Target validation of adenylyl cyclase 5 and adenylyl cyclase 6 in human induced pluripotent stem cell-derived cardiomyocytes

Inaugural-Dissertation

zur Erlangung des Doktorgrades

Dr. rer. nat.

der Fakultät für

Biologie

an der

Universität Duisburg-Essen

vorgelegt von

Pascal Lambertz

aus Essen

Abgabedatum: Februar/2021

Die der vorliegenden Arbeit zugrunde liegenden Experimente wurden bei der Bayer AG in der Abteilung Systems Biology durchgeführt.

1. Gutachter/in: Prof. Dr. Dobromir Dobrev

2. Gutachter/in: PD Dr. Kirsten Leineweber

3. Gutachter/in: Prof. Dr. Gero Hilken

Vorsitzender des Prüfungsausschusses: Prof. Dr. Dirk Hermann

Tag der mündlichen Prüfung: 23.08.2021

DOI: 10.17185/duepublico/74747
URN: urn:nbn:de:hbz:464-20210920-112228-3

Table of contents

I Abbreviations

AC	adenylyl cyclase
AC5	adenylyl cyclase 5
AC6	adenylyl cyclase 6
AMP	adenosine monophosphate
ATP	adenosine triphosphate
AV	atrioventricular
BMP	bone morphogenetic protein
BMP4	bone morphogenetic protein 4
BNP	brain natriuretic peptide
bp	base pairs
CaMKII	calcium/calmodulin kinase II
cAMP	cyclic adenosine monophosphate
cDNA	complementary DNA
CHF	chronic heart failure
CMs	cardiomyocytes
CREB	cAMP response element-binding protein
CRISPR	clustered regularly interspaced short palindromic repeats
crRNA	CRISPR RNA
cTnI	cardiac troponin I
cTnT	cardiac troponin T
DMSO	dimethyl sulfoxide

EDPVR	end-diastolic pressure-volume relationship
eGFP	enhanced green fluorescent protein
ESPVR	end-systolic pressure-volume relationship
FACS	fluorescence-activated cell sorting
FCS	fetal calf serum
FDA	food and drug administration
FGF	fibroblast growth factor
FGF2	fibroblast growth factor 2
GDP	guanosine diphosphate
GOI	gene of interest
gRNA	guide RNA
GTP	guanosine triphosphat
HCN	hyperpolarization-activated cyclic nucleotide–gated channel
HF	heart failure
HFpEF	heart failure with preserved ejection fraction
HFrEF	heart failure with reduced ejection fraction
hiPSC	human induced pluripotent stem cells
hiPSC CMs	human induced pluripotent stem cell- derived cardiomyocytes
hPSC	human pluripotent stem cells
HR	homologous recombination
HTS	high-throughput screening
IBMX	3-Isobutyl-1-methylxanthin
$I_{Ca,L}$	L-type calcium current

I_f	hyperpolarization-activated cation current
I_{K1}	inward-rectifier potassium current
I_{Kr}	rapid delayed rectifier voltage gated potassium current
I_{Ks}	slow delayed rectifier potassium current
I_{Na}	sodium current
IP_3	inositol trisphosphate receptors
iPSC	human induced pluripotent stem cells
I_{to}	transient outward potassium current
KO	knockout
LTCC	L-type calcium channel
LV	left ventricular
LVEED	left ventricular end diastolic diameter
LVEF	left ventricular ejection fraction
MANT	29,(39)-O-(N-methylanthraniloyl)
MTP	microtiter plate
NCX	sodium calcium exchanger
NFAT	nuclear factor of activated T-cells
NHEJ	non-homologous end joining
NO	nitric oxide
NPPA	natriuretic peptide A
NPPB	natriuretic peptide B
PAM	protospacer adjacent motif
PBS	phosphate buffered saline

PCR	polymerase chain reaction
PDE	phosphodiesterases
PKA	protein kinase A
PLN	phospholamban
POPDC	popeye domain containing protein family
PP	pyrophosphate
PTX	pertussis toxin
RAAS	renin–angiotensin–aldosterone system
RNP	ribonucleoprotein
RT	room temperature
RYR2	ryanodine receptor 2
SERCA	sarcoendoplasmic reticulum calcium ATPase
SNS	sympathetic nervous system
SR	sarcoplasmic reticulum
TGFβ	tumor growth factor β
TNP	2,4,6-trinitrophenyl
WT	wild-type
Y	Y27632

II Figures

III Tables

IV Abstract (English)

Heart failure with preserved ejection fraction (HFpEF) is a common disease within the elderly population, with hypertension, diabetes and obesity being frequently associated with HFpEF. Lifestyle- and demographic change in industrial nations is likely to increase the prevalence of HFpEF. To date, no causal treatment is available.

In this thesis, cardiomyocytes derived from the human induced pluripotent stem cell line ChiPSC22 exhibited typical features that are known to drive the pathogenesis of HFpEF (aberrant β-adrenoceptor activity, abnormal calcium handling, induction of the fetal gene program, concentric hypertrophy). This phenotype was associated with a relatively high expression of adenylyl cyclase 5 (AC5) and adenylyl cyclase 6 (AC6), two main proteins of the cAMP-dependent pathway. This transcriptional pattern is characteristic of cardiomyocytes from old mice after pressure overload-induced left ventricular hypertrophy, a classical model of heart failure.

To prove if AC5- and AC6 activity is causative for the development of the HFpEF-like phenotype, AC5 KO- and AC6 KO cell lines were generated from ChiPSC22 using the CRISPR/Cas9 technology. Subsequently, wild-type and KO cell lines were differentiated into cardiomyocytes. Both KOs rescued the HFpEF-like phenotype at the cardiomyocyte level. The effect was more prominent in AC6 KO cardiomyocytes. This was in line with the higher catalytic activity of AC6 in ChiPSC22 derived cardiomyocytes. Moreover, the inhibition of cAMP levels by the non-selective AC5/AC6 inhibitor BAY 1232055 rescued the HFpEF-like phenotype of wild-type cardiomyocytes, confirming the results generated in both KO cell lines.

Taken together, these findings identify AC5 and AC6 and the cAMP-dependent pathway as a new potential driving force in the pathology of HFpEF. Small molecule-inhibition of AC5 and AC6 might open new therapeutic approaches for a disease with a high unmet medical need.

V Zusammenfassung (Deutsch)

Diastolische Herzinsuffizienz ist eine häufige Krankheit im fortgeschrittenen Alter, die mit Risikofaktoren wie Bluthochdruck, Diabetes und Fettleibigkeit einhergeht. Aufgrund des demografischen Wandels und veränderter Lebensweise in industrialisierten Ländern wird die Prävalenz von diastolischer Herzinsuffizienz zunehmen. Bis jetzt gibt es keine ursächliche effektive Behandlung.

In dieser Dissertation wurde die humane induzierte pluripotente Stammzell-Linie ChiPSC22 in Kardiomyozyten differenziert. Diese Zellen zeigten abnormale Calcium-Transienten, eine gestörte β-Adrenozeptor Signalkaskade, eine Induktion des fetalen Genprogrammes und eine konzentrische Hypertrophie. Diese Eigenschaften treten typischerweise bei Kardiomyozyten von Patienten mit diastolischer Herzinsuffizienz auf. Dieser Phänotyp war mit einer relativ hohen Expression von Adenylatzyklase 5 (AC5) und Adenylatzyklase 6 (AC6) assoziiert. Beide Proteine sind zentral am cAMP-abhängigen Signalweg beteiligt. Dieses transkriptionelle Muster ist charakteristisch für Kardiomyozyten von Mäusen, bei denen linksventrikuläre Hypertrophie durch Volumenüberlastung induziert wird, ein klassisches Modell für Herzinsuffizienz.

Um herauszufinden, ob AC5- und AC6-Aktivität ursächlich für den Phänotyp von Herzinsuffizienz-Kardiomyozyten ist, wurden AC5- und AC6 KO Zelllinien mithilfe der CRISPR/Cas9 Technologie aus ChiPSC22 generiert. Danach wurden Wildtyp- und KO Zelllinien gleichzeitig in Kardiomyozyten differenziert. Interessanter Weise glichen die KO Kardiomyozyten nicht dem Bild von Herzinsuffizienz-Kardiomyozyten. Der Effekt war stärker bei AC6 KO Kardiomyozyten ausgeprägt. Das entsprach der höheren katalytischen Aktivität von AC6 in ChiPSC22 Kardiomyozyten. Wildtyp Kardiomyozyten, die mit dem nichtselektiven AC5/AC6 Inhibitor BAY 1232055 behandelt wurden, glichen ebenfalls nicht mehr dem Bild von Herzinsuffizienz-Kardiomyozyten.

Diese Befunde weisen darauf hin, dass AC5 und AC6 sowie der cAMP-abhängige Signalweg diastolische Herzinsuffizienz begünstigen. Eine Inhibition von AC5 und AC6 könnte eine neue therapeutische Option für diastolische Herzinsuffizienz, für die es keine effektive Behandlungsmöglichkeiten gibt, darstellen.

1 Introduction

1.1 Heart physiology

The heart enables the circulation of blood between organs and peripheral tissue. The heart consists of a left and right atrium and a left and right ventricle. The left and right sides of the heart are separated by a septum. The right chambers pump deoxygenated blood from the venous system into the pulmonary circulation for reoxygenation. The left chambers pump the reoxygenated blood back into the systemic circulation.

Venous, deoxygenated blood reaches the right atrium via the vena cava superior and inferior (Figure 1). The tricuspid valve separates the right atrium from the right ventricle. Relaxation of the ventricles leads to opening of the tricuspid valve. Blood flows from the right atrium into the right ventricle. This is supported by the contraction of the right atrium. Contraction of the right ventricle closes the tricuspid valve and opens the pulmonary valve. This transports blood to the lungs via the pulmonary artery. The blood is reoxygenated in the lungs and the oxygenated blood reaches the left atrium via the pulmonary veins. Upon relaxation of the ventricles, the mitral valve opens and the blood flows into the left ventricle. This is supported by the contraction of the left atrium. Upon contraction of the left ventricle, the mitral valve closes, the aortic valve opens and blood leaves the left heart via the aorta (1).

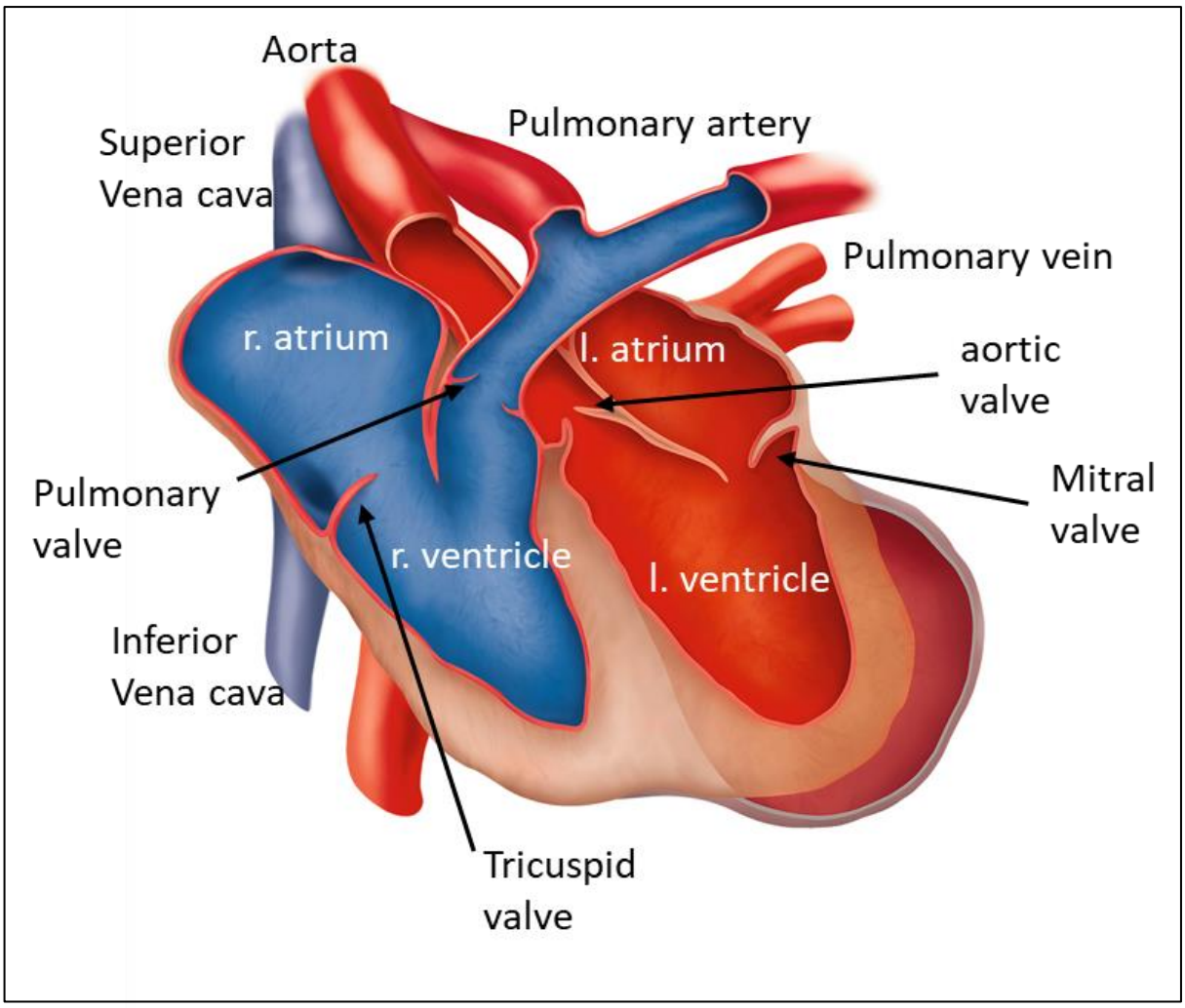

Figure 1: Anatomy of the human heart.
The illustration is adapted from the Bayer identity net media pool (file “Human_Heart.jpeg”).

The sequential contraction of the atria and the ventricles is synchronized by the electrical conductance system of the heart. Normally, electrical stimulation starts at the sinus node. The sinus node is a 3x10 mm large structure localized at the right atrium. It consists of specialized cardiomyocytes with unique electrophysiological characteristics: In contrast to cardiomyocytes from the working myocardium, these cells do not have a constant membrane potential and show spontaneous depolarizations. Spontaneous depolarization is a result of hyperpolarization-activated cyclic nucleotide-gated channels (HCN/ funny channel) activity. Upon hyperpolarization, the HCN channels carry a depolarizing current (I_f). This initial depolarization triggers further depolarization via T- and L-type calcium channels. Spontaneous depolarization is also possible because resting potential stabilizing I_{K1} channels are missing in the sinus node (1).

The electrical impulse propagates from the sinus node over the atria in a fan like manner via gap junctions. These are cell to cell connections with low membrane resistance. The propagation velocity of the electrical signal is about 0,3 – 0,6 m/s. The ventricles are electrically shielded from the atrium. The only location that allows signal transmission is the atrioventricular (AV)-node. It is located at the septum, in between the atrium and the ventricle. When the electrical signal reaches the AV node, the transmission speed of the signal reduces to about 0.04-0.1 m/s, owing to the relatively low abundance of depolarizing potassium channels. This leads to comparatively slow action potential upstroke in AV cell types. The slow conductance prevents high frequencies from being transmitted to the ventricle (e.g. during atrial fibrillation). Higher frequencies would fall in the refractory period of the preceding action potential (see below) (1).

From the AV node, the electrical impulse next reaches the His bundle that branches into a left and a right bundle branch in the interventricular septum. These lead to the Purkinje fibers that innervate the left and right ventricle. The electrical conduction velocity increases in these areas from 1 m/s in the His bundle and the bundle branch to 4 m/s in the Purkinje fibers. In total, complete excitation of all heart areas is completed within 210 ms. The total duration of a ventricular cardiac action potential is longer (300 ms). Because the sodium channels are in an inactivated state for the most part of the action potential (absolute refractory period, see below), healthy cardiomyocytes are protected against the formation of arrhythmia-inducing and maintaining reentry curcuits (1).

The electrical excitability of cardiomyocytes is the basis for the contraction of the atrium and the ventricle (“excitation-contraction coupling”). In general, the action potential of cardiomyocytes can be divided into four phases that will be explained on the example of ventricular cardiomyocytes. At rest (phase 4 of the action potential), the membrane potential of the ventricular cardiomyocyte is between -80 and -85 mV (Figure 2). This phase is characterized by a high potassium conductance of the membrane via the I_{K1} current generated by inward rectifier channels $K_{ir}2.1$, $K_{ir}2.2$ and $K_{ir}2.3$. Electrical impulses from the conducting system are propagated from cardiomyocyte to cardiomyocyte via gap junctions. Once the electrical stimulus arrives at the cardiomyocyte, voltage gated sodium channels open, most notably $Na_v1.5$. The rapid influx of sodium ions (I_{Na}) leads to a depolarization towards the equilibrium potential of

sodium ions. This results in a membrane potential of +20-40 mV (Phase 0). At the same time, the I_{K1} current is inactive due to the inward rectifying properties of the respective channels. Phase 0 is terminated by inactivation of voltage gated sodium channels. The channels remain inactive during the following phases of the action potential until the membrane is repolarized to a value lower than -50 mV. During this time, the cardiomyocyte is in an absolute refractory period where no new action potential can be excited (2).

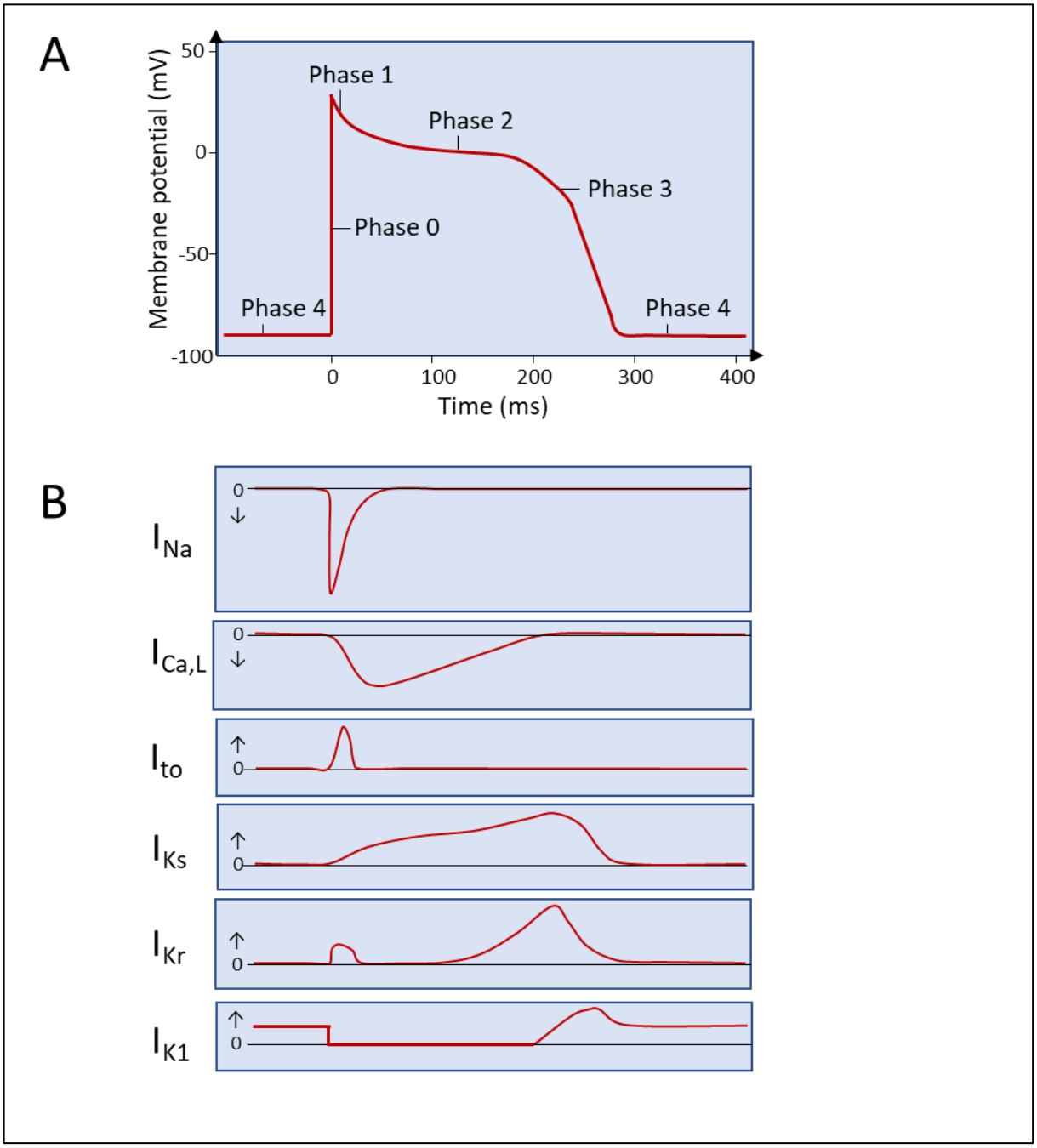

Figure 2: Action potential of a ventricular working cardiomyocyte (A) and the corresponding ionic currents (B).
"↓" mark inward currents. Outward currents are indicated by "↑". The illustration is adapted from (3).

In phase 1, depolarizing calcium currents ($I_{Ca,L}$) via L-type calcium channels $Ca_v1.2$ and $Ca_v1.3$ are activated. Calcium dependent Cl^- channels and voltage gated potassium channels ($K_v1.4$ and $K_v3.4$) are activated and the corresponding outward currents I_{to2} and I_{to1} lead to an early repolarization of the membrane. The Na^+/Ca^{2+} exchanger (NCX) runs in the reverse mode transporting three sodium ions in the extracellular direction and one calcium ion into the cytosol. The net outward current supports the early repolarization. The calcium ions entering the cells via L-type calcium channels and the reverse mode NCX trigger calcium release from the sarcoplasmic reticulum (SR) by activating the type 2 ryanodine receptor (RYR2) in the SR membrane (2). This “calcium-induced calcium release” is facilitated by sarcolemmal invaginations called transverse tubules or T-tubules. These invaginations contain a high density of L-type calcium channels and reduce the distance of L-type calcium channels to RYR2. Calcium binds to cardiac troponin C in the myofilaments. This triggers the crossbridge cycle between actin and myosin leading to contraction of the cardiomyocyte. This excitation-contraction coupling initiates the systole of the ventricle (2).

The early repolarization phase is followed by a plateau (phase 2) where the membrane potential in ventricular cardiomyocytes remains rather stable around 0 to +20 mV for 180-200 ms. This plateau is caused by a tug-of-war between depolarizing and repolarizing currents. On the one hand, depolarizing currents as $I_{Ca,L,}$, late I_{Na} and a forward-mode NCX occur. However, the activity of $I_{Ca,L}$ slowly decreases and repolarizing I_{Kr} and I_{Ks} currents gradually increase. The rapid delayed rectifier current I_{Kr} is driven by opening of $K_v11.1$ channels (HERG). The slow delayed rectifier current I_{Ks} is driven by opening of $K_v7.1$ channels (2).

The increasing activity of I_{Kr} and I_{Ks} and the inactivation of $I_{Ca,L}$ start phase 3 of the action potential. Here, the repolarizing currents exceed the depolarizing currents resulting in a strong repolarization of the membrane potential. Repolarization of the membrane leads to activation of I_{K1} current reestablishing the resting potential between -80 and -85 mV (2). During phase 2 and phase 3 of the action potential, three transport mechanisms lead to removal of calcium from the cytosol. Calcium is transported back into the SR by the sarcoendoplasmic reticulum calcium ATPase type-2a (SERCA2a). Calcium is also transported to the extracellular space by the NCX running in the forward mode (transport of three sodium ions in the inward direction and one calcium ion in the outward direction). Another way for outward transport of calcium is the

plasma membrane calcium-transporting ATPase. Calcium is also taken up by mitochondria. Removal of calcium from the cytosol leads to dissociation of calcium from cardiac troponin C. This terminates the contraction of the cardiomyocyte and initiates relaxation. On the macroscopic level, this results in the diastole of the ventricle (2, 4).

The work of the heart can be illustrated in a pressure-volume diagram. In this diagram, the volume of the left ventricle is plotted against the pressure of the left ventricle (Figure 3). In the diagram, the maximal pressure that is developed by the ventricle is illustrated by the end-systolic pressure-volume relationship (ESPVR) curve. It represents the contractility of the ventricle. Filling of the ventricle is dependent on the compliance of the ventricle. The compliance of the ventricle is illustrated by the end-diastolic pressure-volume relationship (EDPVR) curve. Four different phases of the ventricle can be pointed out: In the first phase, the ventricle becomes completely depolarized. Excitation-contraction coupling leads to a contraction of the ventricle which results in an increase of the intraventricular pressure (Figure 3, point A-B). The pressure is higher than the pressure in the atrium but lower than the pressure of the aorta. As a result, both the mitral valve and the aortic valve are closed. This leads to a intraventricular pressure increase while the blood volume of the ventricle remains unchanged at about 130 mL (isovolumetric contraction) (1, 5).

In the next phase (point B-C), the pressure in the ventricle is higher than the pressure in the aorta which results in opening of the aortic valve and ejection of the stroke volume (about 70 mL) into the aorta. An end-systolic volume of about 60 mL remains in the ventricle (1, 5).

Upon repolarization of the ventricle, the ventricle relaxes and the pressure of the ventricle falls under the pressure of the aorta. As a result, the aortic valve closes and the ventricle undergoes isovolumetric relaxation (C-D). Once the ventricular pressure falls under the pressure of the atrium, the mitral valve opens. As a result, blood flows from the atrium into the ventricle (D-A) increasing the filling to an end-diastolic volume of about 130 mL. This is supported by contraction of the atrium (1, 5).

The analysis of the pressure-volume loop allows calculation of important parameters. The area of the loop corresponds to the stroke work. Subtraction of the end-systolic volume from the end-diastolic volume allows identification of the stroke volume. The

ratio of the stroke volume and the end-diastolic volume times 100 is the ejection faction (about 60-70%). Multiplication of the stroke volume and the heart frequency defines the cardiac output. Another important parameter is dP/dt, that describes the rate of rise/fall of left ventricular pressure (6).

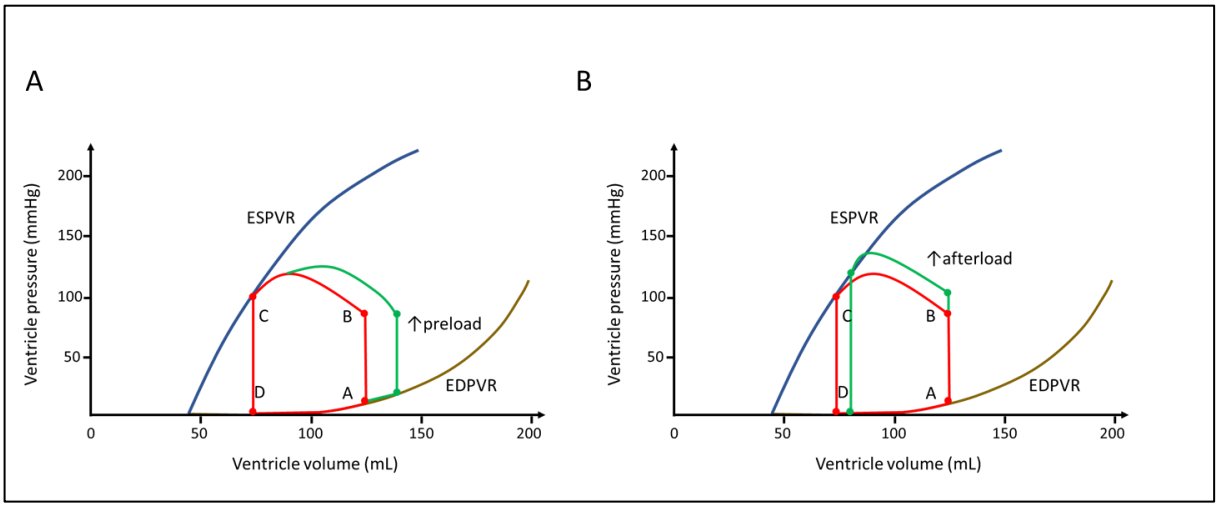

Figure 3: Pressure-volume diagram of the left ventricle under increased preload (A) or increased afterload (B).
The red loop corresponds to the control measurement, the green loop corresponds to increased preload or increased afterload. The end-systolic pressure-volume relationship (ESPVR) curve is indicated in blue. The end-diastolic pressure-volume relationship (EDPVR) is indicated in brown. The illustration is adapted from (5).

The pressure developed by the ventricle is influenced by the law of LaPlace. The law of LaPlace describes the relationship of pressure (P), radius (r), wall thickness (d) and wall tension (K) of a spherical hollow body: $P = Kx\ (\frac{2d}{r})$. This model can also be applied to a simplified version of the heart. In this model, the pressure (P) in the ventricle is a direct function of the tension of the ventricle (K) and the thickness of the ventricle wall (d). On the other hand, the pressure of the ventricle is negatively proportional to the radius (r). During systole, the radius of the ventricle decreases while the wall thickness increases. This allows an increase of pressure even after the complete depolarization of the ventricle (phase B-C in the diagram). During diastole, the radius of the ventricle increases and the thickness of the wall (d) decreases. As a result, a higher active tension of the ventricle is necessary to develop pressure for the next systole (1, 5).

Evolutionary, this problem is solved by the Frank-Starling Mechanism. Filling of the left ventricle results in an increased stretching of the ventricle. Stretching of the cardiac muscle leads to increased sensitivity of the myofilaments for calcium, an increased

calcium release from the SR and an optimal overlap of the myofilaments. All of these mechanisms lead to an increase of the active tension generated by the muscle (1, 5).

The Frank-Starling mechanism also allows the adjustment of the cardiac output of the left and right circulation. An increased pulmonary venous flow leads to increased filling of the left ventricle (increased preload, green loop in Figure 3A). This leads to a higher active tension of the left ventricle, resulting in a larger stroke volume (1, 5).

An increase of the aortic pressure (increased afterload, green loop in Figure 3B) leads to a smaller stroke volume in the first heart cycle and an increased end-systolic volume. In the second heart cycle, the increased end-systolic volume is added to the venous return resulting in a higher end-diastolic volume. This activates the Frank-Starling mechanism which results in a higher stroke volume (1, 5).

1.2 Heart Failure

The pressure volume diagram illustrates that the work of the heart is directly dependent on the contractility and compliance of the left ventricle. A less steep ESPVR curve (smaller contractility) or a steeper EDPVR curve (lower compliance) both reduce the area of the pressure-volume loop (smaller stroke work). A smaller contractility of the left ventricle occurs during heart failure with reduced ejection fraction (HFrEF, Figure 4A). In contrast, a lower compliance of the left ventricle is a hallmark of heart failure with preserved ejection fraction (HFpEF, Figure 4B). In both cases, the reduced stroke work of the heart leads to heart failure (HF), “the inability of the heart to provide peripheral tissue with the required amount of blood and oxygen necessary for their metabolic processes“ (5, 7).

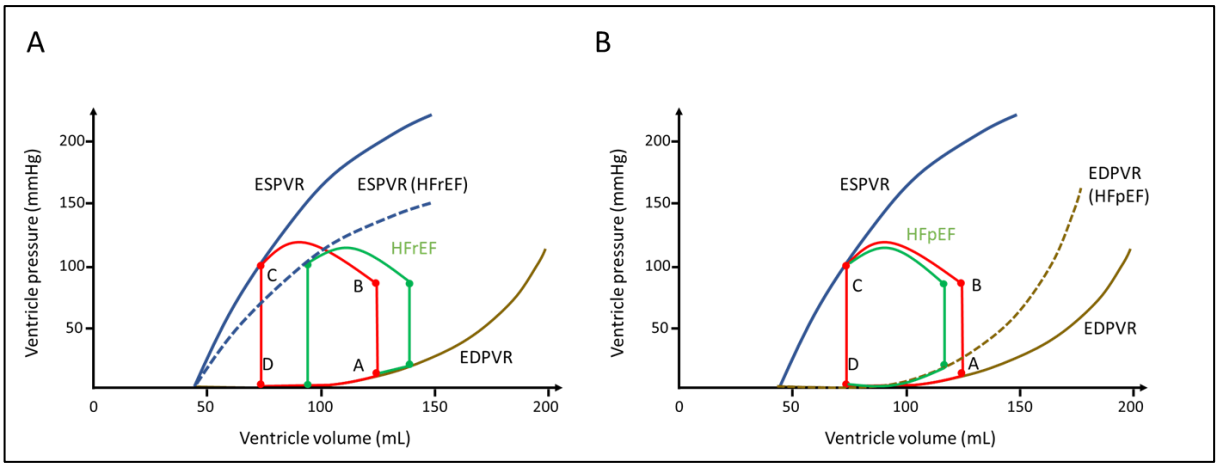

Figure 4: Pressure-volume diagram of the left ventricle under heart failure with reduced ejection fraction (HFrEF, A) or under heart failure with preserved ejection fraction (HFpEF, B).
The red loop corresponds to the physiological pressure-volume loop. The green loop corresponds to the pathological pressure-volume loop. The physiological end-systolic pressure-volume relationship (ESPVR) curve is indicated in blue. The pathological ESPVR curve is marked by a dashed blue line. The end-diastolic pressure-volume relationship (EDPVR) is indicated in brown. The pathological EDPVR curve is marked with a dashed brown line. The illustration is adapted from (5).

HFpEF is mainly caused by peripheral pathological processes like metabolic syndrome, diabetes, obesity or renal dysfunction. All these processes result in systemic inflammation with decreased release of nitric oxide (NO) from the endothelium and increased production of free radicals. Cardiomyocytes respond to free radicals with an increase of stiffness and hypertrophy. On the level of the heart, this often leads to concentric hypertrophy and impaired relaxation of the left ventricle. The reduced compliance of the ventricle manifests in a steeper EDPVR curve in the working diagram of the heart (Figure 4B). As a result, filling of the ventricle is impaired and the ventricle holds a reduced end-diastolic volume. This leads to a smaller stroke volume and a decrease of the heart work despite a hemodynamically normal left ventricular ejection fraction (LVEF) between 50 and 55%. The cardiac output is not sufficient to supply peripheral tissue adequately (1, 5, 8).

In contrast, HFrEF is characterized by a reduction of the LVEF to less than 40%. A reason for the reduced ejection fraction is reduced contractility of the left ventricle due to myocardial infarction, myocarditis or dilated cardiomyopathy. Reduced ejection fraction can also occur when the left ventricle cannot overcome an increased afterload. This is characteristic of coronary artery disease, valvular disease and hypertension. Extra cardiac causes like endocrine diseases, lifestyle and systemic factors can also lead to this disease state. The reduced stroke work of the heart leads to an increase

of the central venous pressure and a higher end- diastolic volume (Figure 4A). However, because the contractility of the ventricle is impaired, the Frank-Starling mechanism fails and the increased preload does not lead to an increased stroke volume. In the diagram, the reduced contractility is illustrated by a less steep ESPVR curve. As a result, the end-systolic volume is increased and the stroke work of the heart is reduced. The ejection fraction is reduced (5).

The reduced ejection fraction is compensated initially by activation of the sympathetic nervous system (SNS) and the renin–angiotensin–aldosterone system (RAAS) (9). These mechanisms can increase cardiac output in the first place. However, chronic activation of these pathways leads to maladaptive changes. For example, β-adrenoceptors are downregulated in cardiomyocytes. Consequently, cardiomyocytes are less responsive towards β-adrenoceptor stimulation (desensitization). Notably, the contractility increasing (positive inotropic) effect of β-adrenoceptors is decreased which deteriorates cardiac contractility further. Another side effect of a high sympathetic tonus is an increase in heart rate that increases the likelihood of arrhythmias. Chronic activation of the RAAS leads to hypertrophic remodeling of cardiomyocytes. Eccentric remodeling of cardiomyocytes leads to chamber dilatation. An increased radius and a decreased wall thickness of the ventricle further impairs the contractility due to the law of LaPlace. Another maladaptive change is the upregulation of atrial natriuretic peptide (ANP) and brain natriuretic peptide (BNP). Initially, this reduces blood pressure. However, blood pressure control fails ultimately because the active form of these peptides becomes reduced under chronic natriuretic peptide signaling (5, 9).

A therapy with RAAS inhibitors, β-adrenoceptor blockers and mineralocorticoid antagonists significantly reduces morbidity and mortality in HFrEF patients (9). Unfortunately, there is no strong benefit of this therapy in HFpEF patients (8). Alternative therapies seek to elevate NO levels by soluble guanylate cyclase activation. Other approaches are based on the reduction of advanced glycation end-products, for example by inhibition of the sodium dependent glucose co-transporter 2 (SGLT2). Overall, there is a clear unmet medical need for effective therapy of HFpEF (10, 11).

Modulation of the cyclic adenosine monophosphate (cAMP) pathway might be a new strategy for the prevention or treatment of HF. In HFrEF, β-adrenoceptor

desensitization is thought to be an adaptation to protect cardiomyocytes from elevated cAMP levels. β-adrenoceptor blockers therapy slows down this vicious cycle. However, β-adrenoceptor blocker therapy comes at the cost of reduced exercise tolerance, reduced relaxation speed and impaired calcium handling (12). Adenylyl cyclase inhibitors could prevent the detrimental effects of cAMP while conserving β-adrenoceptor sensitivity.

Adenylyl cyclase inhibitors could also be useful for HFpEF. Here, traditional β-adrenoceptor blocker therapy fails. One possible explanation could be that β-blockers also inhibit the anti-apoptotic effect of the β_2-adrenoceptor (13). Apoptosis of cardiomyocytes is crucial in the progression of HFpEF (14). Another possible explanation is that there is no clear overactivity of the SNS in HFpEF that could be inhibited by β-blockers (15). In this scenario, targeting downstream effectors of β-adrenoceptor, for example adenylyl cyclases, could reduce baseline activity of cAMP.

1.3 Adenylyl cyclase molecular signaling

Adenylyl cyclases (ACs) convert adenosine triphosphate (ATP) to cyclic adenosine monophosphate (cAMP). The family of ACs consists of 10 membrane bound isoforms and one soluble isoform. All membrane-bound ACs are built up on five domains: An N-terminal cytosolic tail, two transmembrane domains (TM1 and TM2) and two catalytic domains (C1 and C2). TM1 and TM2 anchor the protein in the membrane by six transmembrane-spanning alpha helices (Figure 5). The cytosolic C1 domain is located in between the two transmembrane domains. The cytosolic C2 domain is located at the C-terminus. Both catalytic domains share a homologous structure and can be subdivided in a catalytic (C1a and C2a) and regulatory subunit (C1b and C2b) (16-18).

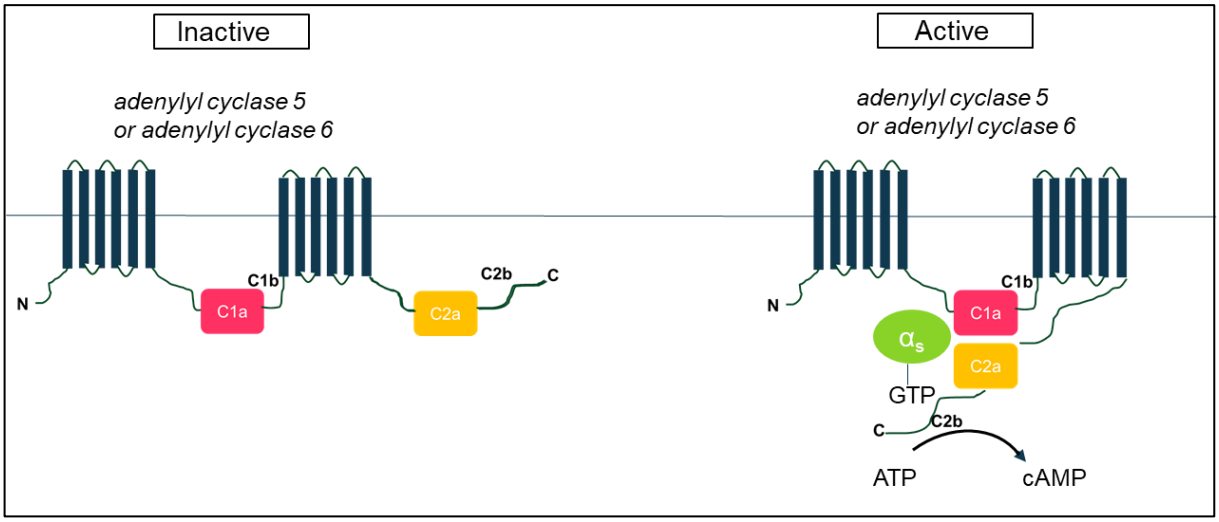

Figure 5: Structure and physiological activation of adenylyl cyclase 5 and adenylyl cyclase 6.

In the inactive state, the catalytic C1a and C2a domains are spatially separated. Activation of β-adrenergic receptors activates $G\alpha_s$ proteins. Activated $G\alpha_s$ protein bind to the adenylyl cyclase TM1 and to the C2 domain. This aligns the C1a and C2a domain in a head to tail like manner. This creates a binding pocket for ATP and two magnesium ions (16-18). The catalytically active state favors the generation of a phosphodiester bond using the alpha-phosphate group of ATP. Release of pyrophosphate (PP) provides the thermodynamic energy for the reaction (18). The product of this reaction is cAMP. Experimental activation of ACs can also be achieved by using the small molecule forskolin. Forskolin can also align and activate the C1a and C2a domains by binding to hydrophobic pockets in the catalytic domains (18). In contrast to $G\alpha_s$ or forskolin, binding of an activated $G\alpha_i$ protein to the C1 domain of ACs leads to inhibition of ACs and decreases cAMP levels (19). Parasympathetic activation of the muscarinic acetylcholine receptor M_2 by acetylcholine is a major activator of $G\alpha_i$ protein. $G\alpha_i$ proteins are also activated through β_2-adrenergic receptors (20). Inhibition of ACs can also be achieved experimentally by addition of pertussis toxin (PTX). PTX catalyzes ADP-ribosylation of the $G\alpha_i$ protein which leads to activation of $G\alpha_i$ and subsequent inhibition of ACs (21).

In the heart, the biological function of ACs is to adapt cardiac output to increased energy and oxygen demand of the body, for example during fight or flight situations: In this scenario, noradrenaline and adrenaline are released from sympathetic neurons in the heart (Figure 6). These neurotransmitters bind and activate the β-adrenergic receptors β_1 and β_2 expressed on cardiomyocytes (12). β-adrenoceptors are G-protein

coupled receptors. In rodents, β_1-adrenoceptors mainly couple to $G\alpha_s$ proteins while β_2-adrenoceptors couple both to $G\alpha_s$ and $G\alpha_i$ proteins (22). In the inactive state, $G\alpha_s$ and $G\alpha_i$ are bound to guanosine diphosphate (GDP) and to a Gβy subunit. Activation of the G-protein coupled receptors leads to exchange of GDP to guanosine triphosphate (GTP). This allows dissociation of the $G\alpha_s$ or $G\alpha_i$ subunit from the Gβy subunit (23). The $G\alpha_s$ protein activates ACs which leads to an increase of cytosolic cAMP. cAMP serves as a second messenger. In cardiomyocytes, cAMP binds to the regulatory subunit of protein kinase A (PKA) which releases and activates the catalytic subunit of PKA. The catalytic subunit of PKA phosphorylates a multitude of calcium handling proteins such as voltage gated L-type calcium channels (24), RyR2 (25) and phospholamban (PLN) (26). Phosphorylation of L-type calcium channels and RyR2 leads to an increased calcium influx into the cytosol from the extracellular region and the SR. This leads to an accelerated rate of contraction of the heart (positive inotropic effect). In addition to that, phosphorylation of voltage-dependent sodium channel $Na_v1.5$ leads to a faster upstroke of the action potential. cAMP and PKA also increase connexin expression, trafficking and phosphorylation. Together, these mechanisms accelerate conduction velocity in the heart (positive dromotropic effect) (27-30). Phosphorylation of cardiac troponin I (cTnI) accelerates dissociation of calcium from the myofilaments. Phosphorylation of PLN increases the uptake of cytosolic calcium ions by SERCA2a. This leads to an accelerated rate of relaxation of the cardiac muscle (positive lusitropic effect) (Reviewed in (31, 32)). PKA might also phosphorylate NCX located in the plasma membrane (33). PKA also phosphorylates and activates the voltage-gated potassium channel $K_v7.1$, which increases I_{Ks} and shortens the cardiac action potential (34, 35). Recently, it has been shown that PKA phosphorylates the intercalated disc protein plakoglobin which increases cardiomyocyte cell-cell junctions by increasing the number of desmoglein 2-specific cell contacts (positive adhesiotropic effect) (36).

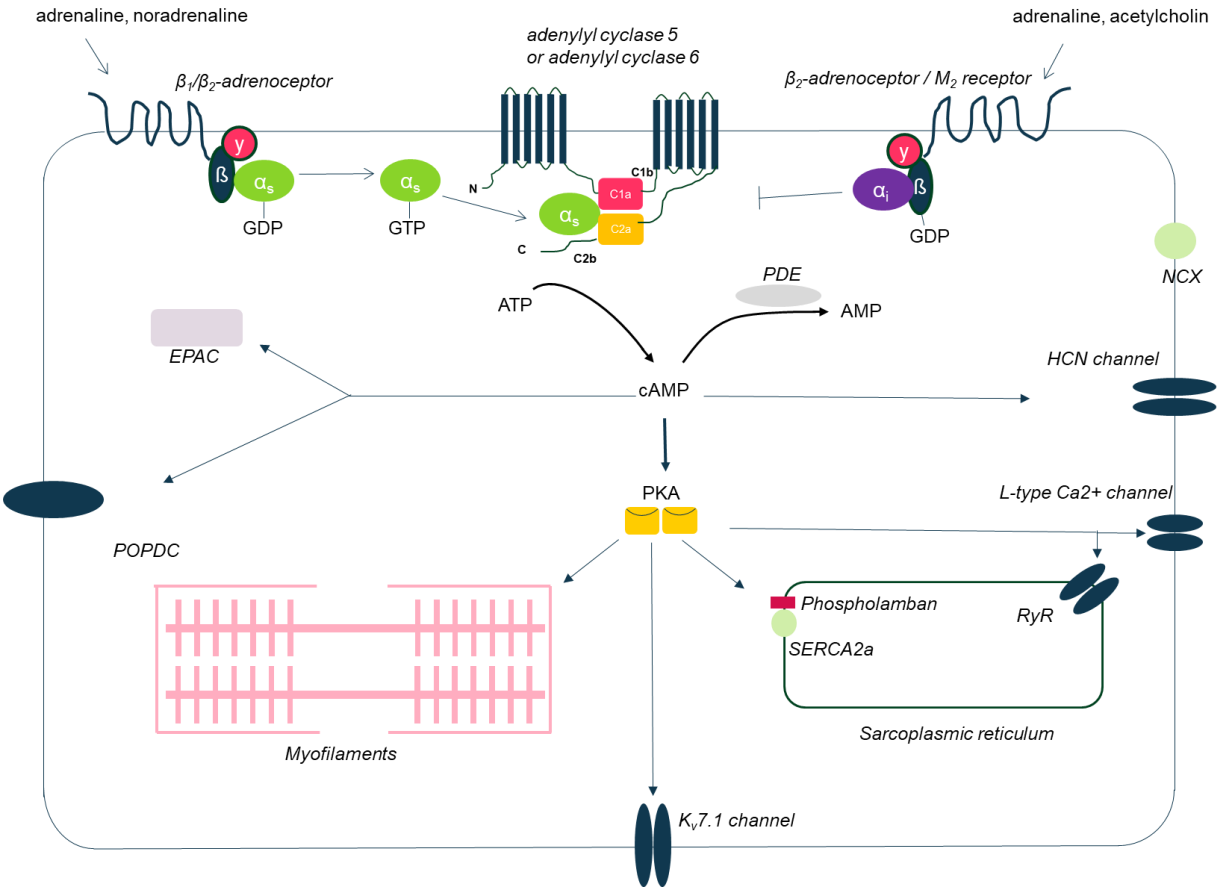

Figure 6: Schematic overview of cardiac AC pathways.

In addition to PKA-dependent effects, cAMP has also direct effects on other proteins. Binding of cAMP to HCN channels in the sinus node increases spontaneous activity of the sinus node which results in increased heart rate (positive chronotropic effect) (37, 38). cAMP can also bind to the intracellular receptor EPAC (exchange protein directly activated by cAMP). Activation of EPAC contributes to cardiac hypertrophy observed under prolonged β-adrenoceptor stimulation. These effects are mediated by the GTPase Ras, nuclear factor of activated T-cells (NFAT), the phosphatase calcineurin, and calcium/calmodulin-dependent protein kinase (CaMKII) (39, 40). A newly defined interaction partner of cAMP is the popeye domain containing (POPDC) protein family. These proteins are highly expressed in the heart and are localized to the t-tubules. Even though the exact mode of action of these proteins is unknown, they interfere with protein membrane trafficking and seem to influence heart rate, the length of the QT

interval and are downregulated in HF (41, 42). cAMP is degraded to 5’ adenosine monophosphate (AMP) by 3′,5′-cyclic nucleotide phosphodiesterases (PDEs) (43, 44).

1.4 Adenylyl cyclase 5 and adenylyl cyclase 6 in health and disease

Type-5 AC (AC5) and type-6 AC (AC6) are the predominant forms in rodent hearts (even though the newest official abbreviation is “ADCY5” and “ADCY6”, the old abbreviations AC5 and AC6 will be used for the gene and protein name for better readability). However, there are inconsistent data concerning the developmental expression of the two isoforms. Northern blot analysis showed that AC6 expression is high in fetal and neonate rat hearts but decreases during the first 10 months after birth. AC5 expression was reported to be low in fetal rat hearts but to increase until birth and thereafter during the first 10 months after birth (45, 46). Scarpace *et al*. also report that AC5 mRNA expression increases between 6 month and 11 month after birth but decreases in older mice between 11 and 24 months (47). They also report a reduced expression of AC6 mRNA between 6 months and 11 months but notice an increase of AC6 expression between 11 months and 24 months.

Hu *et al.* report that the reduction of AC5 expression occurs much earlier. They show that mRNA levels of AC5 are increasing between embryonic and neonate rat hearts but are rapidly decreasing between one week and 24 months after birth. Most importantly, they could show that AC5 protein levels are also decreasing in this time frame using a specific AC5 antibody. Interestingly, pressure overload left-ventricular hypertrophy led to a reactivation of AC5 protein expression (48).

These results suggest that AC5 expression seems to be predominant during development but less important in adult animals. In contrast, AC6 expression seems to be high during embryonic development and in advanced age. However, these findings are not universal. For example, Tang *et al.* found a 59% reduction of AC6 mRNA in left ventricular (LV) samples from 20- vs. 7 month old mouse hearts (49) which clearly contradicts the observations made by Scarpace *et al.*

Next to temporal regulation, AC5 and AC6 seem to be spatially regulated. In mouse cardiomyocytes, AC5 is confined to the t-tubule region by caveolin-3 binding to its N-

terminus. In the T-tubule region, AC5 couples both to the β_1- and β_2-adrenoceptor. However, β_1-AC5 and β_2-AC5 mediated cAMP signaling is silenced because the complexes are coupled to phosphodiesterase type-3 (PDE3) and phosphodiesterase type-4 (PDE4). AC6 lacks a caveolin-3 binding domain in its N-terminus and is therefore not confined to the t-tubule region. AC6 predominantly couples to β_1-adrenoceptors and is not silenced by PDEs (50). Owing to the spatial distribution, the β_1-AC6 cascade is the predominant signaling cascade for $I_{Ca.L}$ activation in rat cardiomyocytes (50). Interestingly, in a rat model for chronic HF (CHF), β_2 receptors are no longer confined to the t-tubule leading to diffuse cAMP signaling. This effect is thought to be a compensatory mechanism for the reduced β_1 signaling in HF (51). The spatial redistribution of the β_2-adrenoceptor might be caused by loss of caveolin-3 during HF (52).

Animal knockout models of AC5 and AC6 have raised hopes that modulation of AC5 and AC6 might be a therapeutic approach for heart diseases. Interestingly, the knockout models suggest that both isoforms play opposing roles in cardiomyopathies. Tang *et al.* generated an AC6 knockout (KO) mouse and investigated the mice in a comparatively young age (6-10 months) (53). Left ventricular cardiomyocytes from AC6 KO mice exhibited an about 60% reduction in isoprenaline- and forskolin-stimulated cAMP levels. This was accompanied by reduced PKA activity, reduced phosphorylation of PLN and impaired SR calcium handling. These molecular changes were accompanied by a functional reduction of the LVEF and contractility during dobutamine stimulation. A later study showed increased mortality of the AC6 KO mouse line under a prolonged β-adrenoceptor stimulation of seven days (54). The study suggests that mortality was not a result of cardiac remodeling or apoptosis of cardiomyocytes. It might rather be a consequence of impaired electrical conduction because the authors observed a prolongation of the PR interval, QRS duration and the QTc interval in the electrocardiogram. In addition, phosphorylation of connexins was altered under baseline and sustained stimulation with isoprenaline (54).

There are many publications that stratify the therapeutic effect of cardiac-specific AC6 overexpression. Gao *et al.* established a mouse line that allows cardiac-specific overexpression of AC6 in three to six months old mice (55). In this model, AC6 mRNA levels can be increased fivefold after removing doxycycline from the drinking water (AC6 “On state”). In the “On state”, forskolin- and isoprenaline-stimulated cAMP levels

were markedly increased. The left ventricular dP/dt and basal heart rates were comparable in transgene off and transgene on mice. However, upon addition of the non-selective α- and β-adrenoceptor agonist dobutamine, the left ventricular dP/dt was markedly increased (55). This study suggested that cardiac-specific overexpression of AC6 can have beneficial effects on cardiac contractility.

The same cardiac-specific, inducible AC6 mouse model was used to investigate the effect of AC6 overexpression in different disease states. Tang *et al.* used the mouse line to show that AC6 overexpression can rescue functional defects of ageing hearts (49). In 20 month old mice, AC6 overexpression led to increased LV ejection fraction, increased LV +dP/dt, increased LV -dP/dt and increased calcium uptake velocity from the SR. These effects were absent in young mice (7 month old). Again, the molecular basis for these effects might be due to increased PKA activity and increased phosphorylation of PLN and cTnI. AC6 overexpression had no effect on cardiomyocyte apoptosis or cardiac remodeling (49).

Lai *et al*. used the same cardiac-specific, inducible AC6 mouse line to show that AC6 overexpression can improve cardiac performance when CHF and myocardial infarction are present (56). After left coronary artery occlusion, mice developed myocardial infarction. In this situation, expression of AC6 increased NKH477 stimulated cAMP levels twofold. They also showed increases in basal LV dP/dt and cardiac output, favorable effects on LV end-diastolic pressure, and a four-fold increase of contractile function. Interestingly, they found increased PKA activity in AC6 “On state” mice. However, they observed no effect of AC6 activation on calcium uptake velocity or phosphorylation of PLN. In addition, they found a 2.7-fold increase in cTnI phosphorylation. This result suggests that in this model, the favorable effect of AC6 overexpression might not be due to improved calcium handling but to direct modulation of cTnI (56).

Interestingly, there is experimental evidence that the cardioprotective effects of AC6 might also be independent of cAMP. Gao *et al*. overexpressed a catalytically inactive AC6 (Ala426->Asp) or wild-type AC6 in adult rat cardiomyocytes via adeno-associated virus (57). Both wild-type and mutant AC6 reduced phenylephrine triggered cell death, apoptosis and hypertrophy. Both constructs also reduced protein levels of PLN and could increase myocyte’s SR calcium content. Mutant AC6 failed to increase basal phosphorylation of PLN but increased phosphorylation of cTnI upon isoprenaline

stimulation. The authors suggest that the cAMP-independent effects of mutant AC6 might be due to protein-protein interactions for example by interaction of the AC6 N-terminus with Snapin (58). In the brain, the N-terminus of AC6 negatively regulates cAMP response element-binding protein (CREB) levels, independent of catalytic activity and localizes AC6 at the nucleus. However, these effects might also be due to a dominant-negative effect of mutant AC6 on cAMP generation (59).

AC6-based gene therapy is currently being explored in humans. Renova Therapeutics conducted a phase-II clinical study with 18 to 80 year old patients suffering from symptomatic HFrEF (both ischemic and non-ischemic, 60). They injected different doses of E1/E3-deleted human adenovirus 5 encoding human AC6 into the coronary arteries of the patients. Patients receiving the highest dose of adenovirus showed an increased LVEF after 4 weeks and increased basal left ventricular peak −dP/dt compared to placebo (60).

Lee *et al.* generated an AC5 KO mouse line (61) whose cardiac performance was characterized at an age of 2.5 months by Tang *et al.* (62). In cardiomyocytes from AC5 KO mice, they detected reduced cAMP levels both under basal (35% reduction) and NKH477-stimulated (44% reduction) conditions. The AC5 KO mice showed a higher basal heart rate and a higher basal LV developed pressure. However, the responsiveness to β-adrenoceptor stimulation was clearly reduced. For example, the potency of dobutamine on relaxation and on LV +dP/dt was substantially decreased. This might be a result of reduced $G\alpha_s$ protein levels in the AC5 KO mouse hearts. On the other hand, knockout of AC5 increased the uptake of calcium in the SR by increasing the affinity of SERCA for calcium. This was in line with increased phosphorylation of PLN in AC5 KO mice (62).

Independently, Okumara *et al.* generated another AC5 KO mouse and investigated its phenotype in four to six month old mice (63). In addition, they studied how AC5 KO mice perform after aortic banding (a surgery leading to LV pressure overload). Wild-type mice responded to aortic banding with an increase of the LV end diastolic diameter (LVEED) and a reduction of the LVEF. In contrast, AC5 KO mice were protected from these compensatory mechanisms. They also noticed that cardiomyocytes from AC5 KO mice were protected from apoptosis. Without aortic banding, these parameters were unchanged between AC5 KO mice and wild-type mice.

Later work of Yan *et al.* found that the same AC5 KO mouse line has an extended life span and is also protected from ageing induced cardiomyopathies (64). For example, left ventricular hypertrophy was the same in young (3-6 month) wild-type and AC5 KO mice. However, older (20-30 month) AC5 KO mice showed reduced hypertrophy and fibrosis of the heart. In addition, cardiomyocytes from older AC5 KO mice exhibited reduced apoptosis. Also, anti-oxidative pathways were enhanced in the hearts of older AC5 KO mice (increased protein level of manganese-dependent superoxide dismutase). However, this study also suggests systemic effects of AC5 knockouts. For example, manganese-dependent superoxide dismutase levels were also increased in the brain and in the kidney of old AC5 KO mice. The anti-oxidative Raf/MEK/ERK pathway was increased also in the kidney, brain and heart of old AC5 KO mice (64).

Hu *et al.* also showed that AC5 protein is increased in the heart upon pressure-overload left ventricular hypertrophy (48). Zhao *et al.* showed that AC5 reactivation could be dangerous because AC5 overexpression can lead to arrhythmias and increased reactive-oxygen-species in mouse ventricular cardiomyocytes (65). These studies have raised hope that AC5 inhibition could prevent the onset of HF or could also be used as a treatment when HF is already present.

Until now, the development of AC5 selective inhibitors was unsuccessful. Two types of AC inhibitors exist: P-site inhibitors mimic a product-bound state and thus slow down AC activity uncompetitively. 29,(39)-O-(N-Methylanthraniloyl)- and 29,39-O-(2,4,6-Trinitrophenyl)-nucleotides (MANT- and TNP nucleotides) inhibit AC activity competitively by preventing the dimerization of the C1 and C2 domain. All inhibitor classes are dependent on phosphate-residues that impair cell permeability of the compounds. Another challenge for the development of AC inhibitors is to achieve isoform- selectivity (reviewed in Dessauer et al, 2017 (17)).

1.5 Human induced pluripotent stem cell-derived cardiomyocytes

Cardiomyocytes derived from human induced pluripotent stem cells (hiPSC CMs) are a powerful emerging tool for cardiovascular research. To understand the generation of hiPSC CMs, the development of the heart and the generation of hiPSCs is described in the following paragraph.

After fertilization, the embryo develops in the spherical structure of a blastocyst. The blastocyst develops into three germ layers ectoderm, endoderm and mesoderm in a process called gastrulation. During gastrulation, an invagination called the primitive streak is formed. Cells migrate through this primitive streak. Cells migrating to the bottom of the primitive streak form the early endoderm while non-migrating cells form the ectoderm. A third population of cells move through the primitive streak in between the two germ layers and forms the mesoderm. The mesoderm also contains the cardiac progenitor cells. These cells migrate bilaterally to the cranial pole of the human embryo on day 15. Here, they give rise to the lateral mesoderm. The lateral mesoderm divides into two parts: The outer somatic mesoderm and the inner splanchnic mesoderm. The splanchnic mesoderm contains the cardiogenic regions. Starting from the two cardiogenic regions, two endocardial tubes form and by the third week, both tubes merge at the ventral midline forming a cardiac crescent. The cardiac crescent soon divides into two major populations, the first heart field and the second heart field. In later stages, cells from the first heart field account for the formation of the left ventricle, parts of the atria and right ventricle and the outflow tract. Cells from the second heart field mainly form the atria, the right ventricle and the sinus venosus. On day 20, a linear heart tube is visible and the first heartbeats arise. Until day 28, the linear heart tube undergoes a looping to the right side. This leads to the formation of a single ventricle. The atria begin to grow into lateral appendages of this primitive ventricle. Starting from day 50 a septum emerges that leads to the formation of the right and left ventricle. Atrial septation starts from day 60 onward. During septation, connections between the atria and the ventricles are retained and soon develop into valves (66, 67).

Several molecular mechanisms orchestrate cardiogenesis. The induction of cardiomyocyte differentiation begins when cardiac progenitors migrate through the primitive streak. This region of the embryo secretes growth factors of the tumor growth factor β (TGFβ) family including nodal and bone morphogenetic protein (BMP) and

growth factors of the fibroblast growth factor (FGF) and Wnt family. Upon migration to the anterior part of the embryo, the cardiac progenitors encounter regions where WNT signaling is inhibited by high levels of Dkk1 and crescent. BMP signaling is antagonized in this region by high concentrations of the growth factors chordin and noggin. Exposure of cardiac progenitors to this growth factor gradient leads to mutual induction of the transcription factors GATA4, NKX2.5 and Mef2c. At the end of this process, NKX2.5 leads to induction of crucial cardiac specific genes like ventricular myosin light chain-2 (MLC2V), cardiac alpha actinin, BNP, cardiac ankyrin repeat protein (CARP), Myocyte Enhancer Factor 2C (MEF2C), calreticulin, NCX1 and A1 adenosine receptor. Expression of the genes Fgf8/10, Isl1, Tbx1/5/20 and e/dHand govern the more specific development of cardiomyocyte subtypes in the first and second heart fields (67, 68).

hiPSCs are stem cells generated from human somatic cells. By definition, stem cells propagate indefinitely and differentiate into any given cell type. Several KO studies led to the identification of 24 candidate genes that confer these characteristic to embryonic stem cells (69). Overexpression of these genes by retrovirus allowed the reprogramming of mouse embryonic fibroblasts into embryonic stem cell-like cells. These cells were termed induced pluripotent stem cells (iPSCs). In the same study, the list of candidate reprogramming genes could be narrowed down to a minimal set of four genes: OCT3/4, SOX2, KLF4 and MYC (70). Subsequently, the same set of genes was shown to generate embryonic stem cell-like cells from human adult fibroblasts. These cells were termed hiPSCs. (71). Another group identified the set OCT3/4 and SOX2 and NANOG and LIN28 to be sufficient to induce pluripotency of human somatic cells (72). Today, these two gene sets are used for the generation of hiPSCs. In the newest generation of hiPSCs, reprogramming factors are introduced by integration-free techniques like sendai viruses, RNA and episomal vectors (69).

Wnt pathway activation and inhibition is crucial in the natural process of cardiomyocyte differentiation. Artificial activation and inactivation of the Wnt pathway enabled cardiac differentiation *in vivo* (73, 74). Zhang *et al.* used this knowledge to establish a protocol for the cardiac differentiation of hiPSCs (75). This protocol tries to mimic the situation in the embryo by applying hiPSCs to high concentrations of fibroblast growth factor 2 (FGF2), bone morphogenetic protein 4 (BMP4) and the Wnt activator CHIR99021 on day 0 of differentiation. C59 addition inhibits Wnt signaling on day 2 of differentiation.

On day 7 after cardiac induction, beating hiPSC CMs are visible. This protocol is used in this PhD thesis (75).

Cardiomyocytes can also be derived from human embryonic stem cells (hESCs). Different protocols exist for the generation of hESC-derived cardiomyocytes and hiPSC cardiomyocytes. Despite this, cardiomyocytes derived from hiPSCs or hESCs (hereafter referred to as hPSC CMs) share many common features. Overall, all hPSC CMs retain many characteristics of fetal cardiomyocytes. For example, hPSC CMs have underdeveloped SR and lack transverse t-tubules. For this reason, calcium handling relies more on plasmalemmal ion channels and transporters. hPSC CMs also have a lower density of mitochondria compared to adult ventricular cardiomyocytes and thus rely more on glycolysis and have only restricted β-oxidation of fatty acids. Morphologically, they are much smaller than adult cardiomyocytes and multinuclear cells are missing. On the transcriptional level, hPSC CMs share also many patterns of fetal gene expression (Reviewed in (76)). Unlike adult CMs, hPSC CMs show spontaneous beating. This spontaneous beating can be attributed to the high density of the HCN currents that are comparable to SAN cells. Additionally, hPSC CMs have a relatively depolarized membrane potential owing to the low density of I_{K1} current. Other characteristic ion channels of ventricular cardiomyocytes are expressed. $Na_v1.5$ and $Na_v1.8$ are expressed early in hPSC CM differentiation. Like in adult ventricular cells, $Na_v1.5$ seems to be the main sodium channel contributing to the inward sodium current I_{Na}. I_{Na} is measurable starting from day 22 but is comparatively small compared to adult ventricular CMs. However, with time in culture, current density significantly increases. Density of $I_{Ca,L}$ also increases during time in culture and achieves comparable levels like adult ventricular CMs. hPSC CMs also exhibit a very comparable expression of the $K_v11.1$ (HERG) channel and thus comparable levels of the I_{Kr} current. (Reviewed in (2)). Because many ion channels of the heart are expressed in hPSC CMs, this model became a versatile tool for safety pharmacology. For example, new drugs must be screened for their ability to block human hERG channels prior to food and drug administration (FDA) approval. Currently, there are endeavors to implement hPSC CMs in this screening cascade (77). In addition, hPSC CMs were successfully used to model human cardiac diseases. For example, hPSC CMs were derived from a family with autosomal dominant long QT syndrome 1 that carry a missense mutation in the KCNQ1 gene. The resulting cells exhibited a prolongation of the action potential duration and increased tachyarrhythmia upon isoprenaline stimulation. The group

could show that the missense mutation led to an aberrant trafficking of the $K_v7.1$ channel which reduces the I_{Ks} current (78). Missense mutations in the KCNH2 gene are associated to decreased I_{Kr} current, prolonged action potential duration and arrhythmic events in hPSC CMs derived from LQTS2 patients. Interestingly, gene editing of the mutation reverses this phenotype (79).

To sum up, hPSC-CMs give the unique opportunity to model human diseases in human cells. These models can lead to the identification of pathogenic mechanisms, drug actions, possible treatment strategies and new interaction partners in regulatory networks. Here, the combination with new gene editing tools is particularly powerful. In recent years, the CRISPR/Cas9 technology has revolutionized this approach.

1.6 CRISPR/Cas9

Bacteria have developed a multitude of CRISPR systems (clustered regularly interspaced short palindromic repeats) for protection against invading viral DNA (80, 81). The CRISPR system used in this PhD thesis is a type II CRISPR system. In bacteria, the system allows the incorporation of invading viral DNA between regularly interspaced short palindromic repeats in the bacterial genome. These repeats are aligned as clusters. During a second infection with the virus, the CRISPR array is transcribed and processed into CRISPR RNA (crRNA). Assembly with a scaffolding tracRNA stabilizes the molecule. The cRNA/tracRNA then forms a complex with a Cas9 nuclease (82). The crRNA contains a variable “protospacer” sequence that is complementary to the viral DNA. This sequence allows binding to invading viral DNA. The Cas9 nuclease then induces a double strand break in the DNA three base pairs upstream of a protospacer adjacent motif (PAM). The canonical PAM sequence of the type type II CRISPR system from S. pyogenes is 5’-NGG (83).

Because this sequence occurs very frequently in mammalian cells, the CRISPR system can be used to edit genes in hiPSCs. To this end, a plasmid containing the Cas9 sequence, a gene-specific crRNA sequence and a tracRNA sequence is introduced into the cell via electroporation or lipotransfection. Cas9 protein, crRNA and tracrRNA are expressed by the cell’s machinery and auto-assemble. Alternatively, complexed recombinant Cas9 protein-cRNA/tracRNA molecules can be directly

delivered into the cell via electroporation or lipotransfection. The functional CRISPR/Cas9 complex then targets the specific gene region according to the crRNA sequence. Cleavage of the target sequence leads to a double strand break. The double strand break is repaired via non-homologous end joining (NHEJ) or homologous recombination (HR). Repair by the first mechanism is error-prone and can lead to the deletion or insertion of base pairs. If located in the exonic region, these indels can lead to frameshift mutations. Starting from the CRISPR site, the resulting protein bears a nonsense-amino acid sequence. In addition to that, the frameshift mutation might lead to a premature stop codon. Translation is terminated leading to a truncated protein. Usually, this should lead to a non-functional protein (84). On top of this, usage of multiple CRISPR sites should also allow the deletion of exons on the DNA level.

2 Aim of this PhD thesis

Data from rodent study support the notion that AC5 inhibition and AC6 activation are two strategies to prevent or treat HF. As a matter of fact, gene therapy for heart targeted AC6 overexpression is being developed and AC5 inhibitors are highly anticipated. Ironically, these strategies are pursued with extensive resources even though human models for AC5 inhibition or AC6 activation are not available. The aim of this PhD thesis is to provide a model for AC modulation in human cardiomyocytes. This model will fill the gap between animal models and translation into human patients. Filling this gap is particularly important since many drug candidates developed in animal models fail later in clinical trials due to species-specific lack of efficacy or toxicity (85). Three human models for AC-modulation are conceivable: Immortalized cardiomyocytes, primary cells and stem cell-derived cardiomyocytes. Immortalized cell lines poorly reflect the patient's situation. Most importantly, their genetic instability confers many features of tumor cells to these cell lines. Primary cells from human heart biopsies are a better option to predict drug effects in the patient. However, the limited accessibility to this type of tissue does not allow extensive studies. The short lifetime of these cells in culture adds to this problem. In addition, patient to patient variability complicates the interpretation of data.

hiPSCs propagate indefinitely and can be differentiated into any given cell type. This new human model has many advantages over primary cells, human cell lines and animal models. In contrast to human cell lines, hiPSCs of the newest generation are

genetically stable and identical to the donor's genome. On the one hand, this improves comparability to patient's cells. On the other hand, isogenic hiPSCs allow stratification of patient sub-populations. For example, patient derived hiPSCs were successfully used to screen for modulators of mutated cystic fibrosis transmembrane conductance regulator (86).
In contrast to primary cells, hiPSCs can be kept in culture indefinitely. Upscaling of differentiation protocols also provides enough material for high-throughput screening (HTS). Patient-to-patient variability, the downside of HTS using primary cells, does not play a role in hiPSC screens. If a large enough differentiation batch is produced, one HTS can be performed with one homogenous cell type. Moreover, three dimensional models built up on hiPSC-derived tissues mimic complex biological interactions. This increases the hit quality from HTS.

The process from drug discovery to drug approval can take up to twelve years. Drug target identification and validation often relies on animal disease models. However, breeding of animal strains is cumbersome and consumes several months or years to be successful. A faster generation of disease models would accelerate the time to drug approval. The CRIPSR Cas9 technology allows unprecedented speed, precision and efficiency in gene editing. hiPSCs are amenable for gene editing by CRISPR/Cas9. Combining CRISPR/Cas9 and hiPSC technology should allow a faster generation of disease models. This would be yet another advantage over animal knockout models.

For these reasons, this PhD thesis will try to establish a CRISPR knockout model of AC5 and AC6 in hiPSC-cardiomyocytes. To this end, a reliable protocol for the cardiac differentiation of the hiPSC clone "ChiPSC22" will be adapted. Next, the expression and activity of AC5, AC6 and other components of the β-adreneoceptor signaling cascade will be monitored during cardiac differentiation. This will allow a characterization of the quality of the model. Data will be obtained by quantitative real-time polymerase chain reaction (qPCR) analysis, fluorescence-activated cell sorting (FACS), western blot, cAMP immunoassays and immunofluorescence staining. As mentioned above, the role of AC5 and AC6 in the developing heart is disputed and human data are completely missing. Thus, these experiments will clarify the role of AC signaling in the developing human heart.

The next part of this PhD thesis will be the development of more advanced functional readouts. The modulation of calcium transients is a crucial mechanism in β-

adrenoceptor signaling. Until now, little is known about these processes in hiPSC cardiomyocytes and all publicly available data only report calcium imaging of spontaneously beating hiPSC cardiomyocytes. Calcium imaging of paced hiPSC cardiomyocytes in a microtiter format will allow the pharmacological characterization hiPSC cardiomyocytes.

After characterization of the hiPSC cardiomyocyte model, a CRISPR knockout of AC5 and AC6 will be generated in the ChiPSC22 cell line. Usage of the CRISPR technology will allow the design of more accurate and reliable AC5- and AC6 KOs compared to previous publications. The AC5 KO mouse lines described by Okumara *et al.* and Tang *et al.* relied on insertion of an antibiotic resistance cassette at the beginning of the AC5 gene (61, 63). A comparable design was used for the generation of the AC6 KO mouse line by Tang *et al.* (53). In both studies, insertion of the antibiotic cassette at the beginning of the gene should lead to an early frameshift event during translation. Thus, the AC5- or AC6 protein sequence is only properly translated until the beginning of the antibiotic cassette. The subsequent protein sequence is likely nonsense due to the frameshift mutation. This experimental approach is likely to give a complete knockout of AC5 and AC6. However, it is not clear whether the knockout is complete. For example, translation from an alternative start codon 3' of the antibiotic cassette might give rise to a truncated, yet functional AC5 or AC6 protein. Because the catalytically important parts of the protein are encoded by the 3' sequence of the AC genes, this event is not unlikely. In this PhD thesis, a more reliable functional knockout of AC5 and AC6 is generated by a CRISPR deletion within the catalytic domain. Even if residual mRNA should be left and translation of an alternative start codon should occur, this deletion will inevitably result in catalytically inactive AC5 or AC6.

In the third part of this PhD thesis, the knockout models will be used to address yet unresolved questions. Most publications have identified AC6 as a cardioprotective factor and AC5 as detrimental contributor to the heart. However, most of these results were acquired in other species and might not reflect the real situation in the human body. This will be the first study to validate these assumptions in human cells. To this end, effects of the knockouts on calcium handling, gene expression, morphology and hypertrophy will be analyzed in the AC5- and AC6 KO cell lines.

Until now, the development of selective AC5 inhibitors was limited. While there is selectivity over AC1-4 and AC7-10, AC6 is equally inhibited by commercially available compounds. The AC5 KO cell line will be used to mimic the effect of selective AC5 inhibition in cardiomyocytes. This will allow the prediction of selective drug effects. In contrast, the AC6 KO cell line will be used to predict the effect of AC6 inhibition in cardiomyocytes. This will help to answer the question which type of AC modulators should be developed (selective drugs vs non-selective drugs). In previous publications, the testing of AC modulators was only performed in biochemical assays using purified enzyme, in HEK 293 cells overexpressing ACs or in animal cardiac membranes. Testing compounds in biochemical assays excludes indirect AC modulators and also identifies molecules that are not cell permeable. Cardiac membrane assays also exclude cell permeable compounds and cannot distinguish between cardiac AC isoforms. Assays using HEK 293 cells only identify cell permeable compounds. Finally, HEK 293 cells have a broad basal expression of ACs hampering the selectivity of this assay. This PhD thesis will characterize AC inhibitors in the human AC5 and AC6 KO models. AC5 and AC6 are the predominant isoforms in the heart. Knockout of one isoform should lead to exclusive expression of the other isoform. Enzymatic activity can be measured using an cAMP immunoassay in intact cells. This will allow the characterization of AC modulators based on cell permeability and isoform selectivity.

3 Methods

3.1 hiPSC culture

The hiPSC clone ChiPSC22 (Takara Bioscience) was cultured in StemMACS™ iPS-Brew XF, human (130-104-368) and on 6-well plates (Corning, 353 224) coated with Matrigel® (Corning, 354263, dilution: 1:72 in KO-DMEM, Gibco®, 10829-018) overnight at 4°C. Cells were splitted regularly on Mondays and Fridays. To this end, the medium of two wells was removed and cells were washed with 1 mL phosphate buffered saline ("PBS", Gibco, 10010-015) Next, 1 mL Accutase (Gibco®, A11105-01) was added to the cells for 9 minutes at 37°C. The reaction was stopped with 4 mL Brew + 10 µM "Y" (StemMACS™ Y27632, Miltenyi 130-103-922) and cells were centrifuged at 200 G for three minutes at 4°C. The supernatant was discarded and the cells were resuspended in 3 mL Brew + 10 µM Y. Cell density was determined by trypan blue staining and manual cell counting. 300.000 c/well were seeded onto a Matrigel®-coated 6-well plate prewarmed to 37°C and containing 2 mL Brew + 10 µM Y per well. The next day, medium was changed to 2.5 mL Brew XF/ well without Y. Tuesday, medium was changed to 3.5 mL Brew XF / well. On Thursdays, this was increased to 5 mL. On Fridays, the splitting was repeated and one million cells per well were seeded onto the plate. Already after 6 hours, medium was replaced with 6 mL Brew XF/well without Y. Medium was not replaced over the weekend. The earliest passage number used was 21 and the oldest passage number used was 40.

3.2 Cardiac differentiation of hiPSCs

10^6 cells of the ChiPSC22 cell line were seeded in one well of a 6 -well plate (Corning, 353 224) on Friday morning in 2.5 ml "Brew" (Brew XF human, Miltenyi, 30-104-368) supplemented with 10 µM Y. In the evening, the medium was completely replaced by six mL without supplements. On Monday morning, the medium was removed and the cells were incubated with 1 ml/well of Brew supplemented with 5 ng/mL Gibco™ Activin A Recombinant Human Protein (Gibco, PHC9561) for five hours. This preincubation improved the yield of cardiomyocytes tremendously. After five hours incubation, the cells were washed with 5 mL PBS (Gibco, 10010-015) and incubated with 1 mL Accutase® supplemented with 10 µM Y for 10 minutes. After neutralization with 2 mL

Brew + 10 µM Y, cells were centrifuged at 200 G for three minutes and resuspended in 2 mL Brew + 10 µM Y. After determination of the cell density, the cells were again centrifuged at 200 G for three minutes and resuspended in day 0 differentiation medium. Day 0 differentiation medium consisted of KnockOut DMEM (1x) Dulbecco's modified eagle medium, +4,5 g/L D-Glucose,+ Sodium Pyruvat, - L-Glutamin (Gibco®, 10829-018) supplemented with 50 U/mL Penicillin-Streptomycin (Gibco®, 15070-063), 1:100 Glutamax (Gibco®, 35050-038), Insulin 5 µg/ mL, 5 µg/ mL Transferrin, 5 ng/ mL Selenious Acid (1:1000 Corning® ITS Premix Universal Culture Supplement, Corning, 354350), 10 µM StemMACS Y27632 (Miltenyi, 130-103-922), 10 ng/mL Recombinant Human FGF basic (154 a.a.) FGF2 (Preprotech, 100-18B), 5 ng/mL Gibco™ Activin A Recombinant Human Protein (Gibco, PHC9561), 0.75 ng/mL BMP-4, human recombinant (BioVision, 4578), 1.75 µM CHIR99021 (Sigma-Aldrich, SML1046-5MG). This was the optimal concentration of BMP-4 and CHIR99021 determined for cardiac differentiation of the wild-type ChiPSC22 clone. These concentrations had to be optimized for each CRISPR-edited clone. Concentrations between 0.5 and 2 ng/mL BMP-4 and 1.5 µM and 3.5 µM CHIR99021 were tested.

The cells were seeded at a density of 350.000 c/mL and 2 mL per well of one well of a 24-well plate (Corning, 353 226) The 24 well plate was previously coated overnight at 4°C with Matrigel® (Corning, 354263, dilution: 1:102 in KO-DMEM, Gibco®, 10829-018). To ensure an even distribution of the cells in the well, the plate was first rocked back and forth in a crosswise movement, and then tapped on the bench in a crosswise movement. The plate was left on the bench unmoved for 30 to 45 minutes and then gently transferred to the incubator. After 24 hours incubation at 37°C and 5% CO_2, medium was changed to 1.5 mL TS medium. TS Medium consisted of KnockOut DMEM (1x) Dulbecco's modified eagle medium, +4,5g/L D-Glucose, + Sodium Pyruvat, - L-Glutamin (Gibco®, 10829-018), supplemented with 50 U/mL Penicillin-Streptomycin (Gibco®, 15070-063), 1:100 Glutamax (Gibco®, 35050-038) and 5 µg/mL Transferrin (Sigma, T8158-100MG), 6.75 ng/mL Sodium Selenite (Sigma, S5261-10G) and 250 µM Phospho-Ascorbat (Sigma, 49752-10G). 48 hours after cardiac induction, medium was switched to TS medium supplemented with 0.5 µM C59 (Tocris, 5148). This medium was renewed 72 hours after beginning of the differentiation. 96 hours after start of the differentiation, the medium was switched back to TS medium. TS medium was renewed every second day until day 13 of the differentiation. At this time point, the medium was switched to RPMI-Thai consisting of RPMI Medium 1640 (1x)

+ L-Glutamin (Gibco®, 28175-034) supplemented with 50 U/mL Penicillin-Streptomycin (Gibco®, 15070-063), 1:100 Glutamax (Gibco®, 35050-038) 0.1% HSA (Sigma, A0237-5G), 250 µM Phospho-Ascorbat (Sigma, 49752-10G), Insulin 5 µg/ mL, 5 µg/ mL Transferrin, 5 ng/ mL Selenious Acid (1:1000 Corning® ITS Premix Universal Culture Supplement, Corning, 354350), 1:12500 Thioglycerol (Sigma, M6145-25 mL). On day 14, cells were dissociated by washing the cells with 2 mL PBS per well and incubation with 250 µL per well TrypLE™ Select Enzyme (10X), (ThermoFisher, A12177-01) supplemented with 10 µM Y for 20 minutes. A single cell suspension was achieved by careful, repetitive pipetting with a 1000 µL Eppendorf pipette and the enzyme was neutralized by addition of 1.5 mL RPMI-Thai supplemented with 10 µM Y. The cells were centrifuged at 200 G for 3 minutes and resuspended in RPMI-Thai supplemented with 10 µM Y. The cells were splitted at a density of 700.000 c/well on a 24-well plate (Corning, 353 226) coated for three hours at 37°C with Laminin-521 (StemCell Technologies, 77003.)

3.3 Freezing and thawing of hiPSC CMs

To facilitate experimental planning, some experiments were conducted using frozen cardiomyocytes. Cardiomyocytes were frozen on day 10 of differentiation. Prior to freezing, hiPSC CMs were treated with 10 µM StemMACS Y27632 (“Y”, Miltenyi, 130-103-922) for two hours. Following the incubation, cells were washed with 1 mL PBS (Gibco, 10010-015) and incubated with 250 µL per well of prewarmed 10x TRYPLE Select (Gibco, A12177-01) for 20 minutes. Cells were dissociated by carefully pipetting not more than 8 times using a 1000 µL pipette. Next, the enzyme was neutralized with six times the volume of RPMI Thai (see chapter Cardiac differentiation of hiPSCs for formulation). After determining the cell density, the cells were centrifuged and resuspended at a density of $4*10^6$ cells per mL of cardiomyocyte freezing medium (StemCell Technologies, 05030), and transferred to -80°C in a Mr. Frosty™ (FisherScientific, 10110051). The following day, the hiPSC CMs were transferred rapidly to liquid nitrogen for long term storage.

For thawing, transport of hiPSC CMs from liquid nitrogen to the waterbath is supposed to be quick. To this end, hiPSC CMs were first transferred from the liquid nitrogen storage to a dewar receptacle containing liquid nitrogen. After transporting the cells to

the lab, cells were transfered into the waterbath swiftly and thawed at 37°C. During thawing, the vial was rotated carefully until only a small ice clumb was visible. Then, the vial was disinfected and 1 mL of RPMI Thai + 10 µM Y was added dropwise. Without resuspending, the cell solution was then transferred to a vial containing 5 mL of RPMI Thai + 10 µM Y. Next, the cryovial was washed once with 1 mL of RPMI Thai + 10 µM Y and this cell suspension was also added to the 5 mL of RPMI Thai + Y. Cells were centrifuged at 200 G for three minutes. The supernatant was discarded and cells were resuspended in RPMI Thai + 10 µM Y and seeded at a density of 600.000 cells per well on a 24 well plate coated with 10 µg/mL Laminin 521 (StemCell Technologies, 7703) for three hours at 37°C.

3.4 Generation of AC5 and AC6 CRISPR KO hiPSC clones

The design of specific CRIPSR sites for an AC5- and AC6 KO were identified by the open source software Benchling (Benchling [Biology Software]. (2017), retrieved from https://benchling.com). Target sequences were selected based on their predicted high "on-target" efficiency (87) and based on their predicted low "off-target" activity. The corresponding gRNAs sequences were synthesized by ThermoFisher as Trueguide™ Synthetic crRNA and annealed with ThermoFisher tracrRNA according to the manufacturer's protocol. Prior to CRISPR experiments, 10^6 ChiPSC22 per well were seeded on a 6-Well plate (Corning, 353 224) in 2.5 mL StemMACS iPS-Brew XF, human ("Brew", Miltenyi, 130-104-368) supplemented with 10 µM Y27632 ("Y", StemMACS Y27632, Miltenyi, 130-103-922). After six hours, the seeding medium was replaced by 6 mL Brew without supplement and cells were incubated at 37°C and 5% CO_2 over the weekend. On Monday, cells were washed with 5 mL PBS (Gibco®, 10010-015) and detached using 1 mL Accutase (Gibco®, A11105-01) supplemented with 10 µM Y for 15 minutes. The Accutase was neutralized by addition of 2 mL Brew supplemented with 10 µM Y and the cells were centrifuged at 200 G for 3 minutes. In the next step, the supernatant was removed and the cells were resuspended in 2 ml Brew supplemented with 10 µM Y. An aliquot of the cells was used for determination of the cell density using TrypanBlue (ThermoFisher, 15250061) staining and a Neubauer chamber. 800,000 cells were centrifuged in a 1.5 mL reaction tube and resuspended in 17 µL Nucleofector solution 2 (Lonza, VPH-5022). Next, 85 µL of transfection solution was added to the cells. The transfection solution was pre-

incubated 30 minutes prior to use at RT and consists of 85 µL Nucleofector solution 2, supplemented with 34 pmol of each gRNA, 11,4 µg TrueCut™ Cas9 Protein v2 (ThermoFisher, A36498) and 1,5 µg PL1_pCI_Puro_2A_eGFP. In the next step, the cell solution was transferred to a Lonza Amaxa cuvette and the cells were nucleofected in a Nucleofector 2b device (Lonza) with pulse program B16. After nucleofection, 1 mL Brew supplemented with 10 µM Y was added to the cells and the whole solution was transferred to one well of a pre-warmed Matrigel® coated 6-Well plate containing 3 mL Brew supplemented with Y. After overnight incubation at 37°C and 5% CO_2, successful nucleofection was verified by excitation of the wells with blue light under a fluorescence microscope. Under this condition, successfully electroporated cells emitted green light due to the expression of eGFP. To select the positively transfected cells, the medium was changed to Brew supplemented with 10 µM Y and 0.5 µg/mL puromycin (Gibco, a1113803). After 24 hours incubation at 37°C and 5% CO_2, the selection was stopped by replacing the medium by Brew supplemented with 10 µM Y. Under this condition, the cells were cultured for additional 48 hours at 37°C and 5% CO_2 for recovery. Following recovery, the cells were washed with 5 mL PBS and incubated with 500 µL Accutase supplemented with 10 µM Y per well for 20 minutes. To obtain a single cell solution, 100 µL of the cells was repeatedly pipetted using a 200 µL Eppendorf tip. Subsequently, 100 µL Brew supplemented with 10 µM Y was added. The cell density was measured and adjusted to a density of one cell per microliter. One microliter of cell suspension was added to each well of a Matrigel®-coated (Corning, 354263, dilution: 1:75) 96-well plate (Greiner, 655090) containing 100 µL Brew + Y. After incubation for five days at 37°C and 5% CO_2 50 µL of Brew + 10 µM Y was added to the cells followed by another addition of 100 µL Brew + 10 µM Y another five days later. Usually, hiPSC colonies could be identified after one week and grew to 70% confluency two weeks after seeding. In this period, medium was replaced by Brew without Y in washing steps.

The following table gives an overview of the gRNAs used and possible off-targets associated with these gRNAs. All predicted off-targets would require several mismatches of the gRNA, most of them at the 3’ end which is extremely important for stability. Many off-targets would also require usage of a non-canonical PAM site by the Cas9 protein.

Table 1: gRNAs for editing of the AC5- and AC6 locus and possible off-targets.

Target	gRNA	possible off target
AC5	caaagattcagcctatagca + AGTGAGTCACCCTGAGCCGG	KHSRP (ENSG00000088247)
		LRFN1 (ENSG00000128011)
		PTPN6 (ENSG00000111679)
		PLIN4 (ENSG00000167676)
		CELA2B (ENSG00000215704)
		HAMP (ENSG00000105697)
		MARCH1 (ENSG00000145416)
		ALK (ENSG00000171094)
AC6	GCGTAGACAGGAGCACATCT + ATGCGGACCCCTAGACTCCC	C16orf95 (ENSG00000260456)
		XRCC4 (ENSG00000152422)
		RP13-794C1.1 (ENSG00000280804)
		BAIAP2-AS1 (ENSG00000226137)
		STX4 (ENSG00000103496)
		CTSA (ENSG00000064601)
		ZFAND1 (ENSG00000104231)
		B4GALT7 (ENSG00000027847)
		SP6 (ENSG00000189120)

3.5 Genotyping of CRISPR KO clones

After passaging of CRISPR-edited clones from the 96-well to the 24 well format, the 96 well was rinsed with 30 µL QuickExtract™ DNA Extraction Solution (Epicenter, QE09050,). Next. The solution was vortexed for 15 seconds and incubated six minutes at 65°C. After mixing the sample again for 15 seconds, the sample was incubated at 98°C for 2 minutes. The DNA concentration was determined using a Nanodrop spectrophotometer (Thermofisher). The DNA concentration was adjusted to 10 ng/µL and 1 µL of this solution was added to a total polymerase chain reaction (PCR) reaction volume of 50 µL. The PCR reaction contained 0.05 U/µL JumpStart™ Taq DNA Polymerase (Sigma, D9307-250 UN), 200 µM dNTPs (Promega, 199537), 1x PCR Buffer (Sigma, D9307-250 UN) and 500 nM gene-specific primers. Primers that are complementary to sequences up- and downstream of the CRISPR deletion sites (PCR1) and a primer pair complementary to sequences in between the CRISPR deletion sites (PCR2) were used for detection of the CRISPR deletion.

The primer pair TCTGGGATCAGGGTGCCA and GGGGTTTGGGCAGTGTGA was used for PCR1 of the AC5 locus. AGCGACAGTGCTGAAAGC and TCCTCCTCTGCCTGTCCC were used for PCR2 of the AC5 locus. Cycler conditions for PCR 1 of the AC5 locus were 1 minute 95°C; 35X (30 seconds 95°C, 30 seconds

64°C, 1.12 minutes 72°C), 2 minutes 72°C, hold at 4°C. Cycler conditions for PCR 2 of the AC5 locus were 1 minute 95°C; 35X (30 seconds 95°C, 30 seconds 64°C, 0.5 minutes 72°C), 2 minutes 72°C, hold at 4°C.

The primer pair GCCCCCACCTTACCCCCAAA and GCAGTCTTCCCCTCCCCCAG was used for PCR1 of the AC6 locus. GGGCTCTGGCGATGTGGAGA and CTCTCTTGCCCACCCAGCCT were used for PCR2 of the AC6 locus. Cycler conditions for PCR 1 of the AC6 locus were 1 minute 95°C, 35X (30 seconds 95°C, 30 seconds 64°C, 2 minutes 72°C), 2 minutes 72°C, hold at 4°C. Cycler conditions for PCR 2 of the AC6 locus were 1 minute 95°C, 35X (30 seconds 95°C, 30 seconds 64°C, 1 minute 72°C), 2 minutes 72°C, hold at 4°C.

Following PCR, 5 µL of the reaction was mixed with 1 µL of 6X blue gel loading dye (New England Biolabs, B7021S) and added to a 1% agarose gel (Carl Roth, 6352.4) stained with 1:10000 SYBR Safe (Thermo Fisher, S33102). Electrophoretic separation of the PCR products was achieved by applying an electrical voltage of 80 V for 45 minutes. DNA was visualized by excitation with blue light using a GelDoc documentation system (Biorad).

3.6 Sequencing of KO DNA/cDNA

Complementary DNA (cDNA) of the wild-type clone and AC5- and AC6 KO clones was generated as described on page 51 and DNA was extracted as described on page 47. Next, cDNA and DNA was amplified using the high fidelity SeqAmp™ DNA Polymerase (Takara Biosciences, 638509). For amplification of AC5 KO DNA, the primer pair TACCTCTAGAGTCGACCCGGtctgggatcagggtgcca and ccacgaccttcTCCACTGCCGGGGTTTGGGCAGTGTGA and the following cycle program were used: 94°C - 1 minute, 40X (98°C - 10 sec, 60°C - 15 sec, 68°C - 33 sec) 68°C - 33 sec. For amplification of AC5 KO DNA, the primer pair TACCTCTAGAGTCGACCCGGGAACGGCTCCTGCTGTCTG and ccacgaccttcTCCACTGCCGAGATGGCCTCGATCATGTCC and the following cycle program were used: 94°C - 1 minute, 40X (98°C - 10 sec, 60°C - 15 sec, 68°C - 24 sec) 68°C - 24 sec.

For amplification of AC6 KO cDNA, the primer pair CCTCTAGAGTCGACCCGGGCCTCGGTGCCAATGTGCTGC and ccttcTCCACTGCCGCGGCCTGGACCACACATCGAACTGC and the following cycle program were used: 94°C - 1 minute, 40X (98°C - 10 sec, 60°C - 15 sec, 68°C - 18 sec) 68°C - 18 sec. Amplification of AC6 KO DNA was performed using primers compatible for cloning into a TOPO cloning vector. These primers were the same used for PCR2 genotyping of AC6 KO clones. The PCR conditions were 94°C - 1 minute, 40X (98°C - 10 sec, 60°C - 15 sec, 68°C - 40 sec) 68°C – 40 sec.

The recipient vector 80_pCI-2A-eGFP (Figure 7) was digested for 30 minutes at 37°C using FastDigest™ NotI (ThermoFisher Scientific, FD0593). The vector digest and the PCR product were separated in an agarose gel electrophoresis as described previously. The amplicon and the linearized vector were excised and gel-purified using the Wizard® SV Gel and PCR Clean-Up System (Promega, A9280). DNA concentration was determined. Next, the PCR product and 50 ng of the linearized vector were united at a molar ratio of 3:1 in a 10 µL reaction containing 0.2 µL T4 DNA polymerase (New England Biolabs, M0203S) and 1 µL NEB 2.1 Buffer (New England Biolabs, B7202S). After mixing, the reaction was kept at room temperature for 2.5 minutes, followed by 10 minutes incubation on ice. During this incubation, an aliquot of competent *E.coli.* was thawed on ice. 5 µL of the reaction were added to 50 µL of the bacterial solution and heat-shocked at 42°C for 30 seconds. After heat shock, bacteria were transferred to ice for two minutes. Next, 500 µL LB broth (Sigma, 61748) was added and the cells were kept agitated at 37°C for one hour. 160 µL of the transfected bacteria were spread onto petri dishes containing LB-agar with 50 µg/mL Carbenicillin (Sigma, C1389). After overnight incubation at 37°C, single colonies could be picked with a 10 µL pipette tip and were transferred to a 50 mL conical tube (Corning, 11820055) containing 5 mL LB + 50 µg/mL Carbenicillin. After overnight incubation at 37°C and 200 rpm shaking, plasmids were extracted using the PureYield™ Plasmid Miniprep System (Promega, A1222). Cloning of AC6 KO DNA was performed using the Topo™ TA Cloning™ (ThermoFisher, 450030) according to the manufacturers protocol. Plasmids were sent to Eurofins Genomics, Cologne for Sanger-DNA sequencing. Results from the sequencing reaction were aligned using the SnapGene software.

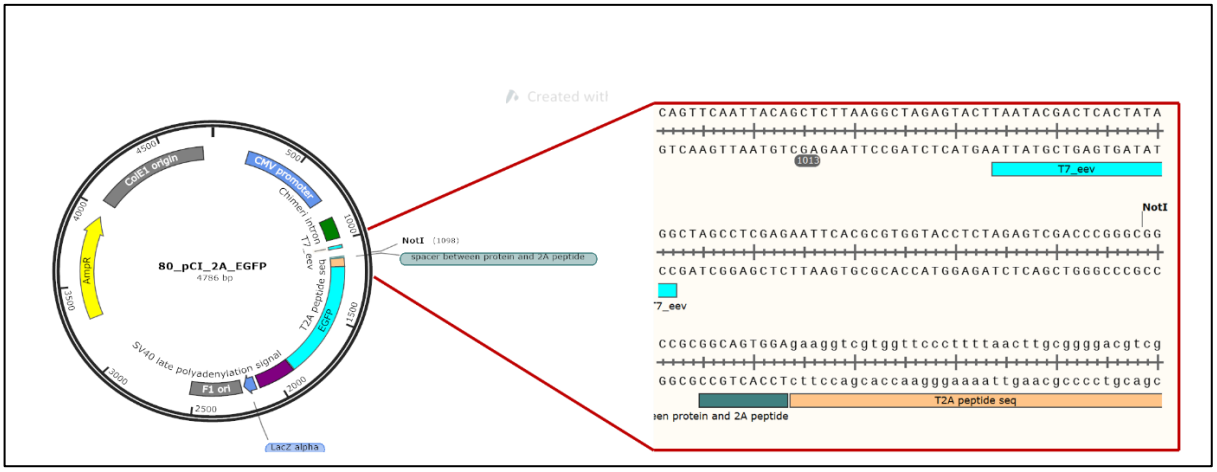

Figure 7: Map of the 80_pCI_2A_EGFP vector used for sequencing of AC5 KO- and AC6 KO DNA and cDNA.
The NotI restriction site is enlarged on the righthand side. The vector map was generated using SnapGene.

3.7 FACS analysis of hiPSC clones

A fully confluent well of hiPSCs was analyzed on Thursdays or Fridays (four/five days after splitting). To this end, cells were washed with 1 mL PBS (Gibco, 10010-015) and the cells were incubated with 1 mL Accutase (Gibco®, A11105-01) + 10 µM Y (StemMACS™ Y27632, Miltenyi 130-103-922). After 10-20 minutes, 2 mL PBS + 2% FCS were added to the wells and the cell solution was centrifuged at 200 G for three minutes. After discarding the supernatant, the cells were resuspended in 1 mL of PBS + 2% FCS. Per staining, 90 µL of the cell solution was incubated with 10 µL of the anti TRA-160-PE (Miltenyi, 130-100-347), SSEA-4 VioGreen antibody (Miltenyi, 130-098-341) and SSEA-1 antibody (Miltenyi, 130-104-937) for ten minutes. Following incubation, cells were washed with 1 mL PBS + 2% FCS and centrifuged at 200 G for three minutes. The supernatant was discarded and the cells were resuspended in 200 µL PBS + 2% FCS and measured using a MACSQuant Flow cytometer (Miltenyi). For analysis of cardiac troponin T (cTnT) in cardiomyocytes, cardiomyoyctes were washed with 1 mL PBS and incubated with 250 µL/well of “TrypLE™ Select Enzyme (10X), no phenol red” (Gibco, A12177-01) for 20 minutes. After neutralization with 8x the volume of RPMI Thai (see chapter Cardiac differentiation of hiPSCs for formulation), the cells were centrifuged at 200 G for 5 minutes. Fixation and staining were performed according to the protocol of the inside stain kit (Mitlenyi, 130-090-477). An anti- cTnT-APC antibody (was used for staining cTnT positive cells (Miltenyi, 130-106-747).

3.8 qPCR analysis

Cells from three wells of a 24-well plate were washed with 1 mL PBS (Gibco, 10010-015) and 250 µL RLT buffer (part of the Qiagen RNeasy Mini Kit, see below) was added to each well. The plate was directly transferred to -80°C. For RNA extraction, the sample was thawed on ice and RNA was extracted using the Qiagen RNeasy Mini Kit (250) (Qiagen, 74106) kit following the manufacturer's description with on-column DNAse digest using the RNase-Free DNase Set (Qiagen, 79254). RNA was reverse transcribed using the High-Capacity RNA-to-cDNA™ Kit (ThermoFisher, 4387406). For qPCR analysis, primers were designed to be exon-exon overlapping and to amplify no off-targets of comparable size. The efficiency of the PCR was determined for every primer pair by performing qPCR with serial dilutions of template DNA from all biological samples. The efficiency of all primer pairs used in this thesis was between 95 and 110%. The DNA concentration of the midpoint of the dilution series was used for the actual experiment. In the subsequent melt curve analysis, only primer pairs were accepted that generated one clear peak without fluorescent shoulders. The PCR product was next analyzed on an agarose gel. Only if the observed size of the amplicon corresponded to the predicted size were the primer used for experiments. For qPCR analysis, the iTaq™ Universal SYBR® Green Supermix (BioRad, 1725122) was used. The following cycle program was run on a Viia7 Real time PCR system (ThermoFisher) for all samples: Initial denaturation (95°C) for 25 seconds, followed by 40 cycles of 95°C for 3 seconds and 60°C for 25 seconds. CT values of the target of interest were normalized to the CT value of the reference gene RPL37A. RPL37A was shown to have stable expression throughout all experimental situations. The efficiency of RPL37A cDNA was comparable to the efficiencies of the targets. The reference gene PCR was always run on the same plate as the target gene PCR. The following primer pairs were used for qPCR:

Table 2: qPCR Primer pair sequences and respective targets.

Target	Primer pairs:	Target	Primer pairs:
AC1	TGCTGACATCGTGGGTTTCA	GNAI2	CGTGCAGTTCGTGTTTGACG
	CAGTGGTTCTCCGTGGCTAA		GGGTACAAAGTCGGCGGT
AC2	GCTGCCAAAAACGTCCGTC	GNAS	GAGAAGCAGCTGCAGAAGGA
	TGAGCAGGGGAGAGGCTTTT		CCAGATTCTCCAGCACCCAG
AC3	AGATCGCGCTCCGGC	MyH6	CGGCCCAGATTCTTCAGGATT
	GCTAGAACTGTGCGGGAACT		GCTCCTTCTCTGACTTGCGG
AC4	GGCCATTACCAGCCTGTTCT	MyH7	ACTTGAGTAGCCCAGGCACA
	TGATGAGAGGCAGAGACCCA		TAGCCGCTCCTTCTCTGACT
AC5	TTGGCACAGGAGCACAACAT	NPPA	CAGGATGGACAGGATTGGAG
	CTGATCTGCAGGAACACGGA		TCCTCCCTGGCTGTTATCTTC
AC6	ACACTCCACCCTGATGCTTG	NPPB	CTTTCCTGGGAGGTCGTTCC
	AAAAGATGCCAACTGCGGTG		GTTGCGCTGCTCCTGTAAC
AC7	CCTTCAGCCAGGGGGACC	CACNA1AC	GACGTGCTGTACTGGGTCAA
	TACATCAGCACAGAGAGGGC		AACTCTCCGCTAAGCACACC
AC8	TATTTGGCCCGGAACGTCAT	PKACA	GAGCAGGAGAGCGTGAAAGA
	TTGTCAAAATCACACCACAGGATA		CTGTGTTCTGAGCGGGACTT
AC9	TCTTGCAGGAGAAGGGAAGG	PLN	ATCACAGCTGCCAAGGCTAC
	TCATCAGGCTGTCTTCTTTGAT		CAGCAGGACAGGAAGTCTGA
ADRB2	GCCTGTGCTGATCTGGTCAT	RPL37A	GTGGTTCCTGCATGAAGACAGTG
	AATGGAAGTCCAAAACTCGCA		TTCTGATGGCGGACTTTACCG
ATP2A2	CCAGTGGCTGATGGTGCT	RYR2	CCTCAGATCCAGAGAAGACGG
	ACTTGAGCGTCTCATCCATG		ACCCACACGTTTAGACTTCTGTT
cTnI	CCCTCACTGACCCTCCAAAC		
	GAGGTTCCCTAGCCGCATC		

For the hypertrophy assay, Endothelin-1 (Sigma, E7764-10UG) was reconstituted in water and diluted to the final concentration in RPMI-Thai medium.

3.9 Simple Western analysis of cTnT phosphorylation

On day 33 of differentiation, cells from three wells of the 24 well differentiation plate were stimulated with 1 µM isoprenaline (Sigma, I5627-5G) for 60 minutes at 37°C. Following incubation, cells were washed with 1 mL PBS and detached by scratching with a 1000 µL Pipette tip. The cell suspension was centrifuged and the pellet was resuspended in ice cold RIPA-Puffer (ThermoFisher, 89900) supplemented with 4 mM

sodium ortho-vanadate (Sigma, S6508-10g), 1 mM PMSF (ThermoFisher, 36978) and Complete Mini protease inhibitors (Roche, 11836153001). The lysate was transferred to a pre-cooled 1.5 mL centrifuge tube and kept agitated at 4°C for 30 minutes. Next, the sample was centrifuged at 12000 rpm for 20 minutes. The supernatant was collected and protein concentration was determined. Samples were stored at -80°C. For detection of phosphorylated cTnI, an anti- p-cTnI antibody (Biorad, MCA2780) was used that recognizes phosphorylation of the protein serine 22 and serine 23. Protein quantification was performed in a simple western assay using the 12-230 kDa Jess or Wes Separation Module (Protein simple, SM-W002) and the Anti-Mouse Detection Module (Protein Simple, DM002) on the WES instrument from ProteinSimple. Prior to the experiment, the dynamic range of the assay was verified by cross titration of antibody concentration against lysate concentration. Signals were normalized to total protein levels using the total protein detection module (Protein Simple, DM-TP01,).

3.10 Immunostaining of contractile proteins

A CellCarrier-384 Ultra Microplate (PerkinElmer, 6057300) was coated with 20 µl/well of 10 µg/ml CellAdhere™ Laminin-521 (StemCell Technologies, 77003) diluted in DPBS $+Mg^{2+}/Ca^{2+}$ (Gibco™, 14040091) for three hours at 37°C. On day 25 of differentiation, Laminin coating was removed by inverting the plate. 8000 c/well ChiPSC22-derived cardiomyocytes were seeded per well in 50 µL RPMI-Thai + 2% FCS + Y (compare chapter “Cardiac differentiation of hiPSCs” for formulation) and left unmoved on the benchtop for 30 minutes. Plates were then carefully transferred to the incubator. Medium was replaced every second day with RPMI Thai. On day 33 of differentiation, cells were washed twice with PBS (Gibco, 10010-015) and fixed with 4% paraformaldehyde for 20 minutes. Cells were rinsed with PBS for 5 minutes and permeabilized in PBS + 0.2% BSA + 0.3% Triton X 100 for 10 minutes. After rinsing for 5 minutes with PBS, cells were incubated with blocking buffer (PBS + 5% BSA + 0.1% Triton X 100) for 60 minutes. Primary antibodys Mouse-anti-Cardiac Troponin T antibody (Abcam, ab8295), Rabbit-anti-N Cadherin antibody (Abcam, ab76057), Alexa Fluor™ 488 Phalloidin (Thermo Fisher Scientific, A12379) were diluted 1:200 in staining buffer (PBS + 2% BSA + 0.1% Triton X 100) and incubated over night at 4°C. The next day, cells were rinsed three times with PBS for 5 minutes. The secondary fluorophore-conjugated antibody (ThermoFisher, Donkey anti-Mouse IgG (H+L) Highly

Cross-Adsorbed Secondary Antibody, Alexa Fluor Plus 594, A32744; Goat anti-Rabbit IgG (H+L) Highly Cross-Adsorbed Secondary Antibody, Alexa Fluor Plus 488, A32731) was diluted 1:200 in staining buffer (PBS + 2% BSA + 0.1% Triton X 100) and 25 µl was added to each well. Cells were incubated for 60 minutes at RT in the dark followed by rinsing twice with PBS for 5 minutes. For embedding, water was removed from plate by leaving it upside-down on a clean paper towel for 1 minute and dabbing several times. Polyvinyl alcohol mounting medium with DABCO® (Sigma, 10981) was heated before use to 50-55°C to decrease viscosity. 20 µl of (anti-fade). Mounting reagent was added by inverse pipetting to prevent air bubble formation. Images were acquired using the Operetta CLS High-Content Analysis System (Perkin Elmer).

3.11 Live cell staining and high content imaging

On day 25 of differentiation, each clone was plated on 20 wells of a Laminin-521-coated 96 well plate (Greiner, 655090) at a density of 40.000 c/well in 200 µL RPMI-Thai + 2% FCS + Y (compare chapter “Cardiac differentiation of hiPSCs” for formulation). This cell density allowed the formation of a continuous monolayer without overlapping of cell bodies. Medium was replaced every second day with 100 µL COR.4U medium (Axiogenesis, Ax-M-HC250E). On day 33 of differentiation, medium was removed and cells were washed twice with 200 µL PBS. Next, cells were loaded for 30 minutes at 37°C with DPBS + Mg/Ca (Gibco™, 14040091) containing a 1:1000 dilution of Nuc Blue Live cell Stain (ThermoFisher, Hoechst 33342, R37605) and 5 µM CellTracker Green (ThermoFisher, CMFDA, C2925). Hoechst 33342 stains nuclei and CMFDA stains cytosol. High content analysis was performed on the Operetta CLS High-Content Analysis System (Perkin Elmer). Per Well, 16 quadrants were recorded resulting in a total of 320 pictures per biological replicate. Cell parameters were calculated using the Harmony® high-content imaging and analysis software. Subsequent FACS analysis ensured that only cell populations with more than 85% cardiomyocytes were used for evaluation.

3.12 Calcium imaging of hiPSC CMs

1 mL of 100 µg/mL Laminin 521 (StemCell Technologies, 7703) was thawed in the fridge for 40 minutes and resuspended in 9 mL DPBS with $MgCl_2$ and $CaCl_2$ (Sigma, D8662). 50 µL of the 10 µg/mL laminin solution was plated per well of a black 96-well plate (Greiner, 655090) and incubated at 37°C for three hours. Afterwards, plates were left in the fridge for one week.

For calcium imaging, only hiPSC CMs were used that were already re-plated once on a 24-well plate coated with Laminin-521 on day 14 of differentiation. The day before seeding, fresh RPMI-Thai medium was added to the cells. On the day of seeding, the laminin coated plate was equilibrated to room temperature for two hours. Then, the coating was removed with a vacuum aspirator and 100 µL of RPMI Thai (+ 4% FCS) was added to the wells (compare chapter “Cardiac differentiation of hiPSCs” for formulation). For splitting, cells from two wells of the 24 well plate were washed with 1 mL PBS (ThermoFisher, 10010015) and incubated with 250 µL per well of prewarmed 10x TRYPLE Select (Gibco®, 12177-01) for 20 minutes. Cells were dissociated by carefully pipetting not more than 8 times using a 1000 µL pipette. Next, the enzyme was neutralized with ten mL of RPMI Thai + 4% FCS and centrifuged in a 15 mL Falcon at 200 G for 6 minutes. The supernatant was aspirated using a 10 mL pipette and the cells were carefully resuspended in 2 mL RPMI Thai + Y using a 5 mL pipette. After filtering the cells through a 100 µM cell strainer (ThermoFisher, 22363549) the cells were diluted to a cell density of 300.000 cells/mL and transferred to a flat cell reservoir. While rocking the cell reservoir back and forth, 100 µL of the cell solution was added to each well of the 96 well plate using a 200 µL tip. Throughout seeding, the 96 well plate remained unmoved on the bench and was left there for 30 minutes for the cells to settle down. The plate was then carefully transferred to the highest step of the incubator and remained unmoved for 18 hours. Two days after seeding, 100 µL COR.4U medium (Axiogenesis, Ax-M-HC250E) was added to the cells and 100 µL were removed. This washing was performed twice and every second day. Calcium imaging was performed one day after washing and seven days after plating. For calcium imaging, 130 µL medium was removed so that 70 µL of medium remained in the well. Next, 30 µL of Calcium 6 (Molecular devices, R8190) diluted in 10 mL COR.4U medium was added and incubated for thirty minutes. Next, 50 µL COR.4U medium were added (pacing worked best with a volume of 150 µL in the well). Cells were

transferred to the fluorescence reader (Hamamatsu, FDSSµCell) prewarmed to 37°C and left there for at least 30 minutes. This device allows pacing of cardiomyocyte monolayers in a 96-well plate. The electrical current is applied by electrodes that are lowered into the well. With this fluorescence reader, pacing and compound addition are not possible simultaneously. In addition to that, well to well variability is so strong that compound effects cannot be normalized to a control well. Therefore, one measurement with unstimulated and with paced hiPSC CMs was performed before compound addition (10 µL). A second measurement was performed after compound addition. Compound effects were calculated as %-change by normalization of post-treated wells to pre-treated wells. Pacing settings were 5 Volt with a pulse width of 10 ms for 25 seconds with a pause of 10 seconds between different pacing frequencies. Compounds tested were isoprenaline hydrochloride (Sigma, I5627-5G), thapsigargin (Tocris, 1138), verapamil hydrochloride (Tocris, 0654), ryanodine (Tocris, 1329), 2-APB (Tocris, 1224), SEA 0400 (Tocris, 6164), ICI 118,551 (Tocris, 0821), ivabradine hydrochloride (Tocris, 6542), BAY 1232055 (internal compound). All Compounds were reconstituted in dimethyl sulfoxide (DMSO, Sigma, D2650-100 mL) and stored as aliquots at -20°C. All subsequent dilutions were performed in DMSO or medium. FACS analysis ensured that only cell populations with more than 85% cardiomyocytes were used.

For the analysis of fluorescence increases, a Bayer proprietary software was programmed by Dr. Greta Ziemann and Stefan Neumann and improved in this PhD thesis together with Dr. Mark Meininghaus. An exemplary measurement of KinEva analysis is shown in Figure 8. KinEva detects fluorescence peaks and fluorescence baseline and fits a curve connecting the measurement points. Based on this function, KinEva calculates calcium transient parameters: The parameter “systolic calcium” is the mean peak height of all maximal signals. “Diastolic calcium” is the mean fluorescence baseline in the measurement. “CaT amplitude” is the mean difference between systolic and diastolic calcium in the measurement. “Peak to peak time” is the mean time between the peaks of two calcium transients. Calculation of the mean time from diastolic to systolic calcium (“Time to peak”) and the mean time from systolic calcium to diastolic calcium (“Calcium decay”) characterizes the steepness of the calcium transient. The software also allows the calculation of the calcium transient integral (“CaT integral”) which is a proxy for the overall calcium oscillation during one

transient. Based on the CaT integral, the PWD90 can be defined as the duration of the calcium transient at 90% of the peak integral. Disclaimer: Based on a “bug” in the software, the “amplitude” value was not rescaled. Therefore, the values are much smaller than expected from subtraction of the diastolic calcium value from the systolic calcium value. This scaling error does not affect the quantification of the parameter. Comparing this parameter from different calcium transients works without any problems.

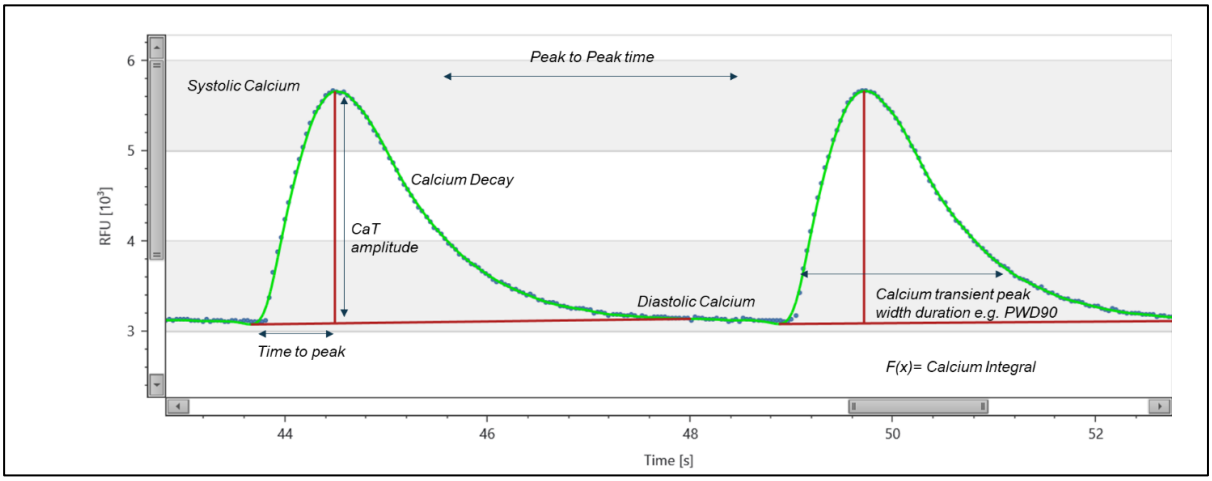

Figure 8: Exemplary “KinEva”- curve fitting of fluorescence increases evoked by calcium transient in hiPSC CMs.
Blue dots mark fluorescence measurements. KinEva detects fluorescence peaks and baseline (marked in red) and fits a curve (green) connecting the measurement points.

3.13 cAMP Assay

To determine the most suitable assay for cAMP detection in hiPSCs, the cAMP - Gs Dynamic kit - 1,000 tests (CisBio®, 62AM4PEB) and cAMP - Gs HiRange kit - 1,000 tests (CisBio®, 62AM6PEB) were compared side-by side using a cAMP standard. To this end, serial dilutions of a cAMP standard (8 µL) were incubated with 8 µL of a D2-cAMP conjugate and 8 µL of an anti-cAMP antibody. Upon excitation with light of a wavelength of 337, emitted light at 650 nm and 620 nm was detected. The 650 nm/620 nm ratio was plotted against the cAMP concentration. The resulting concentration-response curve of the dynamic kit showed an EC90 value of 0.4 nM and an EC10 value of 38.4 nM (Figure 9). Between these two values, the HTRF ratio is almost linear to the cAMP concentration, allowing an accurate determination of cAMP levels based on the HTRF ratio. Thus, the dynamic kit was most sensitive for the detection of rather low

cAMP concentrations. With an EC90 value of 0.7 nM and an EC10 value of 252.9 nM, Cisbio's HiRange kit was found to be most sensitive for higher cAMP concentrations. cAMP levels of hiPSCs and hiPSC CMs changed over time in differentiation. Using both the "Dynamic"- and the "Hi-Range" kit ensured that maximal cAMP levels were always in the linear range of one of the assays. The standard curves were repeated in every assay. This allowed accurate calculation of absolute cAMP levels by interpolation of the HTRF ratio to the standard curve.

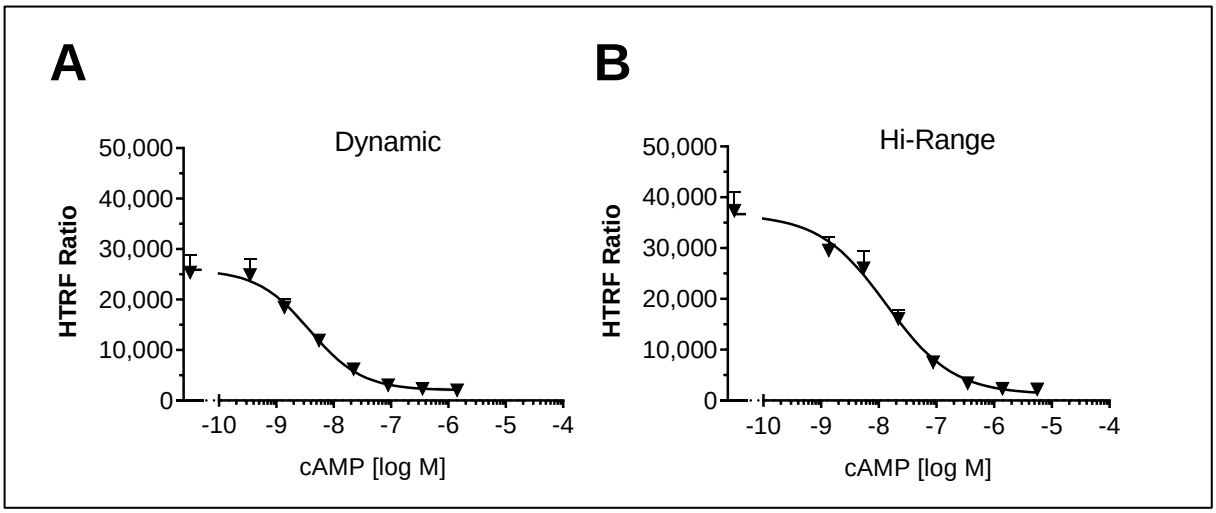

Figure 9: Measurement of a cAMP standard using the Dynamic- and Hi-Range assay kits (CisBio®).
Serial dilutions of a cAMP standard (8 µL) were incubated with 8 µL of a D2-cAMP conjugate and 8 µL of an anti-cAMP antibody. Upon excitation with light of a wavelength of 337, emitted light at 650 nm and 620 nm was detected. The 650 nm/620 nm ratio was plotted against the cAMP concentration.

For seeding, cells were dissociated and resuspended as previously described. Before determination of the cell density and seeding, the cells were passed through a 100 µm cell strainer (Corning, CLS431752-50EA). 3000 cells were seeded per well of a 384-well microtiter plate (Gibco, 781092) that was previously coated for three hours at 37°C with 15 µL of 10 µg/mL Laminin-521 (StemCell Technologies, 77003) diluted in DPBS with MgCl2 and CaCl2 (Sigma, D8662) per well. Prior to seeding, the coating solution was removed by inverting the plate and tapping the plate on tissue culture paper. The seeding medium consisted of RPMI-Thai supplemented with 10 µM Y (compare chapter "Cardiac differentiation of hiPSCs" for formulation). Two days after seeding, the 384-well plate was inverted and tapped on tissue culture paper to remove the cell culture medium. Next, 8 µL of RPMI-Thai supplemented with 0.5 mM of the pan-phosphodiesterase inhibitor 3-Isobutyl-1-methylxanthin (IBMX) was added and

incubated for 10 minutes at 37°C and 5% CO_2. If an inhibitor was tested, the inhibitor was preincubated in this step. To stimulate cAMP synthesis, 8 µL isoprenaline or forskolin was added at a final concentration of 10 µM to 0.01 nM and incubated for 20 minutes at 37°C and 5% CO_2. In previous experiments, cAMP production was found to saturate after 20 minutes incubation with these agonists. Thus, this incubation time guarantees the highest cAMP signal, while still allowing the detection of slower cAMP production as expected by AC5- and AC6 KO. After incubation, the cells were lysed by addition of 8 µL cAMP-d2 and 8 µL anti-cAMP-cryptate in lysis buffer. After incubation at RT for 30 minutes, the sample was excited with light of a wavelength of 337 nm and the excited light of the wavelength 665 nm 620 nm was measured using a HTRF reader (BMG, PheraStarPlus).Stocks of isoprenaline hydrochloride (Sigma, I5627-5G), forskolin (Sigma, F6886-10MG), 3-Isobutyl-1-methylxanthine (Sigma, I5879-100MG), ICI 118,551 (Tocris, 0821), CGP 20712 dihydrochloride (Tocris, 1024), ICI 118,587 (Tocris, 0950) and BAY 1232055 (internal compound) were reconstituted in dimethyl sulfoxide (DMSO, Sigma, D2650-100 mL) and stored as aliquots at -20°C. All subsequent dilutions were performed in DMSO or medium. FACS analysis ensured that only cell populations with more than 85% cardiomyocytes were used.

3.14 Statistical testing

Statistical testing was performed using the GraphPad Prism software, version 8. The software was also used for the creation of all figures. Normality was tested using the D'Agostino & Pearson normality test. An F test was performed to compare the variances of the data sets. If the data sets passed the F test and the D'Agostino & Pearson test, an unpaired two-tailed t-test was performed to verify if the results were statistically significant. If normally distributed data did not pass the F-test, Welch's correction was employed. If data were non-normally-distributed or normality could not be tested because of too small sample sizes ($n<8$), a Mann-Whitney test was employed. Comparison of three or more non-parametric datasets was performed using Kruskal-Wallis testing. For all tests, results with $p<0.05$ were considered statistically significant. All results are expressed as mean ± standard deviation (SD). *p*-values are indicated in each graph.

4 Results

4.1 Characterization of hiPSC CMs

4.1.1 Efficient cardiac induction within 7 days

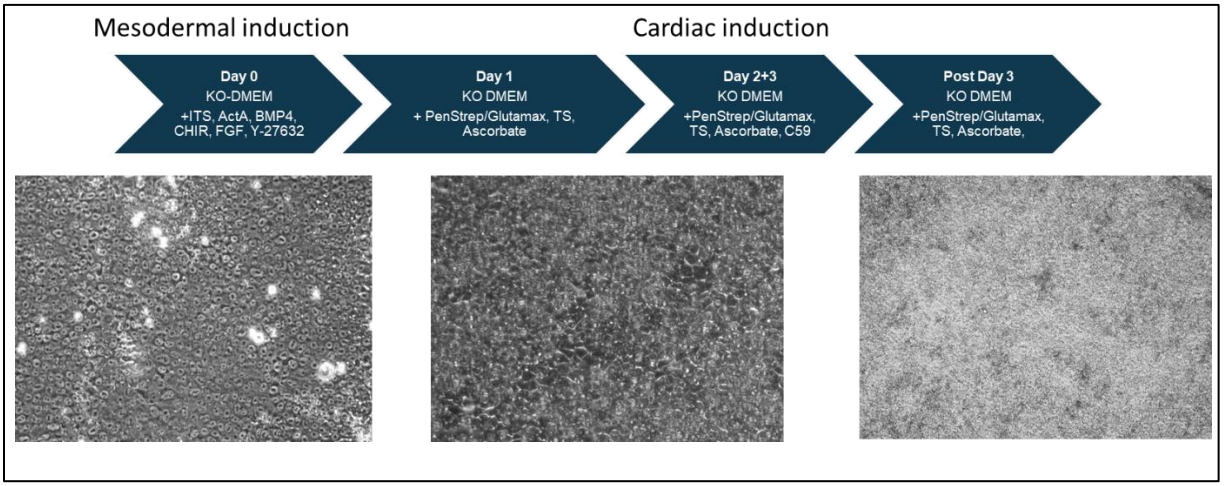

Figure 10: Time course of the cardiac differentiation protocol.
Typical morphology of hiPSCs (left), mesodermal cells (middle) and cardiac monolayer (right).

For the cardiac differentiation of the ChiPSC22 clone, a protocol was adapted from Zhang *et al.* (75). ChiPSC22 exhibited a typical hiPSC morphology before the start of the differentiation protocol (Figure 10, fish egg-like cell shape with round membranes, high nucleus/cytoplasm ratio and unclear cell to cell boundaries). According to the protocol, activation of the BMP pathway and inhibition of the Wnt pathway on day 0 of differentiation induces mesodermal induction. In fact, ChiPSC22 changed its typical hiPSC morphology swiftly to a cobblestone morphology until day 1 (angular cell shape, lower nucleus/cytoplasm ratio, very clear cell boundaries). Reportedly, this morphology is typical of mesodermal cells (internal communication). Following cardiac induction (Wnt inhibition) on day 3, cells formed a monolayer that started beating from day 7 onward. The yield of cardiomyocytes showed very high batch-to-batch variability. However, addition of activin A on day 0 of the protocol improved the cardiomyocyte yield tremendously. Throughout all differentiations of this thesis, the yield remained consistently higher than 85% cTnT positive cells on day 14. When starting the differentiation with 600.000 c/well, usually 700.000 c/well could be counted on day 14 of differentiation. Apparently, cells propagate throughout cardiac induction. Consequently, the total yield of cTnT positive cells was about 600.000 c/Well.

4.1.2 Optimization of culture conditions for stable cardiomyocyte cultures

hiPSC CMs reportedly mature during time in culture (88). Thus, the aim was to keep a stable cardiomyocyte population in culture for as long as possible. Conventional protocols maintain hiPSC CMs on Matrigel® coated surfaces and in serum-supplemented medium. To improve standardization of the protocol, defined conditions were tested. To this end, Matrigel® coating was replaced by coating with recombinantly expressed Laminin-521. A favorable side effect was that confluency of hiPSC CMs was visibly improved on the defined substrate. In addition, Laminin-521 is reported to improve maturation of hiPSC CMs (89). Removal of serum from the medium was desirable because serum occludes hypertrophic effects of compounds like isoprenaline (90). To this end, a defined mixture of nutrients, termed “Thai,” was used to replace the serum. Two different media were compared: Knockout RPMI, which contained only 0.5 mM calcium and IMDM, which contained a more physiological calcium concentration of about 2 mM. Beating behavior of hiPSC CMs did not change between the two media. When measured on day 50 of differentiation, RPMI-based formulations showed less variability in cardiomyocyte yield compared to IMDM-based formulations (Figure 11). The cardiomyocyte yield in defined conditions (RPMI Thai + Laminin) was unchanged compared to undefined conditions (Matrigel® + RPMI +2% FCS). For these reasons, RPMI Thai + Laminin was the combination used in the following experiments.

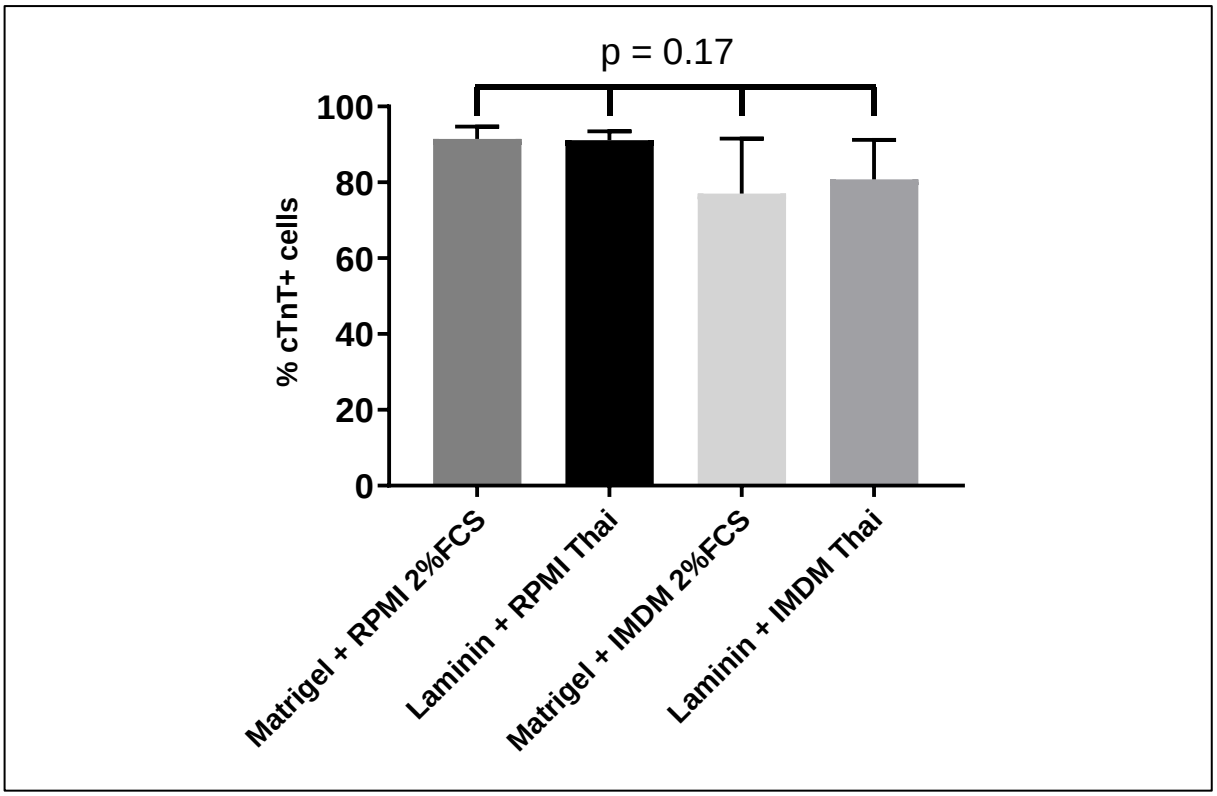

Figure 11: Yield of cTnT positive cells in defined and undefined culture conditions.
Ten days after cardiac induction, ChiPSC22 cells were plated on Matrigel® and cultured in RPMI + 2% FCS or IMDM + 2% FCS (chemically undefined conditions). Alternatively, cells were plated on Laminin-521 and cultivated in RPMI Thai and IMDM Thai (chemically defined conditions), respectively. On day 50 after cardiac induction, cells were dissociated and analyzed via FACS using an anti cTnT antibody. Data are presented as mean of three biological replicates ± SD. The *p*-value is indicated on top of the bars.

4.1.3 Strong transcriptional activation of the $G\alpha_s$-AC pathway in ChiPSC22-CMs

Next, it was interesting to assess if the cardiomyocytes express genes from the β-adrenoceptor signaling cascade. To this end, RNA was isolated at different time points of the differentiation protocol and analysed via qPCR (Figure 12). Strikingly, the expression of $G\alpha_s$ (gene name "GNAS") was much stronger compared to the expression of $G\alpha_i$ (gene name "GNAI2") or the expression of β-adrenoceptors at all time points. Interestingly, only β_2-adrenoceptor expression was detectable (gene name "ADRB2"). Expression was on a very low level and this expression increased slowly, and steadily, until day 33. Expression of $G\alpha_s$ and $G\alpha_i$ also increased in this time frame. However, $G\alpha_s$ showed a much steeper increase of expression until day 33. In animal models, overexpression of $G\alpha_s$ increases $G\alpha_s$ activity, even in the absence of β-adrenoceptor stimulation (91). In combination with the low expression of β-

adrenoceptors and the inhibitory $G\alpha_i$, this suggested that a high $G\alpha_s$-AC activity is present in ChiPSC22-derived cardiomyocytes. This $G\alpha_s$ activity might be independent of β-adrenoceptor stimulation.

A high AC activity was also in line with the expression pattern of AC5 and AC6. In the iPS state (day 0), AC5 and AC6 were expressed on a comparable level. AC6 expression increased very steeply during mesodermal and cardiac induction and peaked on day 25. In cardiomyocytes older than 30 days, the expression of AC6 decreased. In contrast, the expression of AC5 initially decreased after mesodermal induction on day 0. However, the expression increased slowly after day 7 when the first beating clusters of cardiomyocytes were visible. The strongest increase of AC5 expression appeared after day 25. To sum up, AC6 is highly expressed in early hiPSC CMs, whereas AC5 expression is highest in mature hiPSC CMs.

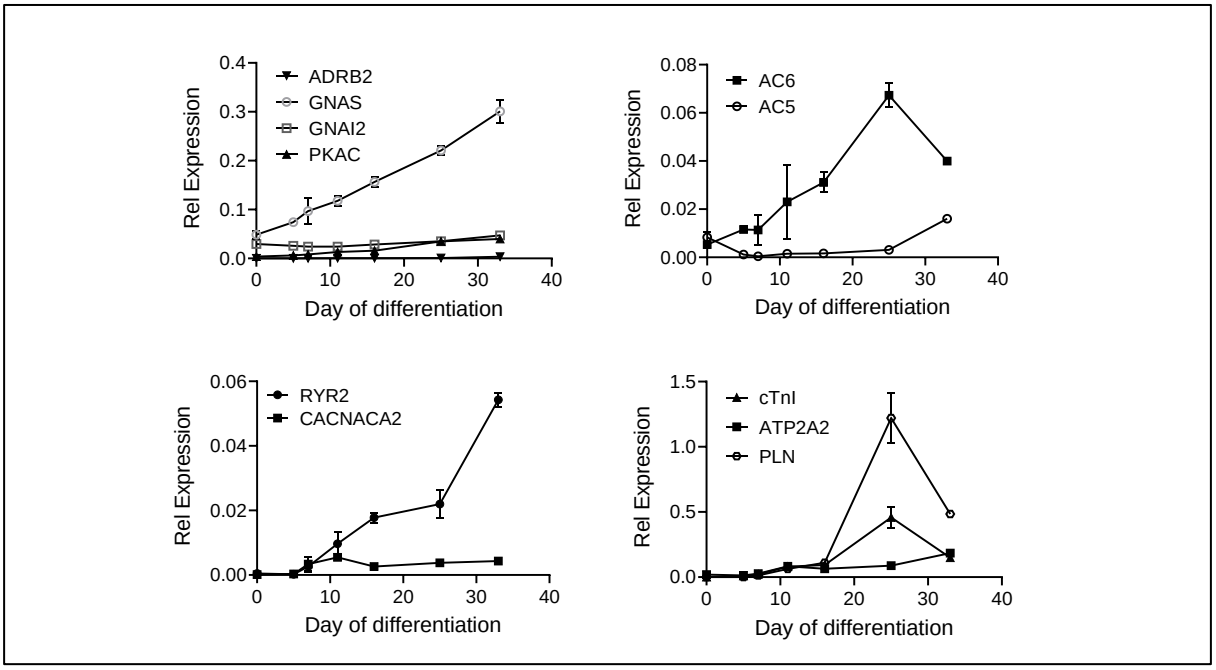

Figure 12: RNA Expression of AC signaling genes and downstream effectors throughout cardiac differentiation.
Relative expression units are normalized CT values of the gene of interest (GOI) to the CT value of the housekeeping gene RPL37A. Data are presented as mean of three biological replicates ± SD.

This expression pattern is reminiscent of old mice that develop HF. With increasing lifetime, the expression of AC6 increases and AC6 is the predominant isoform. However, with the onset of HF, AC5 expression is reactivated (47, 48). The time point when expression of AC6 switches to AC5 (day 25 to day 33) was therefore particularly interesting.

The RNA of AC downstream effectors PKA (gene name PKAC), RYR2, SERCA2a (gene name ATP2A2) and L-type calcium channel (gene name CACNACA2) all increased throughout development until day 33. Interestingly, cTnI and PLN were an exception to this rule. The expression of these genes increased steadily until day 15, followed by strong induction until day 25. Following day 25, the expression decreased sharply. With this, the expression pattern was reminiscent to AC6 expression. It was conceivable that AC6 induces the expression of AC5 and its downstream effectors cTnI and PLN. In fact, analysis of the promotor region of PLN and AC6 revealed CREB motifs. However, stimulation of hiPS CMs on day 25 with isoprenaline did not change the expression of PLN, cTnI, AC5 and AC6 significantly (data not shown).

To sum up, AC5 and AC6 are both expressed at comparable levels on day 33. The expression of all AC-pathway genes is highest on this day or has already reached its maximum. Immunostaining of hiPS-CMs on day 33 revealed that important contractile proteins like cTnT and F-actin are also present on this day (Figure 13). Contractile filaments appeared to be rather unaligned. Most importantly, hiPSC CMs have developed cell-to-cell contacts via N-cadherin. This suggested that functional mechanotransduction takes place in these cells (92). A functional syncytium was a prerequisite to measure calcium transients in a monolayer format. For this reason, it was decided to concentrate the future experiments on hiPSC CMs that are at least 33 days old.

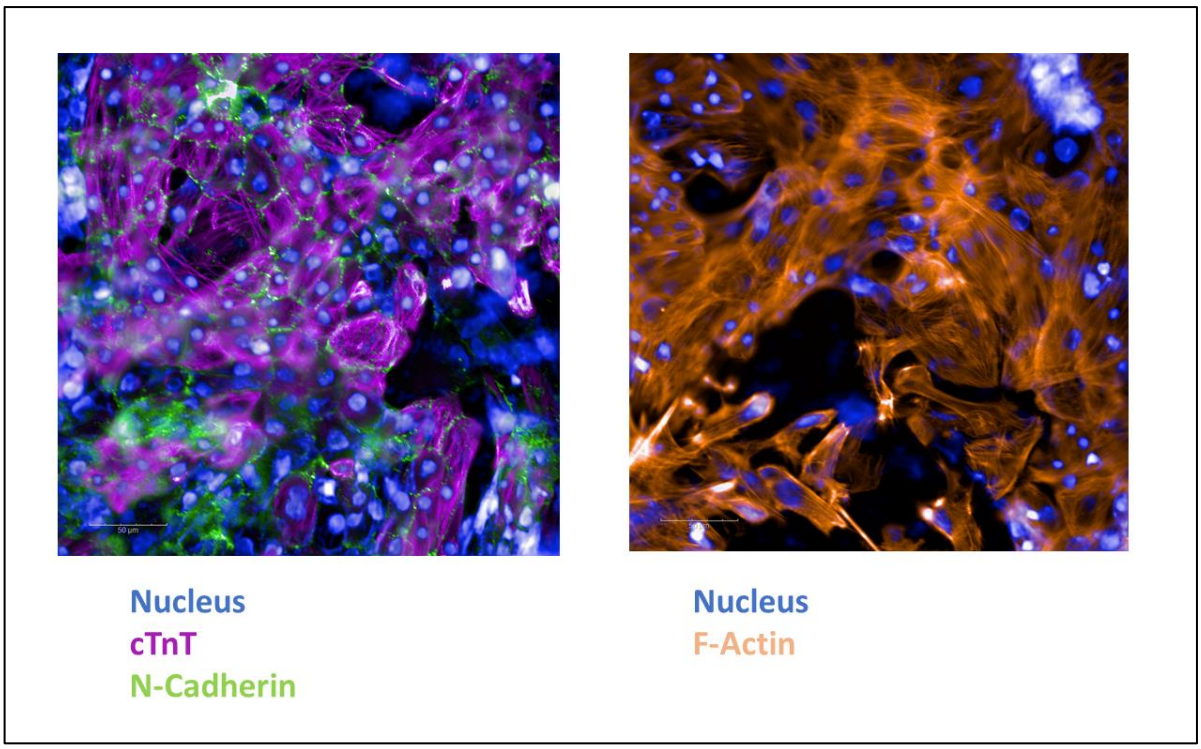

Figure 13: Immunostaining of contractile proteins in hiPSC-CMS on day 33 of differentiation. Cells were fixed with paraformaldehyde. Contractile proteins were stained with a primary IgG antibody for cTnT, N-cadherin or F-actin and a secondary fluorophore-coupled antibody. Nuclei were detected using digital phase contrast.

4.1.4 Atypical calcium handling in ChiPSC22-derived CMs

The previous experiment showed that genes involved in AC signaling, calcium handling and contraction are expressed on day 33 of differentiation. The next step was to show how these factors interact in ChiPSC22-derived CMs. To this end, calcium transients were measured in spontaneously beating cells on day 33 in the presence of calcium handling inhibitors. The L-type calcium channel blocker verapamil completely inhibited calcium transients with an IC_{50} of 176 nM ± 7 nM (Figure 14). In contrast, maximal inhibition with ryanodine (10 µM) only reduced calcium transient amplitude to about 69%. Interestingly, 30 µM 2-APB also reduced calcium transient amplitude to about 70%. This compound activates inositol trisphosphate receptors (IP_3 receptors) at concentrations below 10 µM and inhibits these receptors at concentrations higher than 10 µM. Inhibition and activation of different types of transient receptor potential channels (TRPC) was also reported (information from supplier). This result suggested that intracellular calcium stores account for only a small portion of the calcium transient in ChiPSC22-derived cardiomyocytes. In this respect, the cells were reminiscent of cardiomyocytes from the failing heart (93). The complete inhibition of the calcium

transient by 1 µM verapamil suggested that the calcium transient is completely dependent on the activity of L-type calcium channels. This would support the model of calcium-induced calcium release. According to this notion, intracellular calcium stores are only activated following L-type calcium channel opening. However, the complete block of calcium transients by 1 µM verapamil could also be explained by inhibition of action potentials by unselective inhibition of TRP- or potassium channels.

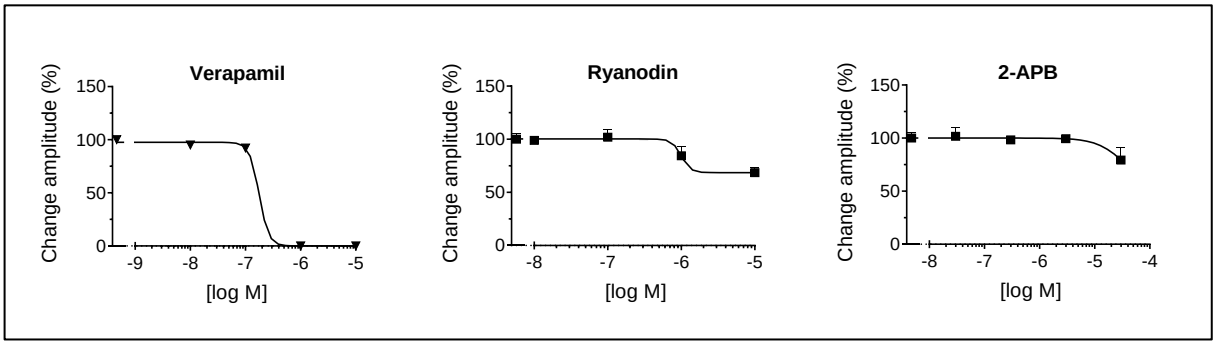

Figure 14: Contribution of the L-type calcium channel (inhibition with verapamil), RYR2 (inhibition with ryanodine) and IP_3 receptors (inhibition with 2-APB) to the calcium transient amplitude.
ChiPSC22-derived cardiomyocytes were loaded with calcium 6 dye on day 33 of differentiation. Fluorescence increases were recorded before and after compound addition at 37°C in spontaneously beating cells. Calcium transient parameters were calculated using KinEva. Results are expressed as the change of the calcium transient parameter after compound addition. Data are presented as mean of three biological replicates ± SD.

Next, calcium transient kinetics (PWD90, decay and time to peak) were assessed, which reflect the function of SERCA and NCX. SERCA terminates calcium transients by the reuptake of calcium to the SR. In contrast, NCX shifts calcium between the extracellular space and mitochondria and between the extracellular space and the cytosol (4). Inhibition of SERCA with thapsigargin increased PWD90 of the calcium transient in a concentration-dependent manner (IC_{50}: 280 ± 9 nM, Figure 15). Maximal inhibition increased the PWD90 to about 144%. The increased PWD90 was a result of both increased calcium decay (191% increase at 10 µM) and increased time to peak (143% increase at 10 µM). Such a strong modulation of the calcium transient kinetics by SERCA inhibition was surprising, given that intracellular calcium stores only accounted for about 30% of the calcium transient. An overactive state of SERCA would explain the strong effect of SERCA inhibition. Under physiological situations, SERCA is regulated by PLN (94). Even though PLN was detectable on the RNA level, no protein could be detected. Thus SERCA might be disinhibited due to absence of

inhibitory PLN, resulting in an overactive state of SERCA in ChiPSC22-derived cardiomyocytes. Application of the NCX-inhibitor SEA 0400 also affected PWD90 decay and time to peak. However, there was no consistent concentration dependency detectable (data not shown). This might be a result of the bimodal function of NCX. NCX can either act in the forward mode or in the reverse mode (95). Inhibition of both the forward mode and the reverse mode might counterbalance each other. Neither thapsigargin nor SEA 0400 application completely abolished calcium transients under baseline or paced conditions. Overall, it appears that calcium cycling from intracellular stores to the cytosol is fairly independent from calcium cycling between the extracellular space and the cytosol. Apparently, the model of calcium-induced calcium release does not completely apply in this cell type.

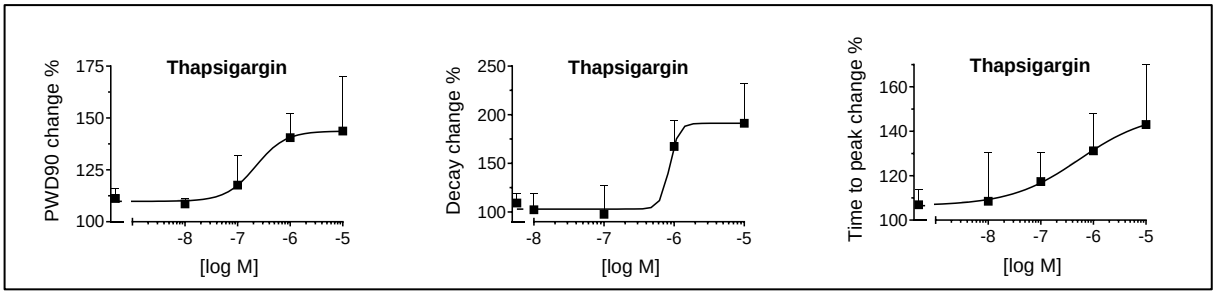

Figure 15: Modulation of calcium kinetic parameters by SERCA-inhibitor thapsigargin.
ChiPSC22-derived cardiomyocytes were loaded with calcium 6 dye on day 33 of differentiation. Fluorescence increases were recorded before and after compound addition at 37°C in spontaneously beating cells. Calcium transient parameters were calculated using KinEva. Results are expressed as the change of the calcium transient parameter after compound addition. Data are presented as means of three biological replicates ± SD.

hiPSC CMs showed automaticity. The mean rate of calcium transients was about 12 transients per minute. However, the range of this parameter was extremely high between a minimum of two beats per minute and a maximum of 16 beats per minute (detailed description in Figure 36).

This variability even occurred over plates seeded with the same batch of differentiation. This result suggested the presence of pacemaker cells in the culture. If the fraction of these cells is very small, uneven distribution of these cells in the different wells of one plate could explain uneven automaticity. In fact, application of the HCN-channel inhibitor ivabradine reduced the frequency of spontaneous occurring calcium transients

in concentration dependent manner with an IC_{50} value of 0.83 ± 0.28 µM (Figure 16). Spontaneous transients completely disappeared upon maximal inhibition with 10 µM ivabradine. Interestingly, calcium transient frequency was also influenced by both verapamil and 2-APB. However, there was no clear concentration dependency of their effects (data not shown). These results suggested that the automaticity of these hiPSC CMs is primarily caused by a fraction of cells expressing functional HCN channels. A high density of HCN channels is typical of sinus node pacemaker cells (37). Thus a fraction of the hiPSC CM culture likely differentiated into this cell type. L-type calcium channels and IP_3 receptors contribute to spontaneous calcium transients.

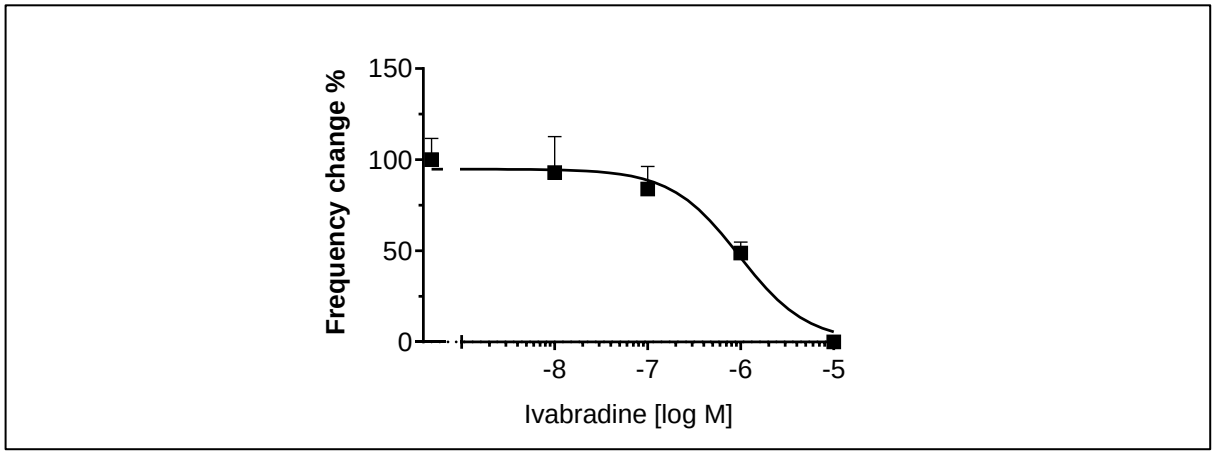

Figure 16: Modulation of spontaneous calcium transient frequency by the HCN-channel inhibitor Ivabradine.
ChiPSC22-derived cardiomyocytes were loaded with calcium 6 dye on day 33 of differentiation. Fluorescence increases were recorded before and after compound addition at 37°C in spontaneously beating cells. Calcium transient parameters were calculated using KinEva. Results are expressed as the change of the calcium transient parameter after compound addition. Data are presented as mean of three biological replicates ± SD.

Next, spontaneous calcium transients were compared to calcium transients stimulated by electrical stimulation (Figure 17). When applying an electrical current with a frequency of 0.5 Hz, calcium transient frequency swiftly increased to 0.5 Hz. This result suggests that calcium transients follow electrical stimuli 1:1. It also suggests that the spontaneous activity of pacemaker cells is overdriven by electrical stimuli. This result was expected because the stimulation frequency was higher than the spontaneous frequency of the calcium transients. No extra peaks occurred between the transients evoked by electrical stimulation. Increasing the pacing frequency to 0.75 Hz resulted in shoulders during calcium decay. These shoulders were situated at the position of each second pacing stimulus. Presumably, cytosolic calcium transients did not return

to the normal diastolic calcium level before the next pacing step. The new pacing step increased this intermediate calcium level by further calcium influx. In the fluorescent readout, this phenomenon would cause the observed shoulder. In many cases, the intermediate calcium level decreased after about 8 seconds of pacing. This resulted in uninterrupted calcium transients that followed the pacing stimulus. Apparently, the cardiomyocytes have the ability to adapt to the new pacing frequency. In other cases, the intermediate calcium level reappeared at every second pacing step, making quantification of calcium transients at this frequency impossible. The effect was even more prominent when increasing the pacing frequency to 1 Hz. In this case, it seemed like two calcium transients were fused. These observations were made in most differentiations. However, some batches were able to follow the pacing frequency without developing calcium transient shoulders. These differentiations could even be paced up to 2 Hz until calcium transient shoulders occurred (data not shown). Experiments using cardiomyocytes older than day 33 exhibited the same phenotype. This suggests that the maturity of cardiomyocytes on day 33 is rather variable. This would also explain the endogenous variability observed in this readout (see also Figure 36).

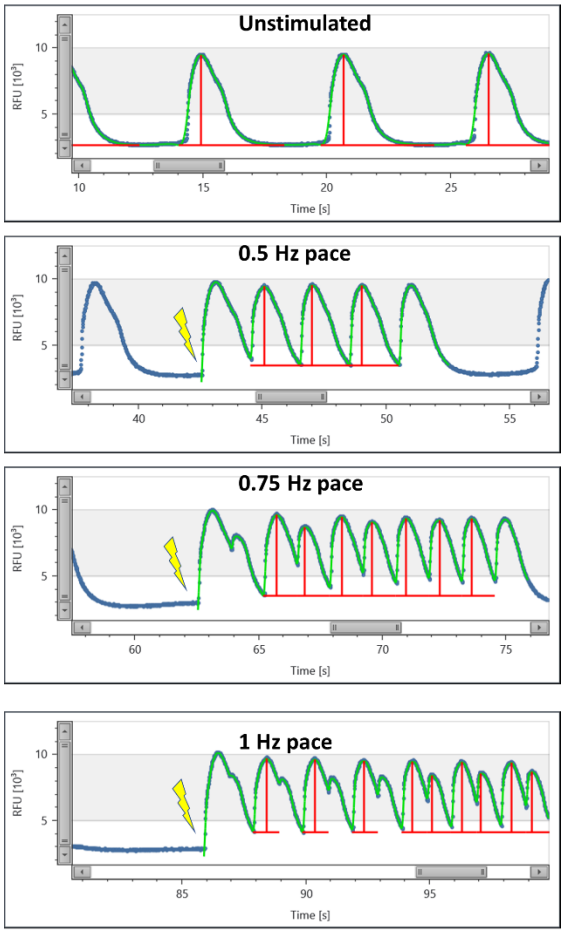

Figure 17: Calcium transients of resting hiPSC CMs or electrically stimulated (0.5-1.0 Hz) hiPSC CMs.
ChiPSC22-derived cardiomyocytes were loaded with calcium 6 dye on day 33 of differentiation. Fluorescence increases were recorded at 37°C under no stimulation or under electrical pacing with 0.5-1.0 Hz. The onset of pacing is marked by a flash. The green part of the fluorescence curve marks the duration of the pacing step. Red lines mark peaks atuomatically detected by the software.

Interrupted calcium transients were reminiscent of cardiomyocytes from HF patients (96, 97). Another hallmark of HF is a negative force-frequency relationship (98). This is caused by lower calcium transient amplitudes and accumulating diastolic calcium levels at high pacing frequency (96). Interestingly, ChiPSC22-derived cardiomyocytes exhibited a negative force-frequency relationship. As aforementioned, the PWD90 was too long for efficient pacing at higher frequencies. In addition, calcium transient amplitude decreased with increasing pacing frequencies (Figure 18), along with an increase in diastolic calcium levels. Actual mechanical force was not measured during this PhD thesis. In default of a better term, the frequency dependent reduction in the

calcium transient amplitude will be termed “negative force-frequency relationship” henceforth. The reader be aware that in this PhD thesis, the term only refers to the calcium transient aspect of this well-established phenomenon.

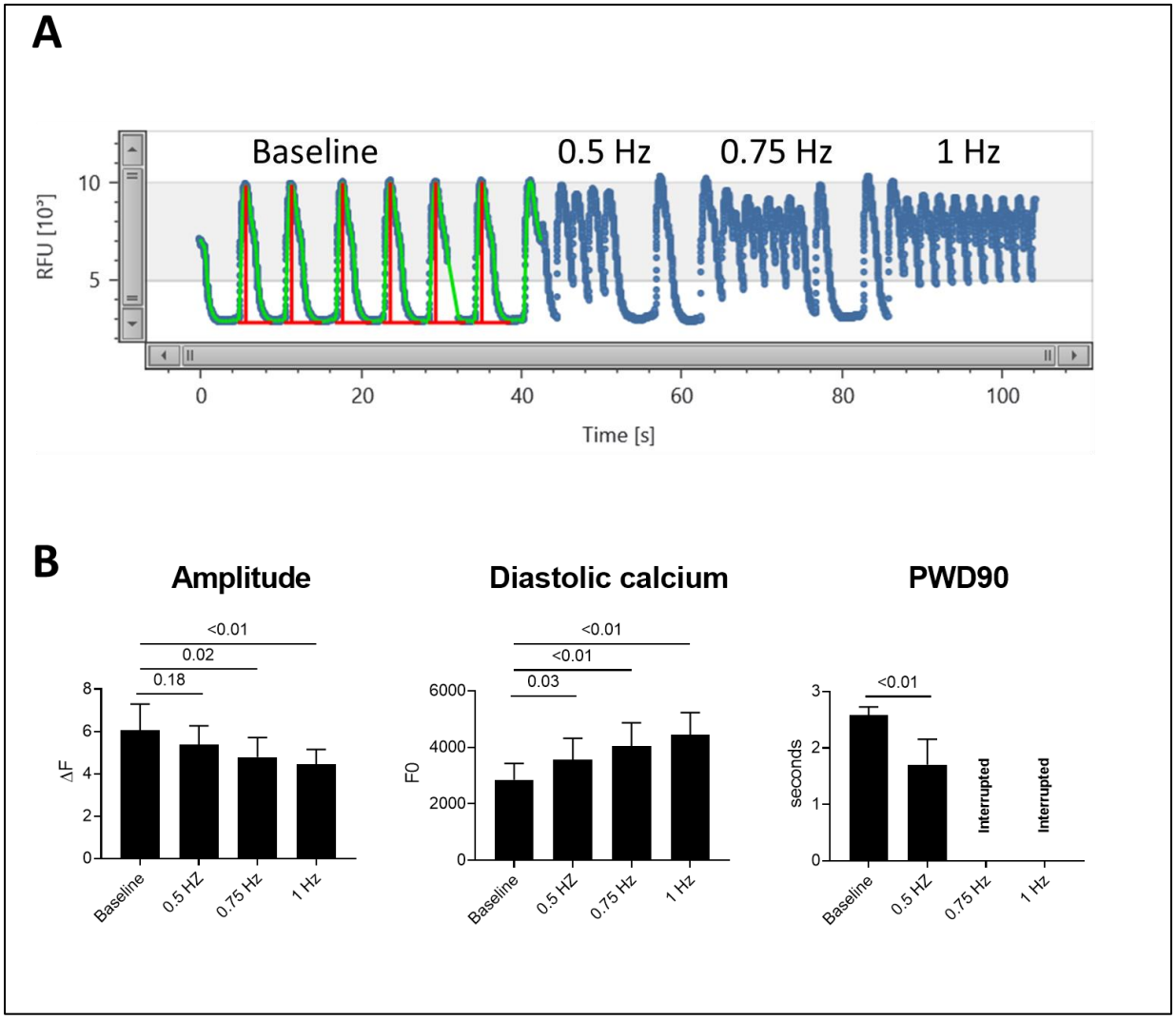

Figure 18: Negative force-frequency relationship in ChiPSC22-derived CMs.
A: Representative recording. B: Quantification of three biological replicates ± SD. ChiPSC22-derived cardiomyocytes were loaded with calcium 6 dye on day 33 of differentiation. Fluorescence increases were recorded at 37°C under resting conditions or under electrical stimulation with 0.5-1.0 Hz. Calcium transient parameters were calculated using KinEva. Data are presented as mean of ten biological replicates ± SD. *p*-values are indicated on top of the bars.

Another parallel to the pathology of HF became obvious when treating the ChiPSC22-derived cardiomyocytes with isoprenaline. Stimulation with isoprenaline did not increase the amplitude of the calcium transient (Figure 19). In contrast, cells responded with an increase of calcium transient frequency to about 150% and a decrease of the PWD90 to about 75%. Addition of the β_2-selecitve inverse agonist ICI 118,551 (1 nM) abolished the effect of isoprenaline on calcium transient frequency and PWD90.

Exclusive signaling via the β_2-adrenoceptor was also verified in subsequent experiments (Figure 33). In HF, the chronic activation of the SNS leads to an increase of the β_2/β_1-adrenoceptor ratio in the ventricle (99, 100). In the failing heart, impaired contractility is compensated by tachycardia (7).

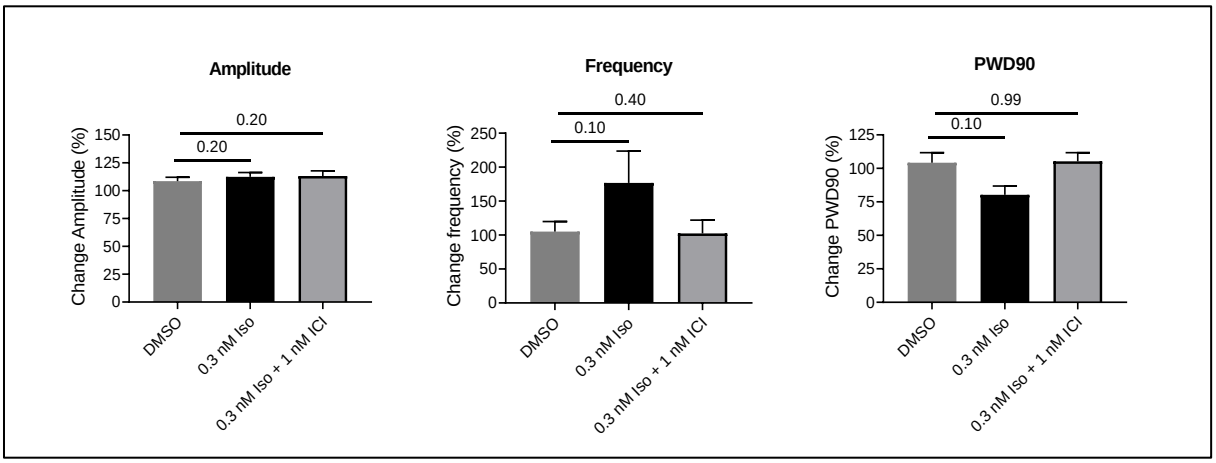

Figure 19: Change of calcium transient parameters upon stimulation with isoprenaline in the absence or presence of the β_2-selective agonist ICI 118,551.
Data are presented as mean of three biological replicates ± SD. *p*-values are indicated on top of the bars.

4.2 Generation of AC5- and AC6 knockout hiPSCs

4.2.1 In silico knockout of AC5 and AC6

The characterization of ChiPSC22-derived cardiomyocytes suggests that the cell line shares many features of cardiomyocytes from HF patients (disturbed calcium-induced calcium release, slow calcium transients, a negative force-frequency relationship, fused calcium transients at high frequencies and small intracellular calcium stores). As in cardiomyocytes from failing hearts, there is an elimination of a positive inotropic effect of β-adrenoceptor agonists and a low expression of β-adrenoceptors. Later experiments also show that ChiPSC22 exhibits expression of natriuretic peptide B (NPPB) and natriuretic peptide A (NPPA). Expression of this fetal gene pattern is a marker of hypertrophy in the failing heart (101, 102).

Interestingly, these effects occur while AC6 expression is dominant. At around day 25 of differentiation, a turning point, AC6 expression declines and AC5 expression

increases. This expression pattern is reminiscent of old mice that develop HF upon pressure overload left ventricular hypertrophy (48). These observations led to the hypothesis that AC6 or AC5 activity could be causative and/or symptomatic of the HF-mimicking state of hiPSC CMs. Knockout of these genes might rescue this phenotype.

The strategy for a functional knockout of AC5 and AC6 was to abolish the catalytical activity of the enzymes. In both enzymes, the C1 and C2 domain dimerize to form a catalytical cleft around the substrate ATP (Figure 20). Both the C1 and C2 domain must be present to form a catalytically active enzyme (103-105). Only few amino acids from the C1 domain directly interact with ATP. Removal of these amino acids by CRISPR editing should disrupt the interaction of the C1 domain with ATP. This should result in a catalytically inactive enzyme.

According to the National Center for Biotechnology Information (NCBI) databank, the AC5 gene transcribes two reviewed, protein coding isoforms NM_183357 (ENSEMBL ID: ENST00000462833.5) and NM_001199642.1 (ENSEMBL ID: ENST00000309879.9). The strategy for a functional AC5 KO was to remove exon 4 of both isoforms (CATCCTGTTTGCTGACATCGAGGGCTTCACCAGCCTGGCGTCCCAGTGCACTG CACAGGAACTGGTCATGACCCTCAACGAGCTCTTCGCCCGCTTTGACAAGCTG GCCGCA). Deletion of this exon removes amino acid 394 to 430 and leads to missense translation from amino acid 431 to 463. These two regions comprise all but one amino acid from the C1-part of the catalytic domain. The eliminated amino acids have multiple roles in the enzymatic reaction: Leu440 and Gly441 interact with the nucleobase. Asp438, Iso439 and Asp442 bind metal ions. Gly401, Phe402 and Thr403 bind to triphosphate. Phe396 and Tyr445 bind bicarbonate. Thr403, Ala411, Gln412, Leu418, Asp419, Phe421, Asp426, Arg434, Lys438 and Ile439 form interactions between the C1 and C2 domain (106). Because many different steps of the enzymatic reactions cannot take place without these amino acids, removal of these amino acids will most likely result in a non-functional protein. In addition, the missense translation leads to a premature stop codon at amino acid 470. Thus, all amino acids C-terminal of amino acid 470 will not be transcribed. This would affect the whole C2 domain. Figure 21 shows a predicted model of the catalytic domain after exon 4 removal.

There is a very small chance for translation of an alternative protein from the CRISPR-edited locus. Deletion of exon 4 may also create a theoretical new open reading frame,

starting at amino acid 464. Translation of this open reading frame is unlikely because of the lack of a ribosomal binding site. The hypothetical truncated protein would contain some amino acids of the C1 domain that form the C1-C2 interface. However, Arg486 would be the only remaining residue of the C1 domain that interacts with the substrate ATP. Thus, only the C2 domain of this theoretical protein would be intact. It is extensively published that monomers or homodimers of C1 and C2 are non-functional. Only C1-C2 heterodimers are catalytically active (103-105). Thus, regardless of the type of protein translated, a functional knockout of AC5 by exon 4 deletion is guaranteed.

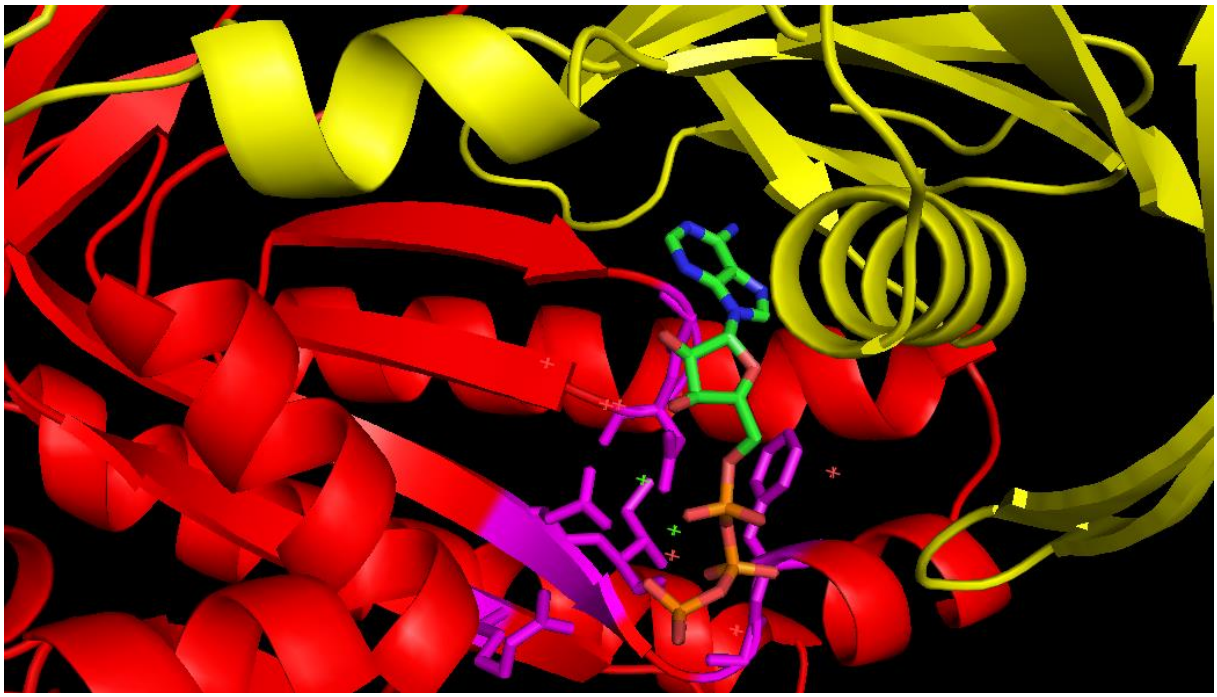

Figure 20: AC catalytic site.
The C1 domain (red) and the C2 domain (yellow) of ACs form the catalytic site around the substrate adenosine triphosphate (green/orange). C1 domain amino acids that interact with ATP are depicted in magenta. X-Ray Crystal structure of C1 domain from *Canis Lupus familiaris* and the C2 domain from *Rattus norvegicus*. (PDB: 3C16). Software: Pymol.

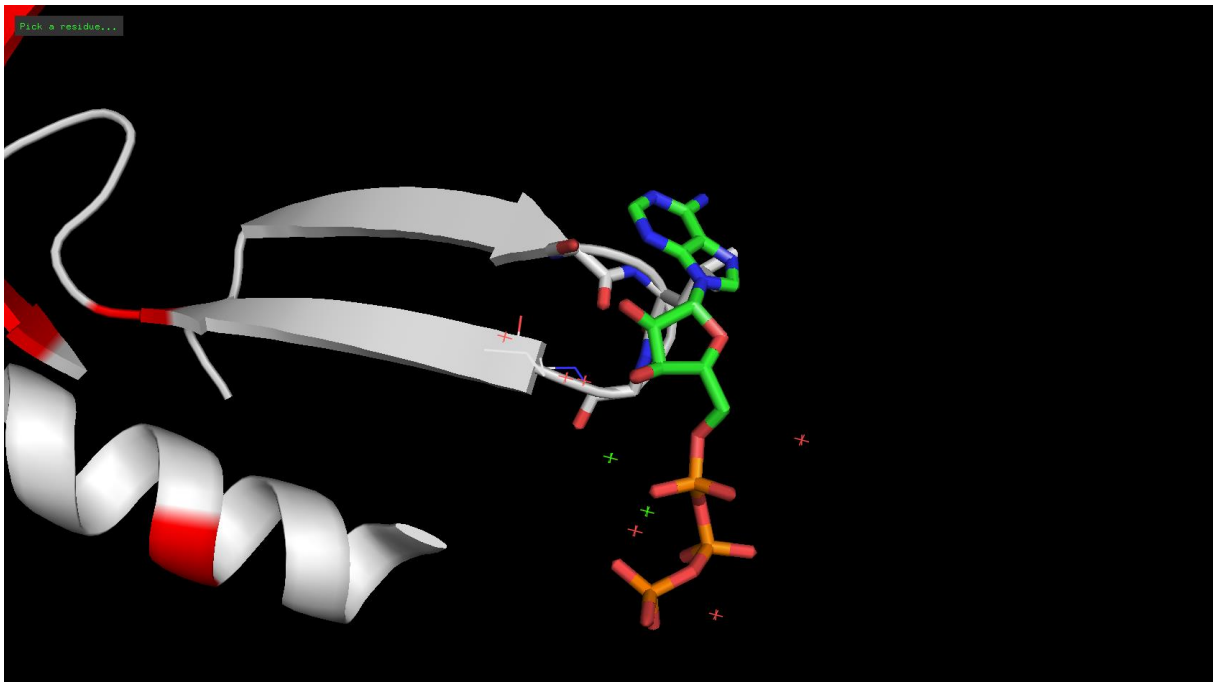

Figure 21: Disruption of the AC5 catalytic domain by exon 4 deletion.
After exon 4 removal, the complete C2 domain is absent due to a premature stop codon. No residues of the original C1 domain (red) contribute to ATP binding. The majority of the C1 domain is mutated due to missense translation (grey) and can only interact with ATP (green/orange) in a very restricted manner and with steric hindrances. In silico mutation of the protein data bank entry 3C16 was performed with Pymol.

AC5 and AC6 are highly conserved proteins. Therefore, an analogous strategy was used for the generation of an AC6 functional knockout. However, different exons encode the C1 part of the catalytic domain. To achieve a similar knockout, exon 3-5 must be deleted in the AC6 locus. This leads to a functional deletion of the C1 domain in both annotated protein isoforms of AC6 (Uniprot IDs O43306-1 and O43306-2).

The intronic sequences GCGTAGACAGGAGCACATCT and ATGCGGACCCCTAGACTCCC were identified as specific gRNA sites for exon 3-5 removal in the AC6 locus. In the AC5 locus, the intronic sequences CAAAGATTCAGCCTATAGCA and AGTGAGTCACCCTGAGCCGG were identified as specific gRNA sites for deletion of exon 4. The open source software Benchling was used to design the specific gRNAs and high efficiency was verified in preliminary experiments. Only few off-target sites were predicted for these gRNAs.

4.2.2 Gene editing and isolation of putative AC5- and AC6 KO clones

For the generation of AC5- and AC6 KO clones, a limited dilution technique was used. An overview of the workflow is depicted in Figure 22. ChiPSC22 clones were electroporated with the Cas9 protein and AC5 or AC6-specific gRNAs. After 24 hours, the cells were selected by puromycin addition for 24 hours and seeded as single cells in a limited dilution. After about one week, colonies were visible and these could be expanded on six well plates after two weeks. Next, DNA was extracted and a PCR was performed using a primer pair complementary to DNA sequences up- and downstream of the CRISPR sites (PCR1). A second PCR used primer pairs that lay in between the two CRISPR sites (PCR2). A gel electrophoretic analysis of the two PCRs is shown in Figure 23 and Figure 24. PCR1 of the wild-type AC5 locus produced an amplicon of about 1.1 kb (Figure 23). From the AC5-CRISPR edited clones, clone 1, 2 and 4 exhibited an ~900 bp DNA band in the agarose gel electrophoresis. A 1.1 kb DNA band that is caused by amplification of the wild-type sequence is not visible in these samples. Deletion of exon four was expected to be ~159 bp. This difference contributes to the size difference of the wild-type 1.1 kb band and the 0.9 kb large band in the gene edited cells. These results suggest that these knockout clones carry a homozygous deletion of exon 4 of AC5. Clones that showed both the 1.1 kb and 900 bp DNA bands (i.e. clone 3 and 5) might be heterozygous clones or a polyclonal cell line. Clone 6 showed only the 1.1 kb DNA band. This clone probably had no larger deletion of the AC5 locus. The putative homologous AC5 KOs 1, 2 and 4 were also analyzed via PCR using a primer pair within the putative deletion site (PCR2). Clones 1, 2 and 4 produced no amplicon in PCR2 while the wild-type cells produced a PCR product of ~600 bp. This experiment suggested that clone 1, 2 and 4 carry a homozygous deletion on the AC5 locus.

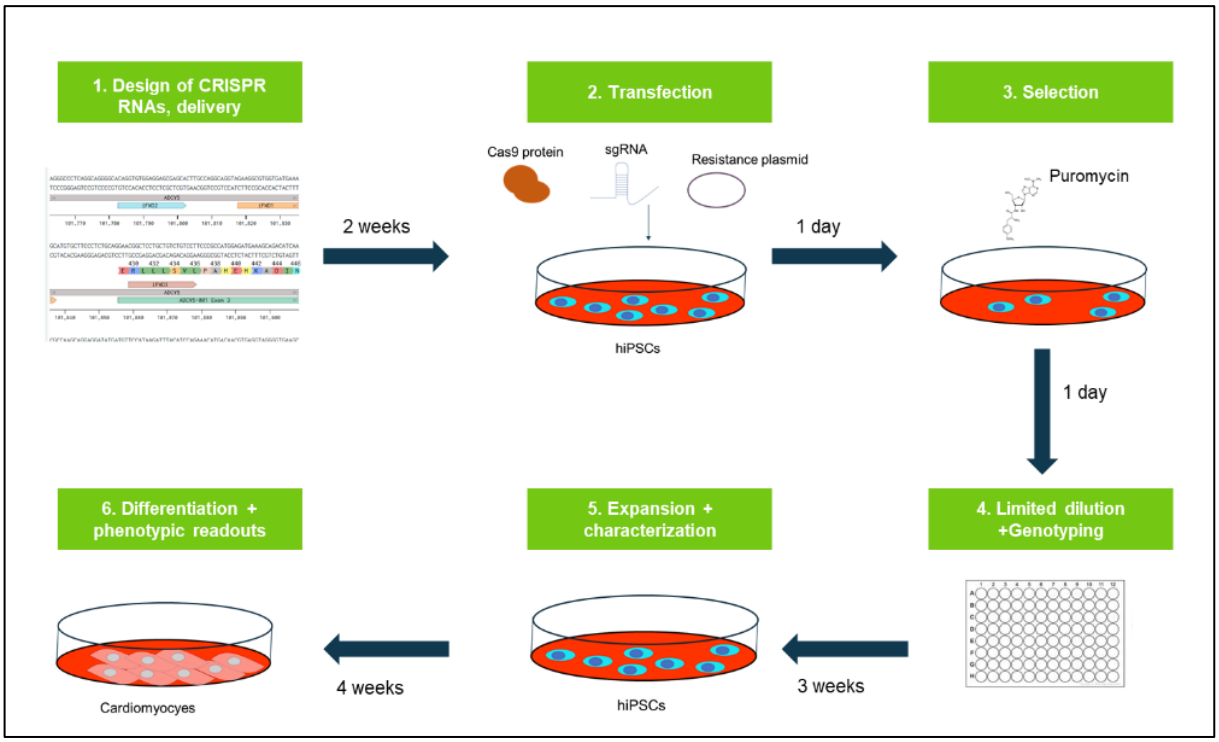

Figure 22: Workflow for the generation and characterization of AC5- and AC6 KO cardiomyocytes.

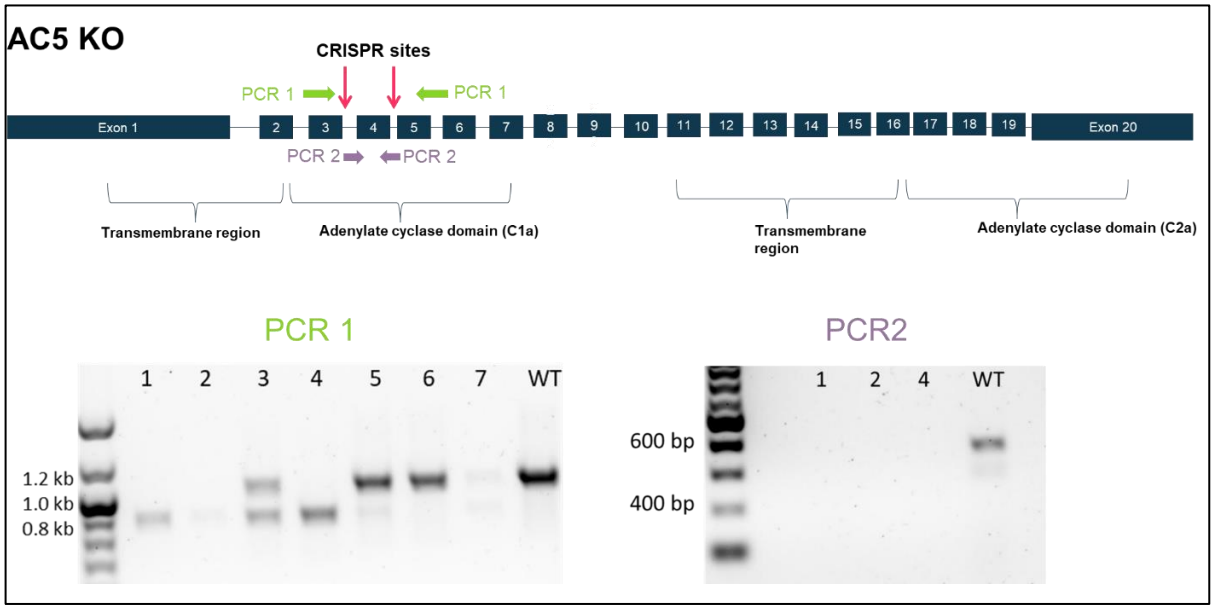

Figure 23: Genotyping of wild-type (WT) and putative AC5 KO clones (1-7) with primers up- and downstream of the putative deletion site (PCR1) or with primers within the putative deletion site (PCR2).

A puromycin-resistance plasmid, AC5-specific guide RNAs and Cas9 protein were introduced into ChiPSC22 cells via electroporation. After a 24-hour treatment with puromycin and a 48-hour recovery, the cells were seeded as a limited dilution on 96 well plates. After three weeks, DNA was extracted and analyzed by PCR using AC5 specific primers. An agarose gel electrophoresis is depicted.

A similar pattern was visible when analyzing ChiPSC22 clones that were submitted to CRISPR-editing of the AC6 locus: Clone D5, D6 and E6B only exhibited a DNA band of ~500 bp in PCR1 (Figure 24). In contrast, amplification of AC6 from wild-type samples yielded a PCR product of ~1.5 kb. The difference of 1 kb corresponded well to the expected size of exon 3-5 deletion (932 bp). Most presumably, these clones carry a bi-allelic deletion in the AC6 locus. Clone E6 exhibited both a DNA band of 1.5 kb and 500 bp. This indicates that this clone has one allele with a deletion in the AC6 locus and one allele without a large deletion. These results were confirmed using PCR2 with primer pairs complementary to sequences within the putative CRISPR sites. In this PCR, clone D5, D6 and E6B showed no amplicon. The wild-type sample produced an amplicon of ~500 bp. Clone E6 showed this amplicon as well. These results are strong evidence that clone D5, D6 and E6B carry homozygous deletions of the AC6 locus and clone E6 carries a heterozygous deletion. The corresponding DNA samples were collected three weeks after limited dilution and immediately before freezing the cells. Thus, these experiments showed that the homozygous deletions of AC5 and AC6 deletion are stable over at least three weeks in culture.

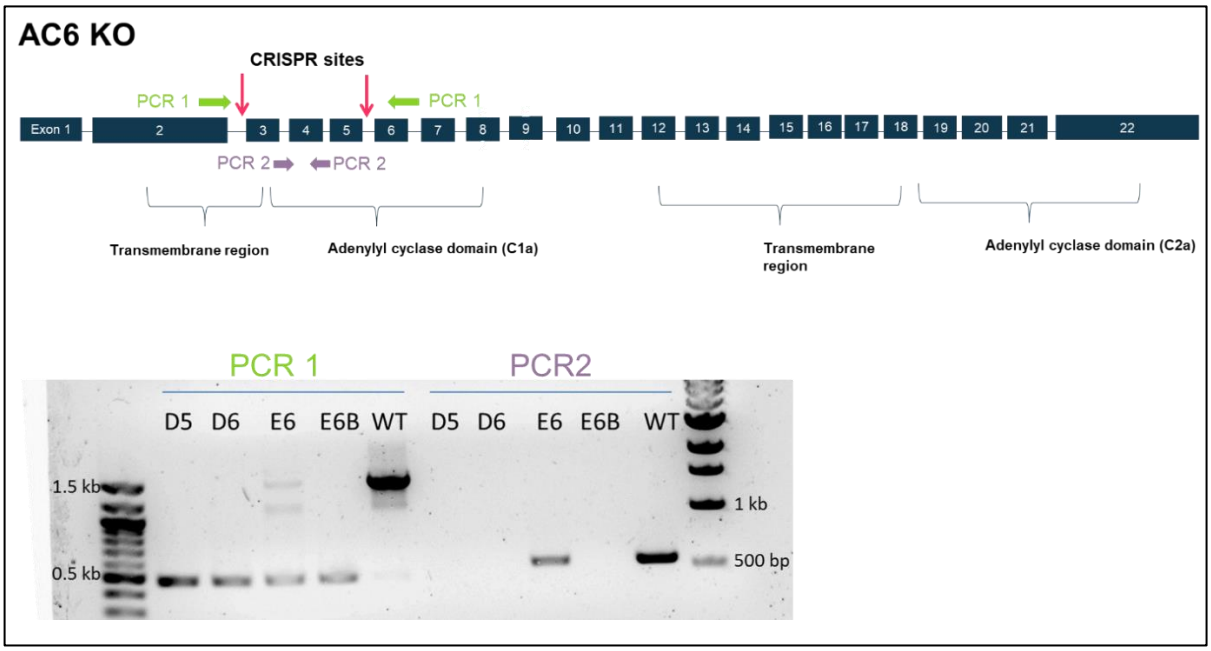

Figure 24: Genotyping of wild-type (WT) and putative AC6 KO clones (D5, D6, E6, E6B) with primers up- and downstream of the putative deletion site (PCR1) or with primers within the putative deletion site (PCR2).
A puromycin-resistance plasmid, AC6-specific guide RNAs and Cas9 protein were introduced into ChiPSC22 cells via electroporation. After a 24-hour treatment with puromycin and a 48-hour recovery, the cells were seeded as a limited dilution on 96 well plates. After three weeks, DNA was extracted and analyzed by PCR using AC6 specific primers. An agarose gel electrophoresis is depicted.

4.2.3 Sequencing of putative AC5- and AC6 KO clone DNA

In the next steps, clones that showed an apparent CRISPR deletion were sequenced. To this end, the PCR using primer pairs upstream and downstream of the deletion site was repeated with a high-fidelity DNA polymerase. In addition, primer pairs were modified so they contained homologous arms complementary to a pCI plasmid. The pCI recipient plasmid was digested with the enzyme NotI and gel purified. The PCR was also gel purified. Both the PCR and the digested plasmid were combined in a sequence and ligation independent cloning reaction (SLIC) and were transformed into *E.coli*. The bacteria insert the PCR fragment into the plasmid by homologous recombination (107). Propagation of the bacterial strain overnight allowed amplification of the plasmid. The plasmid was extracted and submitted to DNA sequencing. Next, the DNA sequences from the AC5 KO and AC6 KO clones were aligned to the wild-type sequence (Figure 25). Alignment of the sequences showed that the DNA sequence between the predicted CRISPR sites was missing in the KO clones. Apparently, gene editing occurred exactly at the predicted CRISPR site (3 base pairs upstream of the 3' end of the gRNA binding site) and the double editing led to a complete deletion of the DNA sequence between both CRISPR sites.

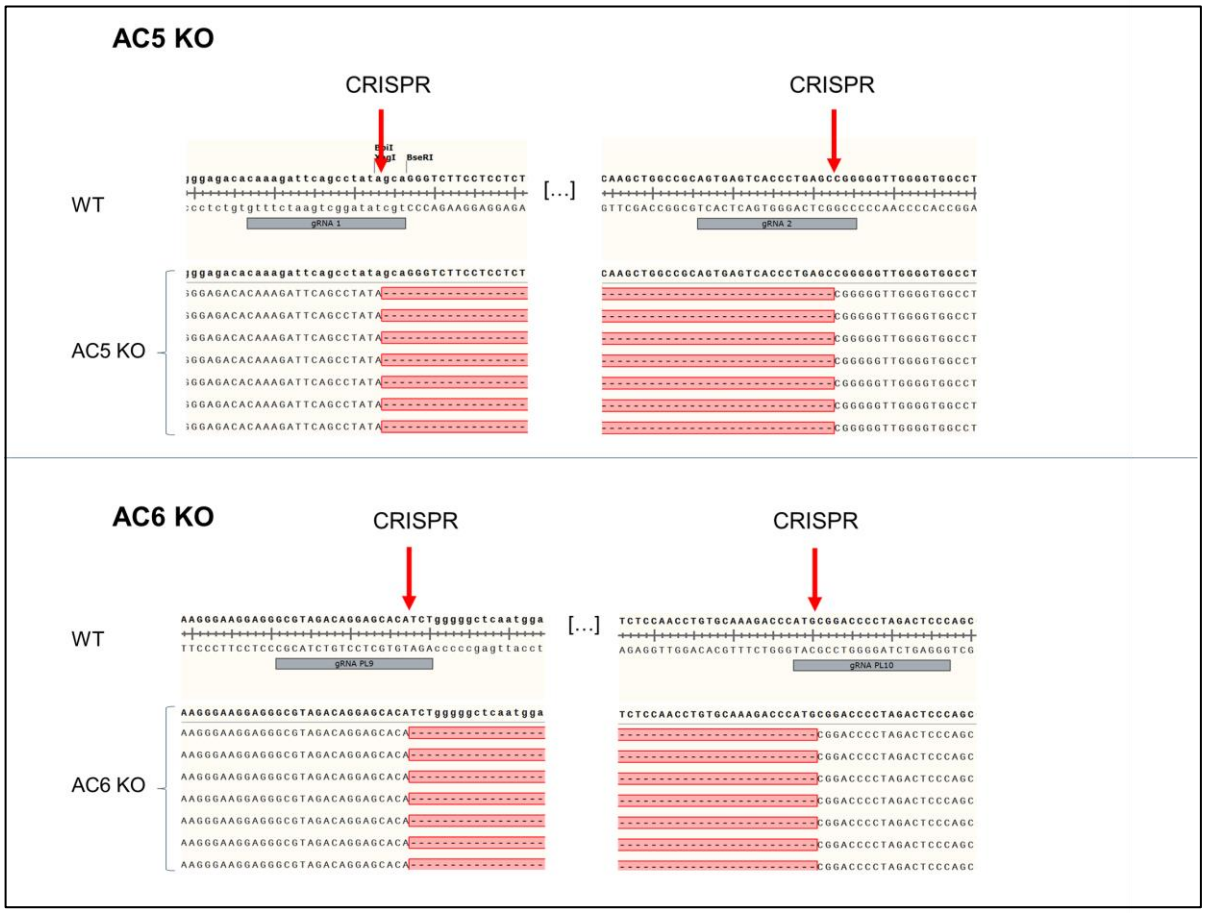

Figure 25: Alignment of AC5- and AC6 alleles from wild-type (WT) and from an exemplary AC5 KO clone and from an exemplary AC6 KO clone.
Binding sites of the gRNAs are indicated in the wild-type sequence (grey). Arrows indicate the predicted CRISPR sites.

4.2.4 Sequencing of putative AC5- and AC6 KO clone cDNA

The previous result was proof that the AC locus was deleted in the predicted manner. However, it could have been possible that cells circumvent the deletion via alternative splicing on the RNA level. Therefore, it was important to show that the CRISPR deletion is also present on the RNA level. To this end, RNA was extracted from knockout clones and reverse transcribed. The resulting complementary DNA (cDNA) was then submitted to the aforementioned sequencing workflow. Alignment of the AC5 KO clone cDNA to the wild-type sequence showed that the exon 4 sequence of AC5 is missing in the AC5 KO clone (Figure 26). Alignment of the AC6 KO clone to the wild-type sequence showed that the sequences of exon 3, 4 and 5 of AC6 is missing in the AC6 KO clone. This experiment was final proof that CRISPR editing led to the predicted deletion on a transcriptional level. The deleted sequences encode the amino acids

necessary for catalytic activity of ACs. Therefore, it is very certain that the catalytic activity of AC5 or AC6 is eliminated in these KO clones.

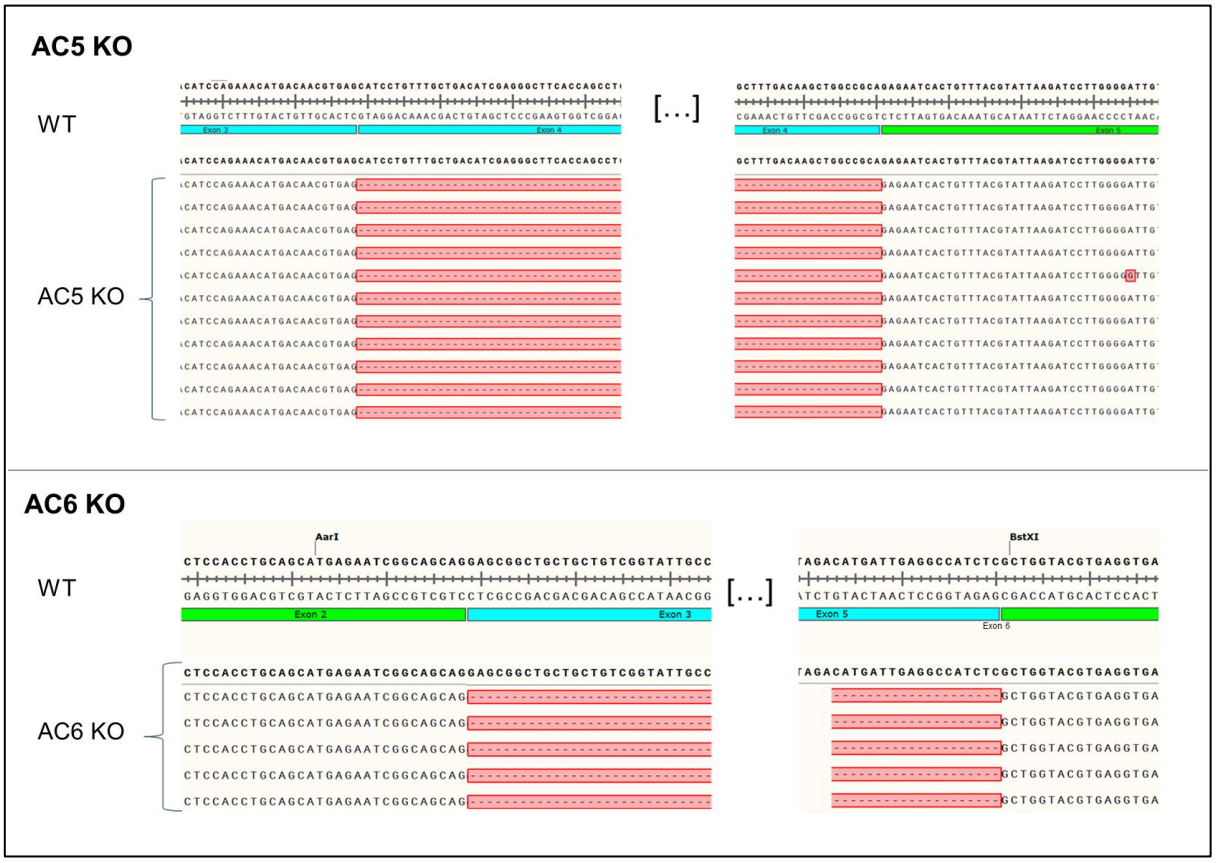

Figure 26: Alignment of AC5- and AC6 cDNA from wild-type and one exemplary AC5 KO clone and AC6 KO clone.
Exon-exon junctions are indicated below the DNA sequence in green and blue.

4.3 Functional testing of AC5- and AC6 KO clones

4.3.1 AC5- and AC6 KO clones retain pluripotency marker expression

FACS analysis revealed that the wild-type ChiPSC22 cell line exhibited permanent expression of the pluripotency marker TRA-1-60 and SSEA-4. Over 90% of the population expressed these two markers. In contrast, the expression of the early differentiation marker SSEA-1 was hardly detectable (Figure 27A). This expression pattern suggests that the wild-type ChiPSC22 cell line is in a pluripotent state.

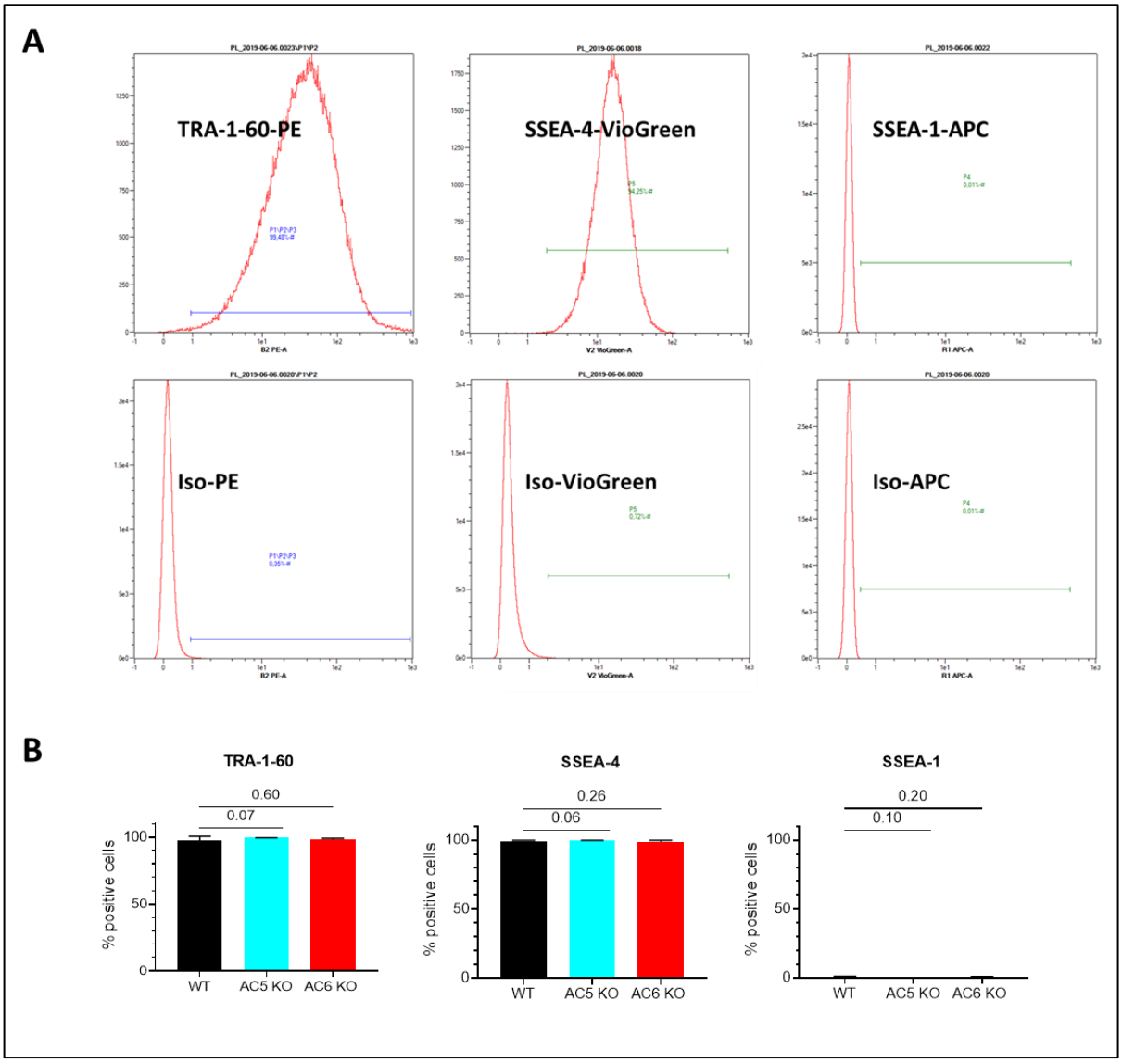

Figure 27: Unchanged expression of pluripotency and differentiation markers in wild-type ChiPSC22 and AC5- and AC6 KO ChiPSC22.
A: Representative FACS-analysis of ChiPSC22 wild-type cells for the pluripotency marker TRA-1-60 and SSEA-4 and the early differentiation marker SSEA-1 B: Quantitative comparison of pluripotency/differentiation markers in wild-type, AC5- and AC6 KO clones (N=5, N=5, N=9, respectively). Data are presented as mean ± SD. *p*-values are indicated on top of the bars.

To assess whether knockout of AC5 or AC6 influences pluripotency, the same FACS analysis was performed in parallel with the wild-type clone, three AC5 KO clones and three AC6 KO clones (Figure 27B). In all cell lines, the expression of TRA-1-60 and SSEA-4 was well above 90% of the whole population. The expression of the differentiation marker SSEA-1 was always below 2% in all cell lines. These results suggest that knockout of AC5 or AC6 does not influence pluripotency of hiPSC cells.

4.3.2 AC5 and AC6 is dispensable for cardiac differentiation

Cardiac induction of the wild-type ChiPSC22 cell line usually generated between 80 to 100% of cTnT-positive cells on day 14 of differentiation. β-adrenoceptor signaling plays an important role in cardiomyocyte physiology. To test whether removal of AC5 and AC6 affects the number of cTnT-positive cells, wild-type and KO clones were dissociated on day 14 of differentiation, stained with an anti-cTnT antibody and analysed via FACS. The expression of cTnT was unchanged between wild-type and KO cells (Figure 28). This was also in line with microscopic analysis that showed a comparable fraction of beating cells in all cell lines. Apparently, AC5 and AC6 are dispensable for cardiac differentiation.

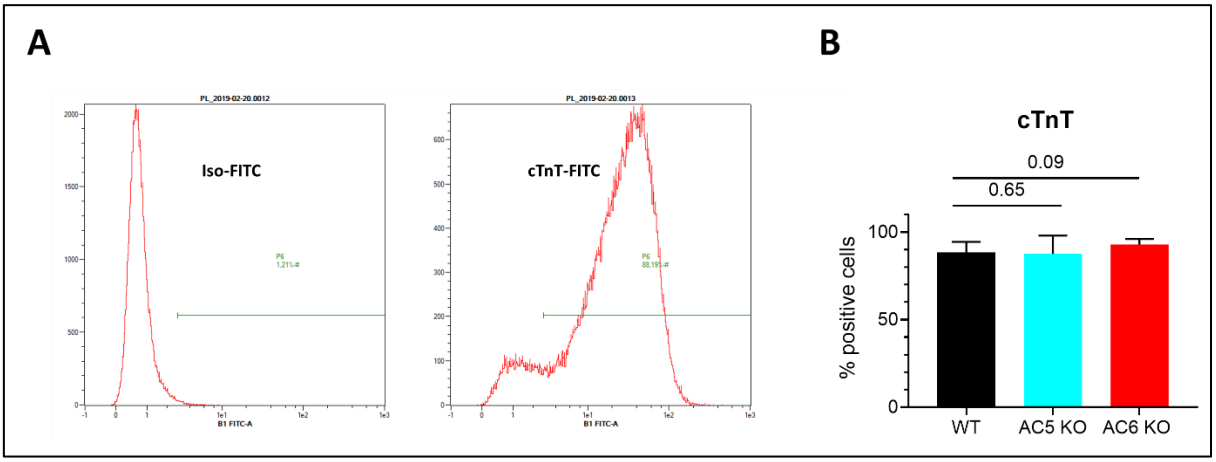

Figure 28: AC5- and AC6 KO does not influence the number of cTnT-positive cells.
A: Representative FACS analysis of wild-type cardiomyoctes using a FITC coupled anti cTnT antibody on day 33 of differentiation. B: Comparison of wild-type AC5 KO and AC6 KO clones after staining with an anti cTnT-FITC antibody. Data are presented as mean ± SD of eight biological replicates. *p*-values are indicated on top of the bars.

4.3.3 Knockout of AC5 and AC6 alters the expression of ACs

Next, it was interesting to see whether a knockout of AC5 and AC6 affects the expression of other ACs. To this end, the expression of all AC isoforms was measured in the iPS state (day 0), in early cardiomyocytes (day 25) and in mature cardiomyocytes (day 33).

In the hiPSC state (day 0, Figure 29), only low expression of ACs was detectable. AC2 and AC1 showed the highest expression levels in all clones followed by AC5 and AC6. All other ACs were only expressed very weakly or were below the detection limit of the assay.

In early cardiomyocytes (day 25), AC6 was predominantly expressed. Expression of other AC isoforms was comparatively low. AC6 KO CMs showed a trend for an almost four-fold decrease of AC6 compared to wild-type cells. This result suggests nonsense-mediated decay of AC6 transcripts after CRISPR editing (108). Interestingly, AC5 KO CMs appeared to show higher levels of AC6 compared to wild-type cells. This result suggests a transcriptional upregulation of AC6 caused by loss of AC5.

In mature cardiomyocytes (day 33), AC5 and AC6 showed the highest expression levels of all ACs. Other ACs were expressed on a much smaller level or were at the detection limit of the assay. There was a trend for an eight-fold reduction of AC5 expression in AC5 KO CMs. This might be attributed to nonsense-mediated decay of AC5 transcripts after CRISPR editing of the AC5 gene. Interestingly, AC6 KO CMs also showed a trend of reduced AC5 expression (about two-fold). Thus it is likely that AC5 expression is dependent on functional AC6. This could also explain why AC5 expression follows AC6 expression during differentiation. AC6 KO CMs showed a trend of four-fold reduction of AC6 expression. In contrast, AC6 expression tended to be upregulated in AC5 KO CMs. Upregulation of AC6 in AC5 KO CMs suggests that AC5 inhibits the expression of AC6. This could also explain why AC6 expression decreases as soon as AC5 expression increases during differentiation. According to these findings, it can be speculated that AC6 expression activates AC5 expression during differentiation. Following day 25, regulation by AC5 reduces AC6 expression.

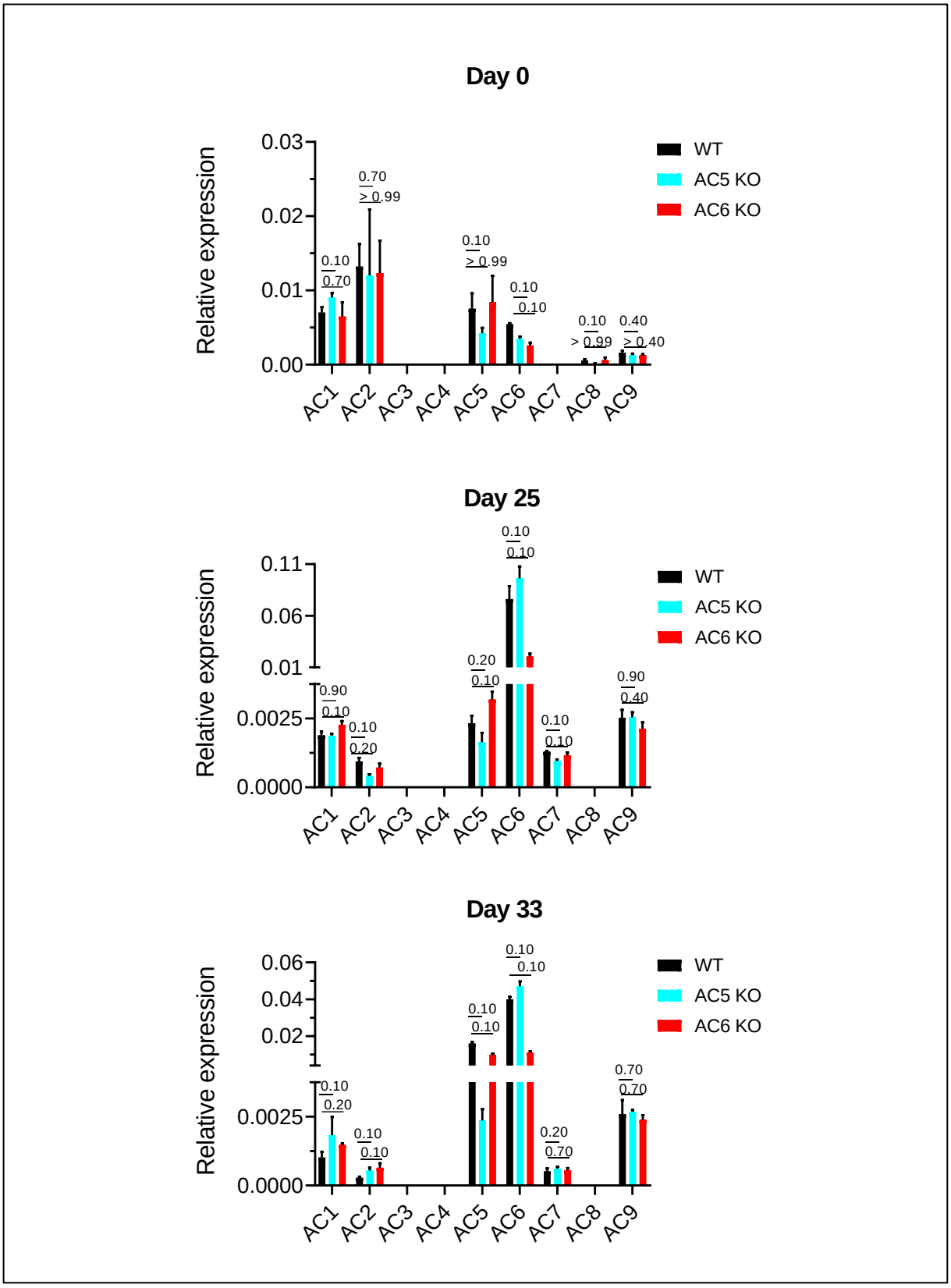

Figure 29: qPCR analysis of all AC isoforms in ChiPSC22 on day 0, day 25 and day 33 of cardiac differentiation.
Expression was normalized to the housekeeping gene RPL37A. A different scale bar was used for all figures because of different expression levels. Data are presented as mean ± SD of three biological replicates. *p*-values are indicated on top of the bars.

4.3.4 CRISPR-mediated deletion of AC isoforms influences differently cAMP production

Next, it was investigated whether knockout of ACs influences cAMP production in the hiPSC state in both early and adult cardiomyocytes. hiPSCs were stimulated with serial dilutions of the AC-agonist forskolin for 20 minutes. Cells were lysed and cAMP levels were detected. Interestingly, this experimental setup only evoked unsaturated concentration-response curves in all clones (Figure 30). On day 0, baseline levels of wild-type and KO clones were comparable (WT: 1.2 +/- 0.04 nM, AC5 KO: 1.3 +/- 0.3nM, AC6 KO: 1.6 +/- 0.7 nM, p> 0.99 and >0.7, N=3). Under maximal forskolin stimulation, cAMP levels tended to be higher in wild-type cells, followed by AC5 KO clones and AC6 KO clones (WT: 54 +/-17 nM, AC5 KO: 37.4 ± 5.3 nM, AC6 KO: 26.4 ± 3.3 nM, p=0.2 and 0.1, N=3).

On day 25 of differentiation, baseline cAMP levels remained unchanged between wild-type- and KO cells (WT: 1.4 ± 0.1 nM, AC5 KO: 1.4 ± 0.4 nM, AC6 KO: 0.5 ± 0.4 nM, p=0.7 and 0.2, N=3). Under maximal forskolin stimulation, cAMP levels tended to be much higher in wild-type CMs compared to AC6 KO CMs (75.5 ± 0.2 nM vs 12.4 ± 4.6 nM, p=0.1, N=3). AC5 KO CMs showed the highest maximal cAMP levels (110.6 ± 12.5 nM). These tended to be higher compared to wild-type (p=0.1). Compared to day 0 of differentiation, the maximal cAMP levels increased in wild-type- and AC5 KO clones but decreased in AC6 KO clones.

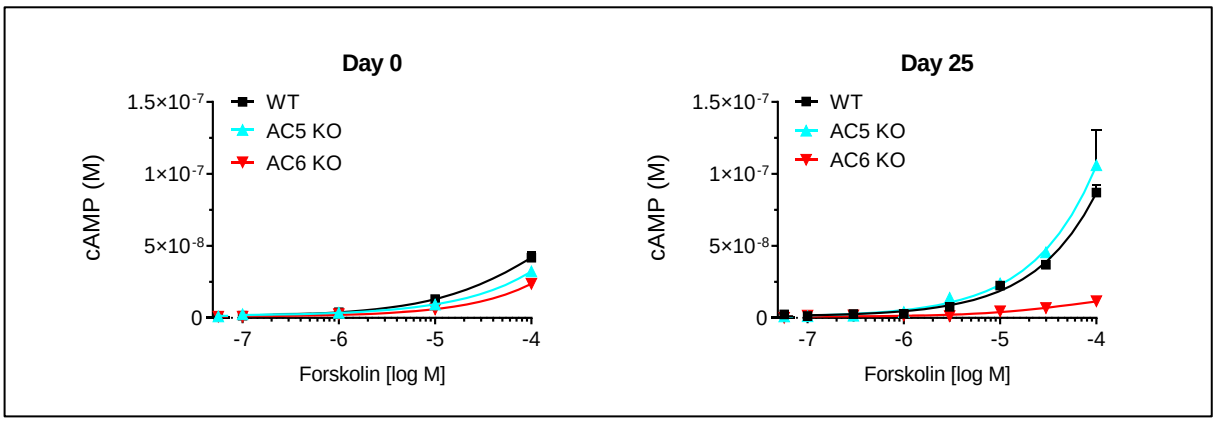

Figure 30: cAMP levels stimulated by AC-activator forskolin in wild-type, AC5 KO- and AC6 KO clones on day 0 and day 25 of cardiac differentiation (representative measurement).
Wild-type-, AC5 KO- and AC6 KO clones were stimulated with serial dilutions of forskolin for 20 minutes. Cells were lysed and cAMP levels were measured using a cAMP HTRF assay. Data are presented as mean ± SD of three technical replicates.

On day 25 of differentiation, it was possible to increase intracellular cAMP levels by stimulation with the β-adrenoceptor agonist isoprenaline (Figure 31). This evoked saturated concentration-response curves that allowed a determination of EC_{50} values. Isoprenaline-stimulated AC5 KO CMs exhibited a tendency of higher cAMP levels than wild-type CMs (maximal response = 233.3 ± 58.4 nM vs. 159.3 ± 43.5 nM, *p*= 0.2, N=3). This observation was in line with the data generated under forskolin stimulation. Again, it appeared that cAMP generation was stronglly reduced in AC6 KO CMs (Maximal response = 31.1 ± 15.9 nM, *p*=0.1, N=3). Compared to wild-type, basal cAMP levels were increased in AC5 KO cells and decreased in AC6 KO cells (WT: 2.8 ± 3.1 nM, AC5 KO: 5.1 ± 4.6 nM, AC6 KO: 1.7 ± 1 nM), although this effect was not statistically significant. EC_{50} values tended to be lower in wild-type cells compared to AC5 KO cells (71.6 ± 7.1 nM vs 201.6 ± 78.2 nM, *p*=0.1, N=3). AC6 KO cells showed an intermediate EC_{50} value (119 ± 19.7 nM, *p*=0.1, N=3).

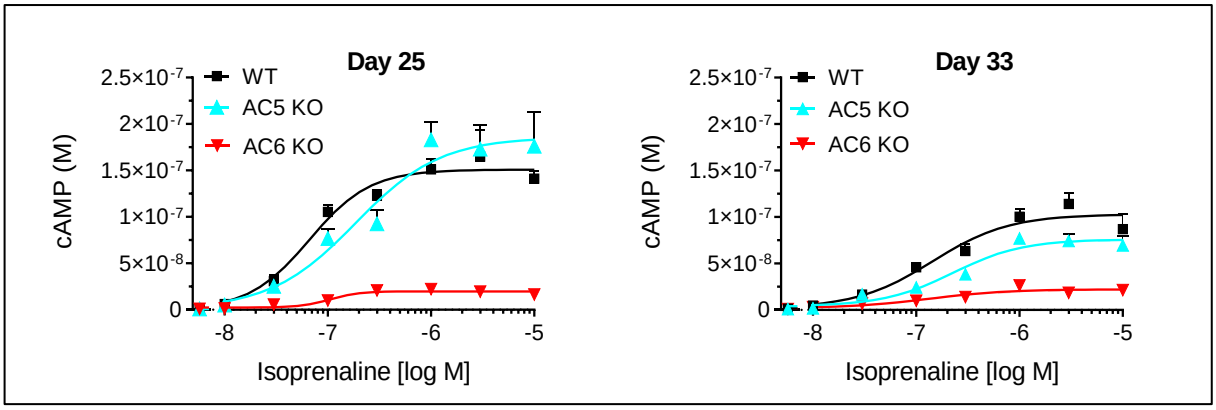

Figure 31: cAMP levels stimulated by isoprenaline in wild-type-, AC5 KO- and AC6 KO CMs on day 25 and day 33 of cardiac differentiation (representative measurement).
Wild-type-, AC5 KO- and AC6 KO CMs were stimulated with serial dilutions of isoprenaline for 20 minutes. Cells were lysed and cAMP levels were measured using a cAMP HTRF assay. Data are presented as mean ± SD of three technical replicates.

In more mature cardiomyocytes (day 33), maximal stimulated cAMP levels were reduced in all clones compared to day 25 (WT: 90.4 ± 10.6 nM, AC5 KO: 53.3 ± 17.4 nM, AC6 KO: 20.9 ± 2.53 nM). The reduction was most prominent in wild-type- and AC5 KO CMs. This could be explained by the lower expression of AC6 on day 33 of differentiation. Interestingly, AC5 KO CMs showed a tendency of lower maximal cAMP levels compared to wild-type CMs (*p*=0.1, N=3). This is in line with the more prominent expression of AC5 in wild-type cells on day 33. The maximal cAMP levels also appeared to be reduced in AC6 KO cells compared to wild-type cells (*p*=0.1, N=3).

Basal cAMP levels were comparable between all clones with a trend of higher cAMP levels in AC5 KO cells (WT: 2.8 ± 3.1 nM, AC5 KO: 5.1 ± 4.6 nM, AC6 KO: 1.7 ± 1 nM, *p*=0.1 and 0.7, N=3). AC6 KO CMs exhibited a trend of lower EC_{50} values compared to wild-type CMs (55 ± 9.9 nM vs. 173.6 ± 85.9 nM, *p*=0.1, N=3). The EC_{50} value of wild-type CMs was unchanged compared to AC5 KO CMs (173.6 ± 85.9 nM vs. 123 ± 50.3 nM, *p*=0.7, N=3)

4.3.5 Gene dose dependent reduction of cAMP levels by CRISPR-mediated knockout of ACs

In the previous experiments, a strong correlation between cAMP levels, expression level and gene editing of ACs was observed. This suggested that the observed effects were specific to CRISPR editing and not related to clonal variation. To corroborate this notion, wild-type cardiomyocytes (AC6+/+), a heterozygous AC6 KO clone (AC6 +/-) and a homozygous AC6 KO clone (AC6-/-) were maximally stimulated with 10 µM isoprenaline for 20 minutes on day 33 of differentiation and cAMP levels were detected (Figure 32). To measure baseline cAMP levels, cells were incubated with DMSO for 20 minutes. Three biological replicates were measured. cAMP levels of unstimulated cells were unchanged. Maximally stimulated cAMP levels were reduced in a gene dose-dependent manner between wild-type cells (98.8 ± 28.7 nM), heterozygous AC6 KO cells (7.5 ± 4.8 nM) and homozygous AC6 KO cells (2.4 ± 0.3 nM). This suggests that the observed reduction in cAMP levels is specific to CRISPR knockout of ACs. However, elimination of one allele already reduced the maximal stimulated cAMP levels to ~8% of the wild-type levels. Elimination of the second allele reduced the cAMP levels to about 2.4%. This suggests that the presence of only one allele is by far too low to support physiological cAMP levels. The system seems to be very sensitive to AC6 activity. In wild-type cells, there is no buffer of redundant AC6 available.

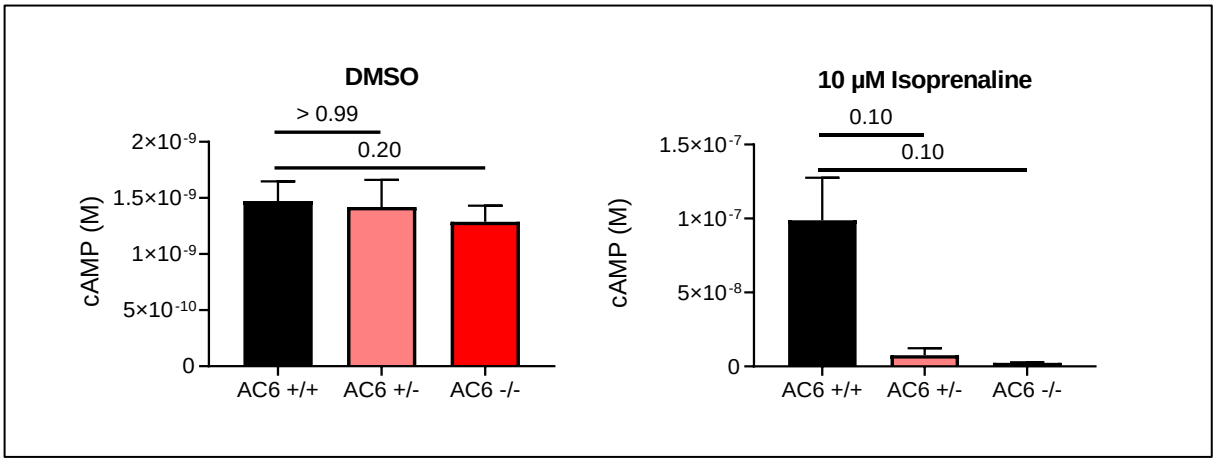

Figure 32: Gene dose-dependent reduction of stimulated cAMP levels.
Wild-type (AC6 +/+), heterozygous (AC6+/-) and homozygous (AC6 -/-) KO clones were stimulated with 10 µM isoprenaline for 20 minutes. For baseline detection of cAMP levels, cells were incubated with DMSO for 20 minutes. cAMP levels were measured using a cAMP HTRF assay. Data are presented as mean ± SD of three biological replicates. *p*-values are indicated on top of the bars.

4.3.6 AC5 and AC6 couple equally to β_2-adrenoceptors in the absence of β_1-adrenoceptors.

Isoprenaline binds the β_1- and β_2-adrenoceptors with comparable dissociation constants (Log $K_D(\beta_1)$= -6.06, Log $K_D(\beta_2)$= -6.64, , Log $K_D(\beta_3)$= -5.52 (109)), and thus affinity. To find out which β-adrenoceptor couples functionally to AC5 and AC6, day 33 hiPSC CMs were stimulated with 0.3 µM isoprenaline in the presence or absence of the β_1-selective antagonist CGP 20712 or the β_2-selective antagonist ICI 118,551 (Figure 33B and Figure 33A). The concentration range of the inhibitors in this experiment guaranteed β_1/β_2 selectivity (110). 0.3 µM isoprenaline was chosen because this concentration is between the EC_{50} and EC_{90} of isoprenaline in wild-type and KO clones. Three biological replicates were measured. ICI 118,551 reduced cAMP levels in a concentration-dependent manner from 25.1 ± 6.6 nM to 1.7 ± 0.6 nM in wild-type cells. The maximal reduction was comparable to baseline cAMP levels in unstimulated wild-type cells (about 1.5 nM). The same effects were seen in AC5 KO cells (inhibition from 11.7 nM ± 1.2 nM to 1.9 ± 0.2 nM, basal cAMP = 5.1 ± 4.6 nM) and AC6 KO cells (8.9 ± 1.1 nM to 0.2 nM ± 0.2 nM, basal cAMP = 1.7 ± 1 nM). In contrast, CGP 20712 did not affect cAMP levels and no concentration-response relationship could be constructed. These results suggest that β-adrenoceptor signaling is exclusively mediated by β_2-adrenoceptor activation. Both AC5 and AC6 couple functionally to this receptor. This result would also explain why it was not possible to detect β_1-adrenoceptor mRNA. The absence of the β_1-adrenoceptor was validated in

a Schild-plot experiment. The concentration-response relationship evoked by stimulation of wild-type cells with serial dilutions of isoprenaline (EC_{50} = 25.2 ± 1.3 nM) was rightward shifted to an EC_{50} of 4.4 ± 2 µM in the presence of 100 nM ICI 118,551 (p=0.10, N=3). No rightward shift occurred in the presence of 1 µM CGP 20712 (51.2 ± 4.1 nM, p>0.99) and the β_1-selective agonist ICI 118,587 did not increase cAMP levels in any cell type (Figure 33D).

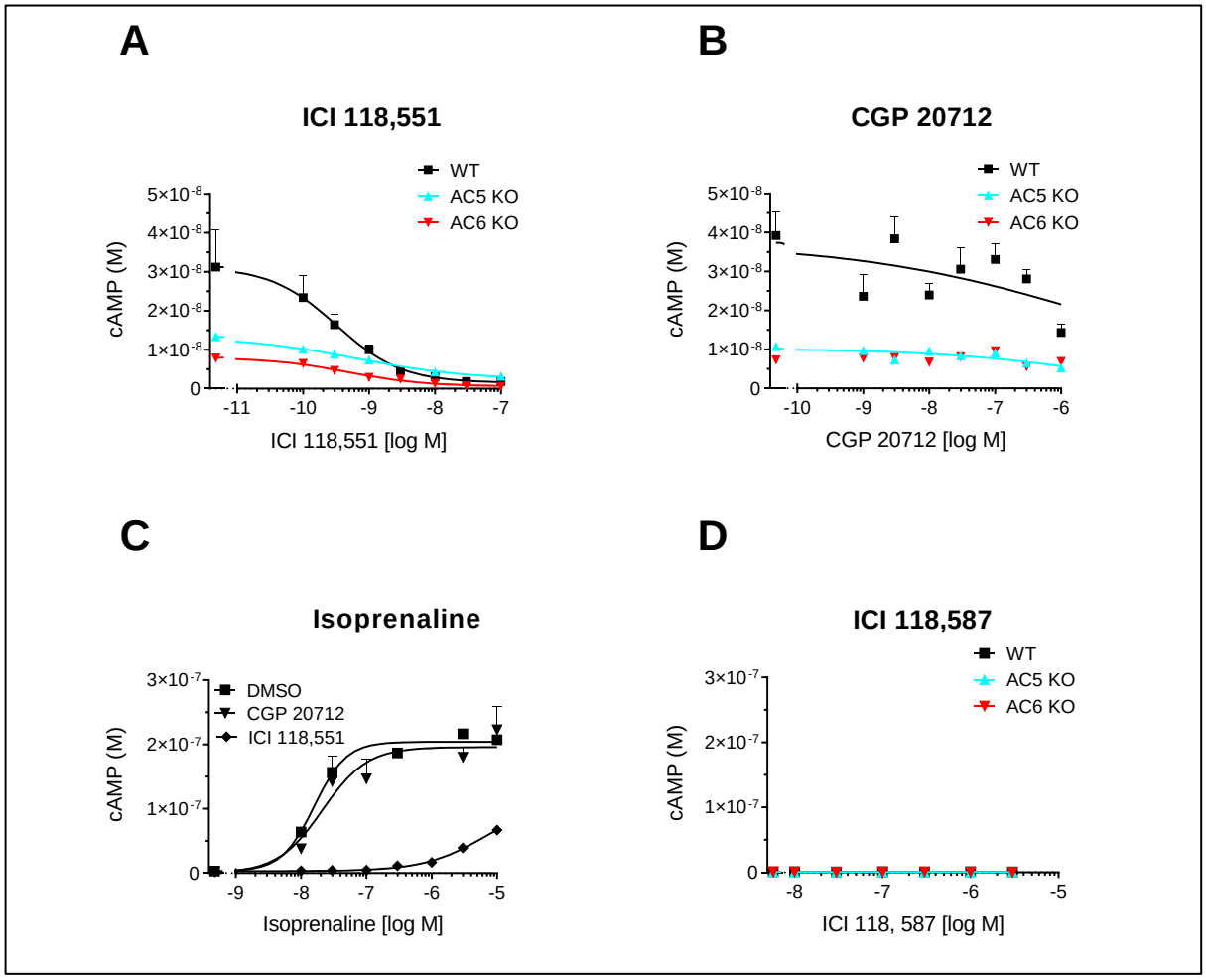

Figure 33: Exclusive coupling of the β_2-adrenoceptor to AC5 and AC6 (representative measurements).
Wild-type and KO CMs were preincubated with serial dilutions of ICI 118,551 (A) or CGP 20712 (B) for 10 minutes followed by 0.3 µM isoprenaline stimulation for 20 minutes until cell lysis and detection. C: Wild-type and KO CMs were pre-incubated with 100 nM ICI 118,551, 1 µM CGP 20712 or DMSO for 10 minutes followed by a 20-minute stimulation with serial dilutions of isoprenaline, cell lysis and detection. D: Wild-type or knockout CMs were stimulated with the β_1 partial agonist ICI 118,587 for 20 minutes followed by cell lysis and detection. Data are presented as mean ± SD of four technical replicates.

4.3.7 AC knockout impairs functional response to β-adrenoceptor stimulation

AC knockouts showed a clear reduction of catalytic AC activity. Next, it was investigated whether this effect also translates into functional effects. Wild-type and KO clones were loaded with calcium 6 dye on day 33 of differentiation and spontaneous calcium transients were recorded in a heated fluorescence reader. Immediately after isoprenaline stimulation, calcium transients were recorded a second time. Figure 34 shows the change of each calcium transient parameter after isoprenaline addition. In contrast to the cAMP HTRF assay, responses to β-adrenoceptor stimulation were already detectable at much lower isoprenaline concentrations.

In wild-type and AC5 KO cells, isoprenaline reduced the time to peak of the calcium transient in a concentration dependent manner. The maximal reduction occurred at 1 nM and was comparable in both cell types (62 ± 7 % vs 68 ± 11%, p=0.2, N=6). Interestingly, 1 nM isoprenaline did not reduce the time to peak in AC6 KO CMs compared to wild-type (96 ± 31 % vs 62 ± 7 %, p=0.01).

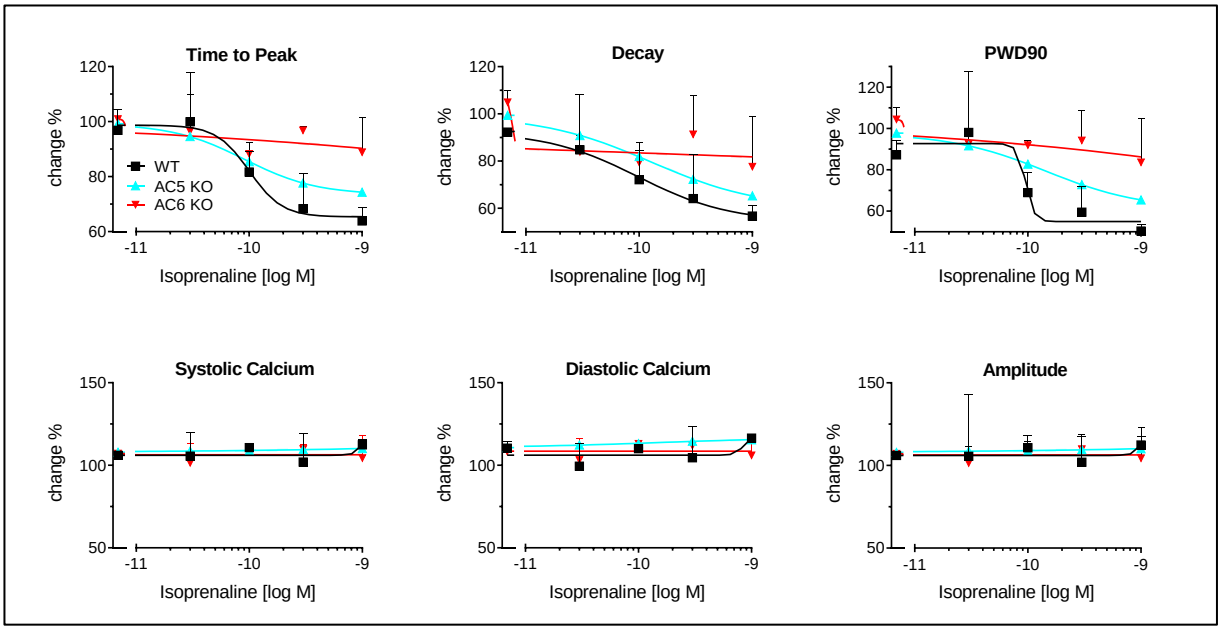

Figure 34: Attenuated functional response to isoprenaline in AC KO cardiomyocytes (representative measurement).
Calcium transient parameters after stimulation with serial dilutions of isoprenaline. Wild-type-, AC5 KO- and AC6 KO cardiomyocytes were loaded with calcium 6 dye. Fluorescence increases were recorded before and after isoprenaline addition at 37°C in spontaneously beating cells. Calcium transient parameters were calculated using KinEva. Data are presented as mean ± SD of four technical replicates.

Isoprenaline also reduced the decay time of the calcium transient in wild-type and KO CMs. However, the maximal reduction by 1 nM isoprenaline tended to be sligthly stronger in wild-type cells compared to AC5 KO- and AC6 KO CMs (55 ± 10% vs. 63 ± 5% vs. 65 ± 19%, *p*=0.09 and 0.3, N=6).

The PWD90 of the calcium transient was reduced upon isoprenaline stimulation in wild-type and AC5 KO CMs in a concentration-dependent manner. The shortest PWD90 was observed after addition of 1 nM isoprenaline in these cell types. However, the maximal reduction of the PWD90 was significantly stronger in wild-type CMs compared to AC5 KO CMs (54 ± 6% vs. 62 ± 13%, *p*=0.05, N=6) and compared to AC6 KO CMs (54 ± 6% vs. 87 ± 31%, *p*=0.02, N=6).

In wild-type and KO CMs, systolic and diastolic calcium levels and the calcium transient amplitude were unaffected by isoprenaline stimulation. The frequency of spontaneous calcium transients always increased in wild-type and knockout cardiomyocytes. However, this parameter was extremely variable and no consistent data could be acquired. For all parameters, no significant difference of the EC_{50} value could be determined when comparing wild-type and KO cardiomyocytes. This ranged around 0.1 nM for all cell types but also showed large variability.

To sum up, the modulation of calcium transients by isoprenaline was weaker in AC KO CMs compared to wild-type CMs, with the strongest reduction being noted in AC6 KO CMs.

The weak isoprenaline-induced response of the PWD90 in KO clones was in line with the phosphorylation level of cTnI. Upon stimulation with 1 µM isoprenaline, phosphorylation of cTnI increased about twelve-fold in wild-type CMs (Figure 35). In contrast, basal phosphorylation of cTnI appeared to be higher in AC5- and AC6 KO CMs and no further change of phosphorylation was observed with isoprenaline (1 µM) stimulation.

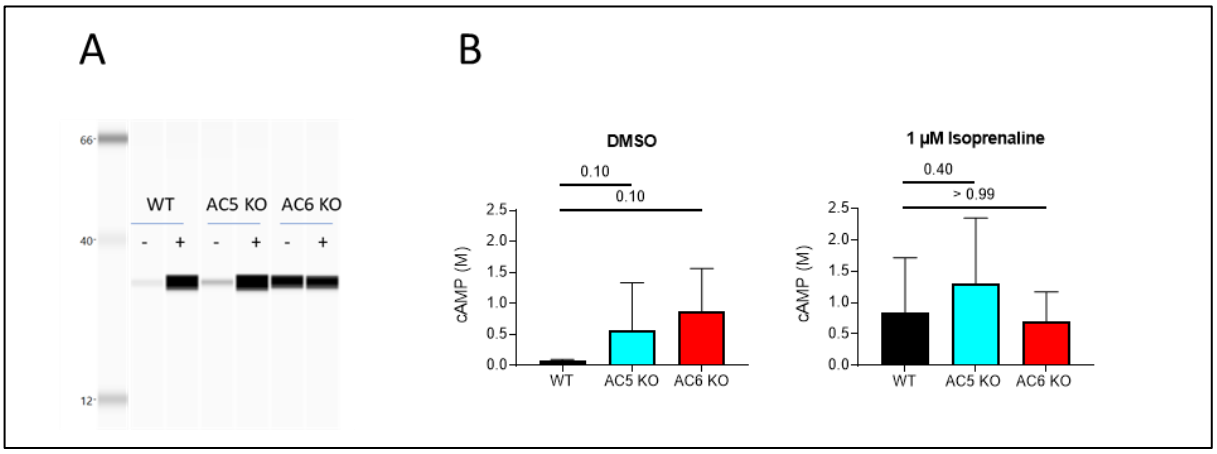

Figure 35: Increased basal phosphorylation of cTnI in AC KO cardiomyocytes.
Simple Western analysis of cTnI phosphorylation. On day 33 of differentiation, wild-type-, AC5 KO- and AC6 KO CMs were stimulated with 1 µM isoprenaline or DMSO (control) for 20 minutes at 37°C before cell lysis. Exemplary blot (A) shows samples from cells stimulated with DMSO (-) or 1 µM Isoprenaline (+). B: Quantification of A. Data are presented as mean of three biological replicates ± SD. *p*-values are indicated on top of the bars.

4.3.8 Knockout of AC5 and AC6 improves calcium transient kinetics

In theory, increased basal phosphorylation of cTnI should accelerate the kinetics of calcium transients (111). Therefore, calcium transients of wild-type and knockout CMs were analysed on day 33 of differentiation. AC6 KO CMs exhibited a significantly shorter PWD90, time to peak and decay of spontaneous calcium transients (Figure 36). The effect was less pronounced in AC5 KO CMs. These results suggest that cardiac calcium cycling is accelerated by knockout of cardiac ACs. Likewise, the calcium transient amplitude was reduced in AC KO clones, although this effect was not significant in AC5 KO CMs. AC6 KO CMs also showed a higher rate of spontaneous calcium transients. Diastolic calcium levels were unchanged in all cell types. A smaller calcium transient integral was characteristic of AC5- and AC6 KO CMs with the effect being stronger in AC6 KO CMs. To sum up, this data suggests that knockout of AC5 and AC6 leads to faster calcium transients and protects cardiomyocytes from high calcium levels.

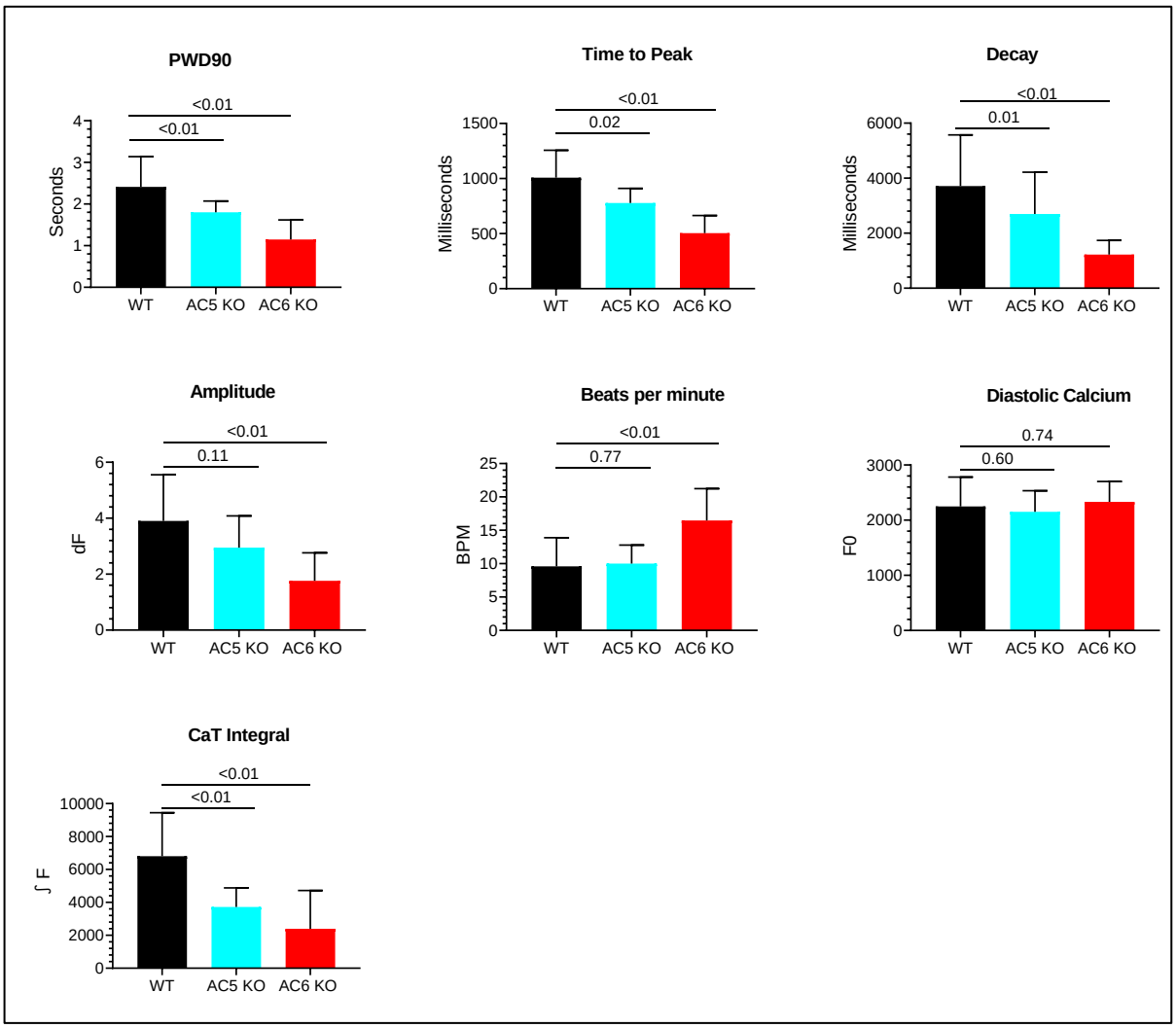

Figure 36: Accelerated calcium transient kinetics in AC-KO cardiomyocytes.
Wild-type, AC5 KO- and AC6 KO CMs were loaded with calcium 6 dye. Fluorescence increases were recorded at 37°C in spontaneously beating cells. Calcium transient parameters were calculated using KinEva. Data are presented as mean ± SD (WT: N=13, AC5 KO: N=13, AC6 KO: N=7). *p*-values are indicated on top of the bars.

Accelerated calcium cycling could be due to increased expression of calcium transporters and calcium channels in KO clones. In qPCR analysis, expression of calcium channels and transporters was unchanged (Figure 37). Interestingly, expression of PLN appeared to be upregulated in KO clones. AC6 KO CMs showed a trend of increased cTnI expression.

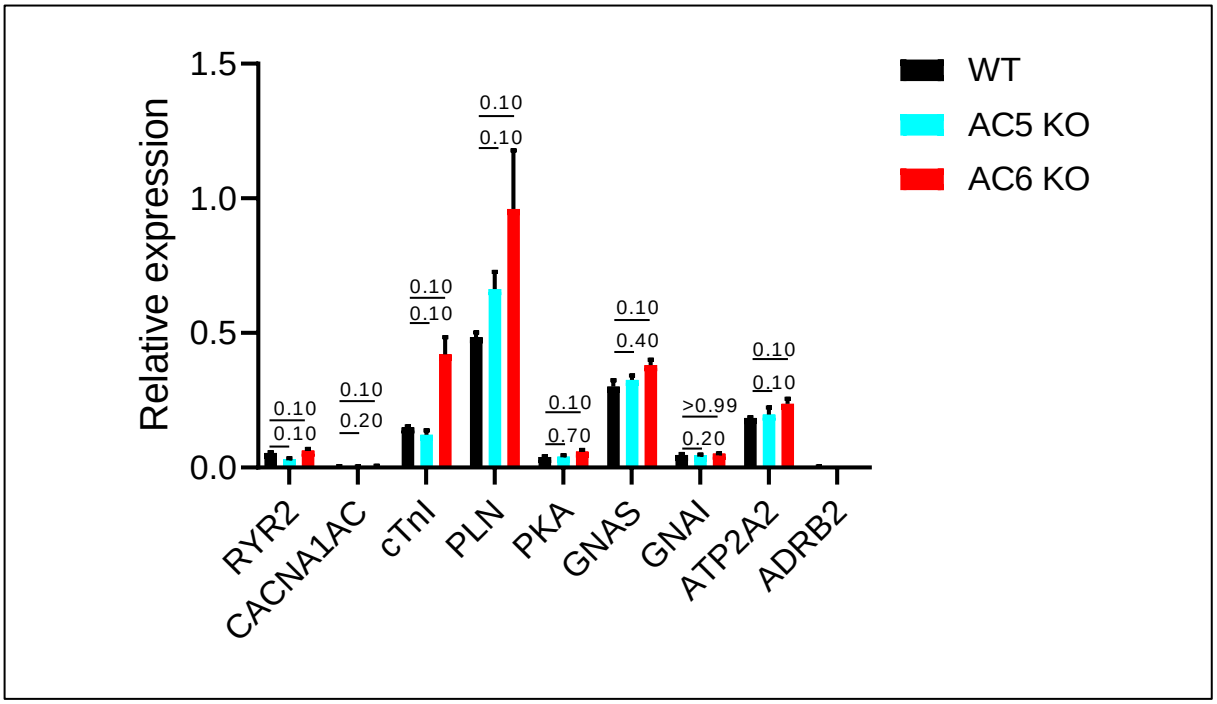

Figure 37: qPCR analysis of calcium handling genes in wild-type and AC KO cardiomyocytes on day 33 of differentiation.
Data are presented as mean of three biological replicates ± SD. *p*-values are indicated on top of the bars.

4.3.9 AC5 KO protects hiPSC CMs from fused calcium transients

It was conceivable that the reduced calcium transient PWD90 and reduced calcium transient amplitude of the AC5- and AC6 KO CMs protect the cells from fused calcium transients at high pacing frequencies. To test this hypothesis, wild-type and AC KO CMs were seeded on a 96 well plate with 20 technical replicates per clone on day 33 of differentiation. Next, calcium transients were recorded at 0.5 Hz and 1.0 Hz. The number of technical replicates that showed fused calcium transients was quantified. The experiment was repeated with 24 differentiations (WT and AC5 KO clone) or 11 differentiations (AC6 KO clone). An example is depicted in Figure 38A along with the quantification of all experiments in Figure 38B. Wild-type cells showed no fused calcium transients when paced at 0.5 Hz. When paced at 1.0 Hz, the mean wild-type cardiomyocytes showed calcium transient shoulders in 58.5% of technical replicates. In contrast, the mean AC5 KO differentiation showed calcium transient shoulders in only about 4.3% of technical replicates. In AC6 KO CMs, the mean likelihood of fused calcium transients was also smaller compared to wild-type cells (37% vs. 58.5%).

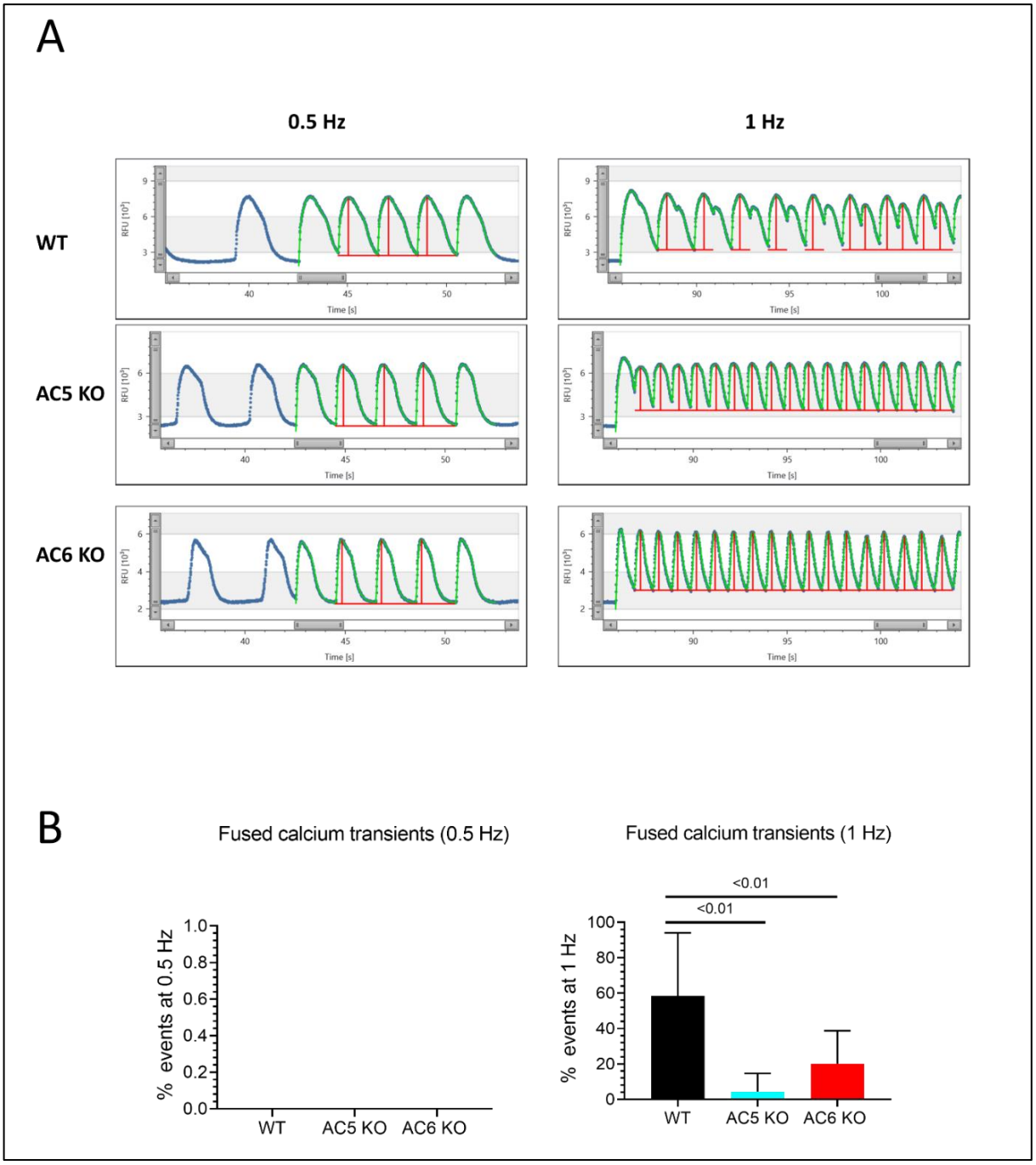

Figure 38: AC5- and AC6 KO protects hiPSC CMs from fused calcium transients.
Wild-type-, AC5 KO- and AC6 KO CMs were seeded on a 96 well plate with 20 technical replicates. After loading with calcium 6 dye, fluorescence increases were recorded at 0.5 and 1.0 Hz. A: Representative calcium transients recorded at 0.5 Hz, and 1.0 Hz in wild-type-, AC5 KO- and AC6 KO CMs. B: Quantification of fused calcium transient events of paced wild-type and KO CMs at 0.5 Hz and 1.0 Hz. Data are presented as mean of biological ± SD (WT: N=24, AC5 KO: N=24, AC6 KO: N=11). *p*-values are indicated on top of the bars.

4.3.10 Knockout of AC6 attenuates negative force-frequency relationship

To determine whether removal of ACs reverses the negative force-frequency relationship observed in paced wild-type cells, the calcium transient amplitude of wild-type and KO CMs were compared under baseline conditions and paced conditions on day 33 of differentiation (Figure 39).

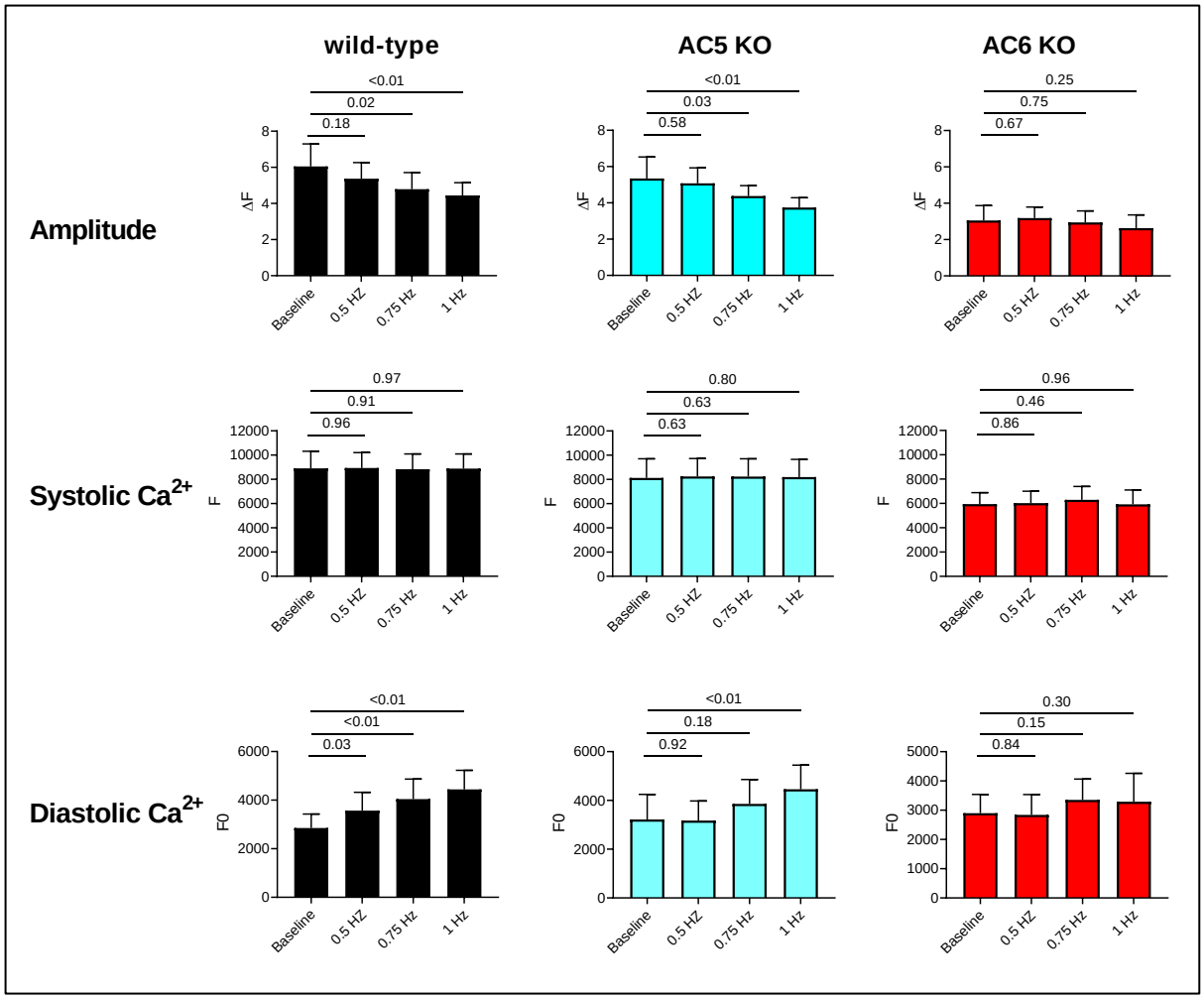

Figure 39: Negative force-frequency relationship is attenuated in AC6 KO CMs.
Wild-type-, AC5 KO- and AC6 KO CMs were loaded with calcium 6 dye. Fluorescence increases were recorded at 37°C for 30 seconds in unstimulated cells (baseline) or electrically stimulated cells (0.5 Hz-1.0 Hz). Calcium transient parameters were calculated using KinEva. Data are presented as mean of ten biological replicates ± SD. *p*-values are indicated on top of the bars.

Wild-type CMs showed a frequency-dependent reduction of calcium transient amplitude. This effect was preserved in AC5 KO CMs. AC6 KO CMs had a reduced calcium transient amplitude at baseline with no further increase under paced conditions. The reduced amplitude was not a result of reduced systolic calcium levels. In all clones, these were unchanged between all frequencies. The reduced calcium

transient amplitude was rather a result of elevated diastolic calcium levels in wild-type- and AC5 KO CMs under paced conditions. AC6 KO CMs were protected from increased diastolic calcium levels under paced conditions.

4.3.11 AC5- and AC6 KO CMs are protected from concentric hypertrophy

The analysis of basal calcium transients revealed that wild-type cardiomyocytes are exposed to higher levels of intracellular calcium compared to AC5 KO and AC6 KO CMs. High calcium levels can activate hypertrophy via induction of a fetal gene program (102, 112, 113). Microscopic analysis revealed that AC5- and AC6 KO CMs had a smaller cell size and a more elongated phenotype compared to wild-type cells on day 33 of differentiation (Figure 40A). The cells appeared to be more oriented along the line of mechanical force developed during contraction. This might reflect an improvement of contractility in AC KO cells. In this sense, the cells resembled more mature cardiomyocytes (114, 115). These findings were confirmed by high content analysis (Figure 40B). Staining of nucleus and cytosol allowed automated quantification of cell area and cell shape. The analysis of ten biological replicates with 800,000 cells each revealed a significantly smaller cell area of AC6 KO CMs compared to wild-type CMs. AC5 KO CMs also showed a trend of smaller cell area with no statistical significance. Interestingly, subsequent FACS analysis of a fraction of these cells showed that the three-dimensional cell volume was unchanged between wild-type and KO clones. Only on the two-dimensional plane, wild-type CMs filled out more space. The fraction of cardiomyocytes was over 95% in all samples. High content analysis also confirmed the more elongated morphology of KO clones by calculating the cell width/length ratio. However, this effect was only significant for AC6 KO CMs. The roundish, large morphology of the wild-type cardiomyocytes was redolent of cardiomyocytes from hearts with concentric hypertrophy. In fact, the hypertrophy-like phenotype of wild-type cardiomyocytes was also reflected in a trend of a higher expression of the fetal gene NPPB and MYH7 (Figure 40C). Interestingly, there was a trend of lower expression of MYH6 in wild-type cells. A reduction of the MYH6/MYH7 ratio is a hallmark of hypertrophic remodeling (116, 117).

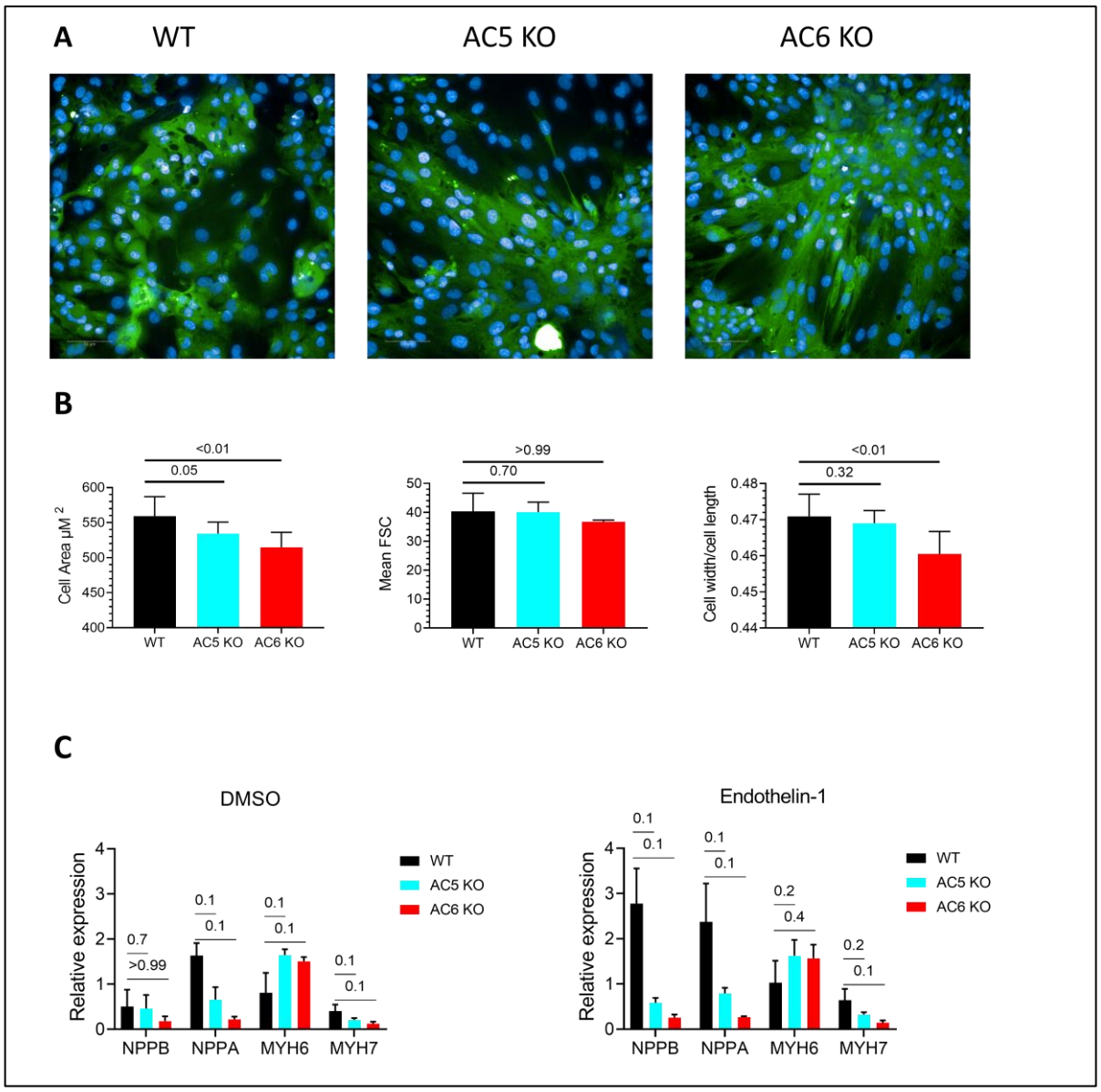

Figure 40: AC KO cardiomyocytes are protected from hypertrophic response.
A: Live-cell staning of cytosol (CMFDA, green) and nucleus (NucBlue, blue) of wild-type- and KO clones. B: Quantification of live cell stainings with high content analysis (Cell Area µm^2 and ratio cell width/cell length, N=10) and quantification of cell volume using flow cytometry (forward scatter, N=3). C: qPCR analysis of fetal gene expression in DMSO only (control) or Endothelin-1 (1 nM) stimulated wild-type and KO cardiomyoyctes (N=3). Data are represented as mean ± SD. *p*-values are indicated on top of the bars.

Taken together, activation of this gene program is a hallmark of hypertrophic cardiomyocytes from HF patients (101, 102). The fetal gene expression and larger cell size of wild-type cells led to the hypothesis that wild-type cardiomyocytes are more prone to the development of a HF-like phenotype. To validate this hypothesis, cells were stimulated with Endothelin-1 for 24 hours. This agent is known to induce hypertrophy in cardiomyocytes (118). Endothelin-1 led to a strong increase of NPPB

in wild-type cells but not in KO clones. Likewise, the expression of NPPA increased substantially in wild-type cells only. The expression of MYH6 and MYH7 was unchanged. To sum up, the morphological and molecular features suggest that elimination of ACs protects hiPSC CMs from hypertrophy.

4.4 An AC5/AC6 non-selective inhibitor rescues the hypertrophic phenotype of wild-type cardiomyocytes

An AC inhibitor (BAY 1232055) was identified in a biochemical high-throughput screen (internal communication). The structure of this hit is depicted in Figure 41A. To determine the selectivity of this compound, wild-type-, AC5 KO- and AC6 KO hiPSC CMs were incubated with serial dilutions of the inhibitor for 10 minutes, followed by stimulation with 300 nM isoprenaline, cell lysis and cAMP determination after 20 minutes (Figure 41B). In these experiments, the IC_{50} of BAY 1232055 was comparable between wild-type- and AC5 KO cardiomyocytes (WT: 2.55 µM +/- 0.49 µM, AC5 KO: 1.64 +/- 0.44 µM). This result suggested that the compound has comparable selectivity for AC5 and other ACs expressed in wild-type cardiomyocytes. Determination of the IC_{50} was not possible in AC6 KO cardiomyocytes, perhaps because of the very low cAMP levels. The next step was to see if inhibition of cAMP by this novel small molecule affects calcium transient parameters in wild-type cardiomyocytes. In fact, BAY 1232055 reduced the calcium load of wild-type cardiomyocytes in a concentration-dependent manner to 20% of control value, with an IC_{50} of 15.2 ± 3.9 µM (Figure 41C). PWD90 was only reduced by the highest concentration of BAY 1232055 (30 µM) to 36% of control value. Compound concentrations of 3 µM or greater also prevented interrupted calcium transients during pacing with 1 Hz (Figure 41D).

To analyse the consequences of AC inhibition for hypertrophy, wild-type cardiomyocytes were incubated for 24 hours with 1 nM endothelin-1 in the presence or absence of 30 µM BAY 1232055. Cells incubated with the inhibitor showed a trend of five-fold reduction of NPPB (Figure 41E). Likewise, the cell size of wild-type cardiomyocytes was significantly reduced after incubation with 30 µM BAY 1232055 (Figure 41F).

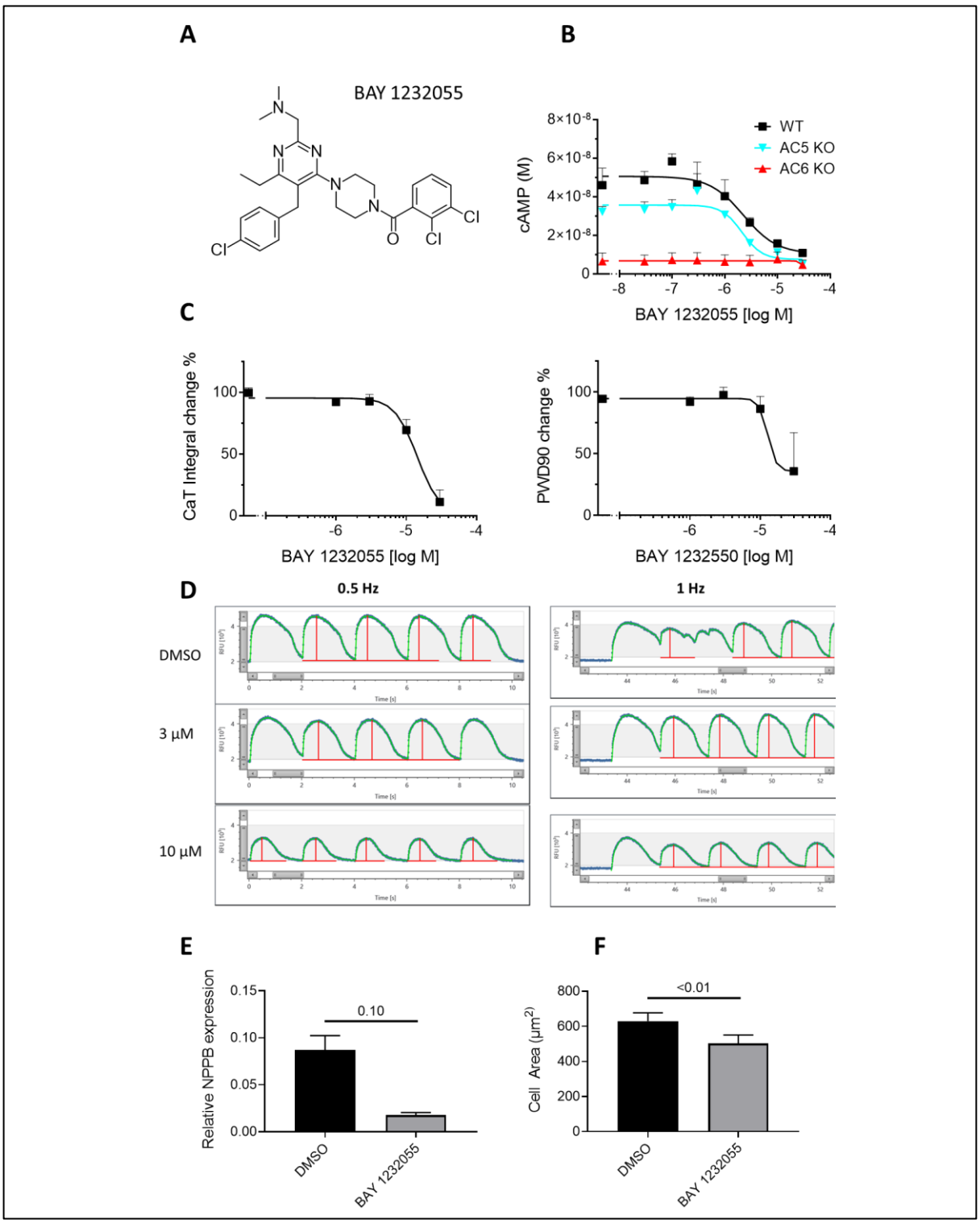

Figure 41: AC inhibitor rescues wild-type cardiomyocytes from HF-like phenotype.
A: Structure of BAY 1232055. B: Inhibition of isoprenaline-stimulated cAMP levels in wild-type and KO cardiomyocytes by BAY 1232055 (representative measurement). C: Change of the calcium transient integral and PWD90 in wild-type cardiomyocytes upon addition of serial dilutions of BAY 1232055 (mean of three biological replicates ± SD). D: Calcium transients of wild-type cardiomyocytes at 0.5 Hz and 1.0 Hz recorded 3 minutes after addition of DMSO, 3 µM or 10 µM BAY 1232055. E: qPCR analysis of NPPB expression in wild-type cardiomyocytes after 24-hour incubation with 1 nM endothelin-1 in the presence or absence of 30 µM BAY 1232055 (N=3). F: High content analysis of wild-type cardiomyocyte cell size after 24-hour incubation with or without 30 µM BAY 1232055 (N=10). *p*-values are indicated on top of the bars. Data are presented as mean ± SD.

These experiments showed that AC inhibition reduced calcium transient amplitude and reduced calcium transient duration at baseline (Figure 41C). This result suggests that ACs are active even in the absence of β-adrenoceptor agonists. Autonomous activity of ACs could be a result of constitutively active $G\alpha_s$ protein that signals independently of β-adrenoceptor activation. Another explanation could be constitutively active β-adrenoceptors that are active even in the absence of an agonist. To identify which factor potentially contribute, the β_2-adrenoceptor was blocked with serial dilutions of the inverse agonist ICI 118,551. The β_2-adrenoceptor was identified as the only β-adrenoceptor in this system. Application of an inverse agonist should reduce the percentage of active β-adrenoceptors even in the absence of an agonist. However, ICI 118, 551 did not affect calcium transient integral or calcium transient duration in the absence of a β-adrenoceptor agonist (Figure 42), although it modulated calcium transients in the presence of a β-adrenoceptor agonist (page 72, Figure 19). This experiment suggests that constitutive active β-adrenoceptors do not modulate calcium transients in these cells. Thus, constitutively active $G\alpha_s$ proteins remain a likely mechanism responsible for the basal modulation of calcium transients by ACs.

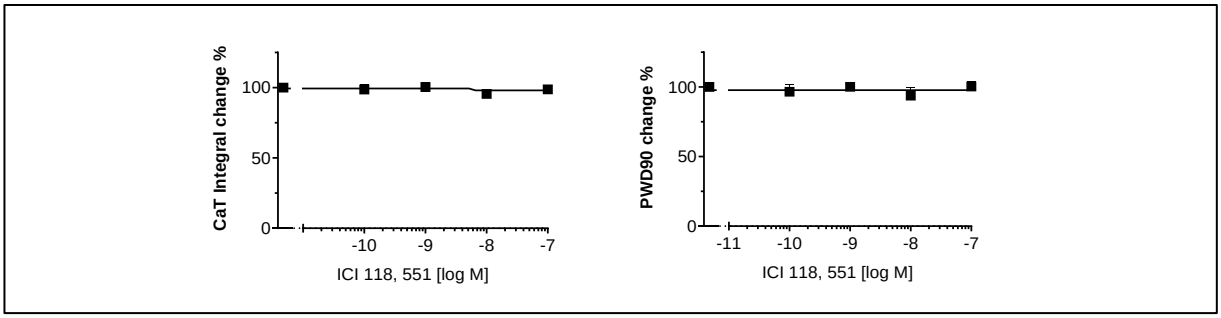

Figure 42: β_2-adrenoceptor inhibition does not influence basal calcium levels or duration of the calcium transient.
Change of calcium transient parameters after addition of serial dilutions of the β_2-selective inverse agonist ICI 118, 551. Wild-type-, AC5 KO- and AC6 KO CMs were loaded with calcium 6 dye. Fluorescence increases were recorded before and after compound addition at 37°C in spontaneously beating cells. Calcium transient parameters were calculated using KinEva. Data are presented as mean ± SD.

5 Discussion

5.1 Characterization of hiPSC CMs

The experimental results of the current thesis suggest that wild-type ChiPSC22-derived cardiomyocytes exhibit a hypertrophic phenotype marked by unrestrained AC signaling and chronic calcium overload. The first evidence was the expression levels of AC-pathway genes throughout differentiation (Figure 12). Remarkably, the expression of $G\alpha_s$ was much more abundant than the expression of $G\alpha_i$ or β-adrenoceptors. Mouse studies show that increasing the amount of $G\alpha_s$ already leads to stronger $G\alpha_s$ activity and a faster activation of ACs even in the absence of an agonist (91). Typically, $G\alpha_s$ transgene mice develop dilated cardiomyopathy (119). The high $G\alpha_s$ /$G\alpha_i$ ratio in ChiPSC22 cardiomyocytes suggests that a high and uncontrolled basal stimulation of ACs takes place in these cells. In line with this, basal cAMP levels are reduced by knockout of AC6 (chapter 4.3.4) and knockout of AC5 and AC6 reduced calcium transient amplitude of unstimulated cardiomyocytes (Figure 36). From the developmental view, autonomous activity of the $G\alpha_s$-AC axis appears logical. Exposure of early cardiomyocytes to β-adrenoceptor agonists is probably low before full development of the sympathetic innervation and the adrenal gland. To activate this pathway in the absence of physiological agonists, autonomous activity of $G\alpha_s$ and AC appear a logical alternative. The early induction of $G\alpha_s$ and AC6 is paralleled by an upregulation of L-type calcium channel. Sarcolemmal calcium cycling might be an adaption to maintain $G\alpha_s$ and AC6 activity. Following day 15, the expression of genes involved in SR calcium cycling (RYR2, SERCA, PLN) also increased. This suggests that a new store system for intracellular calcium is created. The latter might be necessary when expression of $G\alpha_s$ and AC6 expression is increased. Downregulation of PLN on day 25 might constitute a further adaptation to improve calcium storage capacity by removing the PLN-mediated inhibition of SERCA. In line with this notion, PLN protein was not detectable on day 33 in western blot (six different antibodies were tested). In addition, inhibition of SERCA with thapsigargin led to a strong prolongation of calcium transients (Figure 15). This suggests that SERCA is not inhibited by PLN and is in an overactive state. Consequently, the calcium reservoirs are already working at its limit in wild-type ChiPSC22 CMs. In line with this, pacing at frequencies higher than 0.5 Hz led to an increase of the diastolic calcium and a reduced calcium transient

amplitude (Figure 18). Likewise, the duration of the calcium transient was not reduced sufficiently to synchronize the calcium transients at higher pacing frequencies. Apparently, the large amount of calcium cannot be handled by the already overactive system. Interestingly, activation of the β-adrenoceptor pathway did not further increase calcium transient amplitude (Figure 19). All these observations suggest that unrestricted $G\alpha_s$-AC activity leads to an excessive intracellular calcium load. Increased calcium load by AC5 expression was already reported in earlier studies (65). Further increasing the cardiomyocyte calcium load is not possible by β-adrenoceptor stimulation. Likewise, electrical stimulation cannot reduce PWD90 sufficiently. Overall, the system appears working its maximal capacity.

Excessive calcium levels are known to activate CaMKII and the phosphatase calcineurin that activate the fetal gene program (112). In line with this, RNA of typical fetal gene program genes (NPPB, NPPA and MYH7) are detectable in ChiPSC22 cardiomyocytes on day 33 of differentiation. The fetal gene program triggers cardiomyocyte remodeling into a hypertrophic phenotype (102, 113). In fact, ChiPSC22 wild-type cardiomyocytes showed an unpolar, roundish morphology with misaligned contractile filaments.

In the human heart, a limited capacity for calcium storage, induction of the fetal gene program and a hypertrophic phenotype occur in two major scenarios. One scenario is cardiomyocytes of the human embryonic heart. These cardiomyocytes show underdeveloped calcium handling, reduced contractility, short and unorganized myofibrils, a low density of adrenoreceptors and a round cellular morphology (120). Parallels to this scenario are not surprising given that the differentiation of hiPSC CMs should recapitulate the development of cardiomyocytes in the human embryonic heart. The other scenario is cardiomyocytes from the failing heart. This disease is characterized “by the inability of the heart to provide peripheral tissue with the required amount of blood and oxygen necessary for their metabolic processes” (7). Similar to ChiPSC22-derived cardiomyocytes, cardiomyocytes from the failing heart exhibit an increased duration of the calcium transient, a negative force-frequency relationship and accumulating diastolic calcium levels under high heart rates (96). Fusion of calcium transients at high frequencies as observed in ChiPSC22 cardiomyocytes occurs in hypertrophic cardiomyopathy. This leads to an increased end-diastolic tension and a decrease of active tension during contraction (96, 97). An increased

duration of the calcium transient is a result of lower SERCA activity and smaller SR calcium stores in HF (93). SR calcium storage also seems to be reduced in ChiPSC22 cardiomyocytes because ryanodine only modestly decreased calcium transient amplitude (Figure 14). However, SERCA activity seems to be in an overactive state in ChiPSC22-derived CMs. Cardiomyocytes from the human failing heart also exhibit disorganized t-tubules. Removal of RYR2 from the L-type calcium channel's proximity is thought to decouple calcium-induced calcium release (96, 121). Disorganization of the t-tubules is characteristic of hiPSC CMs. This was not directly verified in ChiPSC22. However, neither SERCA inhibition nor NCX inhibition completely abolished calcium transients under baseline or with pacing. This indicates that sarcolemmal and SR calcium cycling are indeed decoupled in this cell type. On the other hand, spontaneous and paced calcium transients were completely inhibited by 1 µM verapamil (Figure 14). This underlines the notion of L-type calcium channel-induced calcium release via RYR2. However, verapamil can also affect potassium channels at this concentration (122).

qPCR analysis of ChiPSC22 revealed that the HF-like phenotype of ChiPSC22 cardiomyocytes on day 33 is preceded by a strong expression of AC6 in early cardiomyocytes until day 25. Following day 25, AC6 expression was downregulated but AC5 expression was upregulated (Figure 12). This expression pattern was reminiscent of a mouse model of pressure overload-induced cardiomyopathy. In this model, aortic banding leads to left ventricular hypertrophy and subsequent HF (48). AC6 expression was high and AC5 expression was low before surgery. However, upon aortic banding, AC6 expression declined and AC5 expression increased.

5.2 Generation of a functional AC5- and AC6 KO in hiPSC CMs

The findings outlined above led to the hypothesis that AC5 and AC6 activity is causative or symptomatic to the development of a HF-like state in ChiPSC22-derived cardiomyocytes. To validate this hypothesis, a functional knockout of AC5 and AC6 was successfully performed in the ChiPSC22 cell line. *In silico* mutation of the catalytic site translated into the exact deletion on the RNA level in the CRISPR experiments (Figure 26). All protein coding isoforms were targeted with this deletion. Possible off-targets of CRISPR editing were not sequenced. However, most of these off-targets

were not flanked by a canonical CRISPR site and would only be targeted with several mismatches to the gRNA. A list of possible off-targets can be found in Table 1. No specific antibody was found in this PhD thesis for the detection of AC5 and AC6. Therefore, it was not possible to prove deletion on the protein level. Hence, the CRISPR deletion was explicitly designed in a way that makes translation of a catalytically active protein impossible based on the current state of research (103-105). Of course, effects of a truncated, catalytically inactive protein cannot be completely ruled out. The activation of non-canonical pathways was already shown for a catalytically inactive AC6 (57). However, the protein was completely intact except for a single point mutation. In this PhD thesis, only a truncated N- or C-terminus could theoretically be translated, depending on the start codon. Moreover, CRISPR deletion also led to a strong downregulation of the RNA transcript on day 33 of differentiation (Figure 29). This could also reduce the amount of protein. In future experiments, final proof for deletion on the protein level could be achieved by mass spectrometric analysis. Alternatively, detection by western blot could be possible. In this PhD thesis, differential restriction sites of hydroxylamine were identified in the AC5 and AC6 sequences. Hydroxylamine digest of AC6 would result in fragments of 5, 638 and 502 amino acids. In contrast, digest of AC5 would result in fragments of 6, 283, 357 and 575 amino. These fragments could be detected with an unspecific AC5/6 antibody. Based on the presence or absence of the fragments, one could distinguish between AC5 and AC6 protein.

Downregulation of AC5- and AC6 RNA transcripts is probably an effect of nonsense mediated decay, triggered by premature stop codons (108). Interestingly, knockout of AC6 also led to a downregulation of AC5 RNA levels. Stabilization of AC5 by AC6 was already described previously, however on the protein level (53). AC5 and AC6 are the major cardiac isoforms on day 33 of differentiation. AC6 KO CMs still exhibit a significant production of cAMP (Figure 31). This suggests that catalytical activity of AC5 is still present despite AC5 downregulation. On the other hand, knockout of AC5 led to a small upregulation of AC6. On day 25, AC5 KO CMs even exhibited higher cAMP levels than wild-type CMs. This suggests that AC5 KO is indeed catalytically compensated by AC6. However, this effect disappears on day 33 of differentiation at a time point at which most experiments were performed. These results suggest that AC5 transcription is activated by AC6. In contrast, AC6 expression is inhibited by AC5. This could also explain the expression of both isoforms throughout differentiation. AC6

expression is high from day 0 to day 25 of differentiation, which induces AC5 expression. Once AC5 expression increases, this leads to downregulation of AC6 following day 25. The transcriptional regulation is not dependent on cAMP levels because stimulation with isoprenaline did not alter the expression of AC5 or AC6 on day 33 (data not shown).

AC KO clones retained the expression of pluripotency markers (Figure 27). There were reports that discussed a function of ACs in maintaining pluripotency in stem cells (123). Apparently, AC5 and AC6 are not necessary for this function. A high expression of AC6 in early cardiomyocytes followed by expression of AC5 in more mature cardiomyocytes is completely in line with studies in rodents (45-47). Despite the early expression in cardiomyocytes, knockout of AC5 and AC6 did not influence the cardiomyocyte yield in the culture (Figure 28). However, each CRISPR clone required a specific ratio of CHIR99021 and BMP4 for efficient differentiation. There was a trend of slightly higher CHIR99021 and BMP4 levels for efficient differentiation of AC5- and AC6 KO clones. These results suggest that AC5 and AC6 do play a role in early cardiac differentiation but are dispensable for the differentiation of human cardiomyocytes. These findings are in line with the fact that genetic removal of either AC5 or AC6 KO is not lethal in mice (55, 63).

As expected, AC5- and AC6 KO cardiomyocytes were less responsive towards β-adrenoceptor stimulation on day 33. This effect was evident both on the enzymatic level (Figure 31) and on the functional level (calcium handling and phosphorylation of cTnI, chapter 4.3.7). This effect was stronger in AC6 KO CMs than in AC5 KO CMs. This fits with the higher expression level of AC6 compared to AC5 on this day. Phosphorylation of cTnI was analysed via the “Simple Western” method from ProteinSimple. The size of p-cTnI measured in this assay (~33 kDa) was larger compared to the predicted molecular weight of p-cTnI (~25 kDa). However, three different antibodies all produced a signal of 33 kDa (data not shown). According to the provider, molecular weights measured in Simple Western do not always reflect the size measured in western blot, for unknown reasons. Because of this, the signal detected is probably caused by phosphorylation of p-cTnI. Phosphorylation could be a result of increased PKA activity or increased PKC activity because both phosphorylate serine 23 and serine 24 (124), although altered counterregulating phosphatase activity could also contribute.

In both wild-type and KO cardiomyocytes, β-adrenoceptor signaling was mediated exclusively by β_2-adrenoceptor signaling: The β_2-selective inverse agonist ICI 118,551 reduced isoprenaline-stimulated cAMP levels in a concentration-dependent manner in wild-type and KO cardiomyocytes (Figure 33). In contrast, a β_1-selective antagonist CGP 20712 showed no consistent effect. In a Schild plot experiment, only the presence of ICI 118,551 led to a rightward shift of concentration-response relationship to isoprenaline. A β_1-selective agonist ICI118,587 did not lead to increased cAMP levels in any cell type. In addition, only RNA of the β_2-adrenoceptor was detectable in qPCR. These results are in line with Wu *et al.*, who showed that the β_2-adrenoreceptor is the predominant isoform in hiPSC CMs on day 30 of differentiation (125). These results also show that both AC5 and AC6 couple functionally to the β_2-adrenoceptor. Coupling of AC6 to the β_2-adrenoceptor contradicts Timofeyef *et al.,* who showed that in mice, AC6 only couples functionally to the β_1-adrenoceptor. In contrast, AC5 couples functionally to both the β_1- and β_2-adrenoceptor (50). However, Timofeyef *et al.* used a different readout ($I_{Ca,L}$). Timofeyef *et al.* also reported differential inhibition of AC5-β_2 complexes by phosphodiesterase (PDE) 3 and 4. This was not investigated in this PhD thesis: All cAMP-assays were performed in the presence of the pan-PDE inhibitor 0.5 mM 3-Isobutyl-1-methylxanthin to increase assay sensitivity.

5.3 CRISPR-mediated KO of AC5 and AC6 rescues the HF-like phenotype of hiPSC CMs

Interestingly, AC5- and AC6 KO cardiomyocytes did not show the HF-like phenotype of wild-type cardiomyocytes. In the absence of β-adrenoceptor stimulation, the basal calcium load was significantly reduced in AC5- and AC6 KO CMs (Figure 36). Most presumably, AC5 and AC6 increase the calcium load of the cells via activation of the $I_{Ca,L}$ current as reported by others (50). Baseline PWD90 was also significantly reduced in both KO clones. This was a result of both a reduced calcium transient decay time and time to peak. The negative force-frequency relationship was abolished in AC6 KO CMs (Figure 39). In baseline, application of the β_2-selective inverse agonist ICI 118,551 did not reduce calcium transient amplitude or PWD90 in wild-type CMs (Figure 42). This result suggests that high basal activity of AC5 and AC6 increases calcium load of cardiomyocytes independently of β-adrenoceptor stimulation. Apparently, baseline AC

signaling is decoupled from β-adrenoceptors. The notion of baseline AC activity is supported by the fact that AC6 KO CMs also showed smaller basal cAMP levels than the wild-type at all time points of differentiation. Although the latter did not show statistical significance, the detection of low cAMP levels is limited by the sensitivity of the assay (Chapter 3.13). Therefore, basal cAMP level in AC6 KO CMs could be in reality even smaller. In addition, the low concentration range of baseline cAMP levels is most crucial to the modulation of calcium transients. On day 33 of differentiation, isoprenaline stimulated cAMP synthesis with an EC_{50} of about 174 nM in wild-type CMs (chapter 4.3.4). In contrast, calcium transients were modulated by isoprenaline with EC_{50} values of only about 0.1 nM (Figure 34). This suggests that low cAMP levels can strongly influence calcium transients. However, all cAMP assays were performed in the presence of a pan-PDE inhibitor. In contrast, calcium imaging was performed in the absence of this inhibitor. This could also explain the discrepancy between normal basal AC5 activity in the cAMP assay and high basal AC5 activity in the calcium imaging assay. Further work should address the potential role of different PDEs.

Several factors could explain the improved basal calcium transient kinetics in AC5- and AC6 KO cardiomyocytes. AC5 KO CMs exhibited a higher basal phosphorylation of cTnI (Figure 35). This effect was even stronger in AC6 KO CMs. Enhanced baseline phosphorylation of cTnI reduces the affinity of myofilaments for calcium. As a result, more free intracellular calcium is available for transport via SERCA and NCX, resulting in accelerated relaxation (111). Increased basal phosphorylation of cTnI in AC KO clones is counterintuitive because AC KO should lead to reduced basal PKA activity. However, KO of AC6 also resulted in increased expression of cTnI on the RNA level (Figure 37). Increased abundance of cTnI could also lead to increased basal levels of phosphorylated cTnI. Unfortunately, protein levels of unphosphorylated cTnI could not be detected accurately because the antibody did not allow quantification. AC5 and AC6 KO could also increase basal cTnI phosphorylation by inhibition of phosphatase activity. For example, Tang *et al.* reported increased phosphorylation of PLN and a lower activity of PP1 in AC5 KO mice (62).

The activity of NCX was not investigated in this thesis. Thus, an increased NCX expression or altered expression of ion channels in AC5- and AC6 KO cardiomyocytes might also contribute to the accelerated kinetics of calcium transients. However, the expression of NCX and calcium channels was unchanged in wild-type and KO clones

(Figure 37). Structural differences might also influence calcium transient kinetics. The cell area of wild-type CMs was larger and the cells were significantly rounder than the knockout CMs in a high content assay (Figure 40). Cell size is linear to membrane capacitance (126). Increased membrane capacitance leads to slower action potential propagation (127). The large cell size of wild-type cardiomyocytes must lead to slower impulse propagation. This would also result in slower calcium propagation to the cell center. A slower calcium wave would be the result. It was also shown that a round cell shape can lead to increased calcium load of osteoclast compared to elongated cell shapes (128). This might also apply to ChiPSC22 wild-type cardiomyocytes. Theoretically, the rounder and larger cell shape of wild-type cardiomyocytes should also increase the distance between RYR2 and L-type calcium channels. This would slow down calcium-induced calcium release. A reduced baseline calcium transient amplitude in AC5- and AC6 KO clones might be also a result of decreased phosphorylation of RYR2 and L-Type calcium channels. These questions should be investigated in subsequent work. Accelerated calcium cycling could also be a consequence of the smaller calcium transient amplitude. The two transport mechanisms responsible for calcium decay (SERCA and NCX) have a maximal transport capacity that limits the transport rate. From this standpoint, the transport of smaller levels of calcium is probably faster than the transport of high levels of calcium. On the other hand, higher calcium transient amplitudes would also result in higher concentration gradients between cytosolic calcium and extracellular- and SR calcium. This gradient could improve transport of calcium by SERCA and could have bimodal effects on calcium influx and efflux via NCX. In fact, compounds that reduced calcium transients (verapamil and nifedipine) had no effect on PWD90 in ChiPSC22 wild-type CMs (data not shown).

The larger cell size and larger cell width/cell length ratio of wild-type cardiomyocytes is reminiscent of myocytes from HFpEF patients. The heart of these patients develops concentric hypertrophy with an increase of the relative wall thickness. This is caused in part by hypertrophy of cardiomyocytes. These cardiomyocytes grow in the transverse direction while the cell length remains constant leading to a roundish cell shape (129). In line with this, wild-type cardiomyocytes showed increased expression of fetal genes MYH7, NPPB and NPPA (Figure 40). These are reportedly active during hypertrophic remodeling of cardiomyocytes (102, 113). In fact, stimulation with a pro-hypertrophic compound (endothelin-1) further increased NPPA, NPPB and MYH7

expression in wild-type cardiomyocytes but not in AC5/AC6 KO cardiomyocytes. Under all conditions, MYH6 expression was smaller in wild-type cells compared to AC5 KO cells. MYH6 and MYH7 are both expressed in adult atrium and ventricle. However, MYH6 is more abundant in the atrium and MYH7 is more abundant in the ventricle. During HF, the ratio of MYH6/MYH7 becomes smaller in both atrium and ventricle (116, 117). In this regard, wild-type cells resembled cardiomyocytes from HF patients. MYH7 encodes the β-myosin heavy chain that is slower than the α-myosin heavy chain (130). Upregulation of MYH7 in wild-type cells might also be an adaption to the slower calcium transients. Wild-type cell size was not significantly increased when analyzed via FACS (Figure 40). In contrast to high content analysis, flow cytometric analysis via forward scattered light measures three-dimensional cell size. Thus, it seems that wild-type cardiomyocytes are only larger in the two-dimensional plane. On the other hand, only three biological replicates were measured in the FACS assay. Thus, this issue requires further verification with a larger sample size.

The observed effects were always stronger in AC6 KO CMs compared to AC5 KO CMs. AC6 accounts for the majority of cAMP production on day 33 (Figure 31). Thus, it is likely that cAMP is responsible for excessive calcium load, delayed calcium transient kinetics and the hypertrophic phenotype of wild-type cells, although it is unclear whether the cAMP-mediated effects are acute effects or long-term effects. As mentioned earlier, ChiPSC22 CMs exhibited a high degree of variability in calcium handling. Most differentiations had slow calcium transients but some outliers showed faster calcium transients that were comparable to KO clones. Interestingly, these outliers appeared also less responsive to isoprenaline. In addition, older wild-type cardiomyocytes (day 50) also showed improved calcium transient kinetics. These results suggest that variability in the KO differentiations was a result of different degrees of maturation. It also suggests that improved calcium transient kinetics in AC-KO clones is a result of improved maturation. The lower baseline expression of fetal genes in the AC KO clones supports this notion. Thus this possible maturation effect should be considered when interpreting the results of this thesis. Also, different CHIR99021 and BMP4 amounts were necessary for the differentiation of the different clones. In general, knockout clones required higher amounts of these growth factors. Thus, it could also be that the observed effects are a result of the different concentrations of CHIR99021 and BMP4 during early development. Another caveat of

this thesis is that possible CRISPR off-targets were not validated (Table 1). It is possible that CRISPR editing of other genes leads to the observed effects. However, off-targets were predicted to be very unlikely because CRISPR editing of all possible off-targets would require mismatching of gRNAs and sometimes even usage of a non-canonical PAM sequence by the Cas9 protein. The process of clonal isolation could also be responsible for the different behavior of knockout clones.

To circumvent these experimental problems, it would be admirable to perform AC5 KO and AC6 KO in already differentiated cells and in the same clonal cell line. Having created AC5- and AC6 KO cell lines, the next step would be to supplement the cells with an inducible copy of AC5 and AC6. After a second round of clonal isolation, the inducible AC5- and AC6 KO hiPSC clones would be isolated. The inducible clones would then be differentiated into cardiomyocytes. Throughout differentiation, the inducible genes could be titrated to the endogenous expression level of wild-type cells. This would be feasible when using a doxycycline-inducible promoter. To analyze the immediate effect of an AC5- or AC6 KO, doxycycline would be removed from the culture. To achieve this goal, different ways of gene transfer into the AC5 KO and AC6 KO cell lines were compared (CRISPR knock-in, lentivirus, transposases). CRISPR- and lentivirus-based techniques worked extremely well in HEK 293 cells. Unfortunately, these techniques were not amenable for hiPSCs. Preliminary experiments using a transposase suggest that stable integration of AC5 and AC6 into AC5 KO and AC6 KO cell lines would be feasible (data not shown).

Since testing of these inducible cell lines was not possible in the time frame of this PhD thesis the dissection of the cAMP-dependent from maturation-dependent effects was performed with an AC inhibitor in wild-type cardiomyocytes. BAY 1232055 was initially discovered in a biochemical high-throughput screen for the identification of AC5 inhibitors conducted by Dr. Adrian Tersteegen (internal communication). Dr. Mark Meininghaus validated AC inhibition in commercially available human embryonic stem cell-derived cardiomyocytes (internal communication). In this PhD thesis, inhibition of isoprenaline-stimulated cAMP levels by BAY 1232055 produced comparable IC_{50} values in wild-type- and AC5 KO CMs (Figure 41). This suggests that the compound is non-selective for AC5 or AC6. Short-term inhibition of ACs (3 minutes incubation) by BAY 1232055 protected wild-type CMs from excessive calcium levels. This effect was very similar to CRISPR-mediated KO of AC5 or AC6. The concentration-dependent

effect occurred between 1 µM and 30 µM of BAY 1232055. This is also the concentration range where isoprenaline-stimulated cAMP levels are inhibited by the compound. Similar to CRISPR-mediated KO of ACs, BAY 1232055 also reduced PWD90 in wild-type cardiomyocytes. However, this effect might not be specific to AC inhibition because it only occurred at a BAY 1232055 concentration of 30 µM. On the other hand, 30 µM was necessary for maximal inhibition of isoprenaline-mediated AC activity. BAY 1232055 concentrations between 3 µM and 30 µM also protected wild-type cardiomyocytes from fused calcium transients during pacing with 1 Hz. A reduction of the PWD90 only occurred at 30 µM BAY 1232055. This suggests that a smaller calcium load alone protects cardiomyocytes from fused calcium transients. Similar to AC knockout, incubation of wild-type CMs with 30 µM BAY 1232055 for only 24 hours also attenuated endothelin-1-mediated BNP expression. Cell size was also significantly reduced in wild-type CMs treated with 30 µM BAY 1232055 for 24 hours. These results suggest that the effects of CRISPR-mediated knockout of AC are also directly caused by diminished AC activity. Interestingly, these effects occurred at baseline with no β-adrenoceptor stimulation. This validates that there is high level of basal AC signaling, uncoupled from β-adrenoceptor activity. Different degrees of maturation cannot be the sole explanation for the different phenotype of wild-type and KO cardiomyocytes. It seems that AC inhibition has short-term effects that reduced the calcium load of the cell and long-term effects that prevent development of a hypertrophic phenotype. The reduction of calcium transient duration by BAY 1232055 was not very prominent. The reduced calcium transient duration in AC-KO clones might therefore be a long-term effect of AC inhibition. It would be important to investigate whether the reduction of the calcium transient duration by BAY 1232055 will be more prominent with long-term drug incubation. If BAY 1232055 enhances cTnI phosphorylation, this would unmask cTnI as the factor responsible for long-term effects on calcium kinetics. In the end, BAY 1232055 should also be tested in AC KO CMs. If the effects are specific to ACs, the effect should be attenuated in the AC KO clones.

Together, these results support the hypothesis that AC5 and AC6 are causative for the development of a HF-like phenotype of ChiPSC22 cardiomyocytes. Knockout of AC5 and AC6 both rescue this phenotype. Based on these findings, the following working model of an AC-driven HF is proposed (Figure 43A). In hiPSC CMs, $G\alpha_s$-AC activity is partly uncoupled from β-adrenoceptor activity. Activation of calcium channels by uncontrolled AC-PKA signaling pathways leads to excessive cardiomyocyte calcium

load. Initially, this is compensated by upregulation of intracellular calcium stores and downregulation of β_1-adrenoceptors, which eliminates the positive inotropic effect of β-agonists. Despite downregulation of the β_1-adrenoceptor, diastolic calcium levels remain high and activate the pro-hypertrophic calcineurin/CaMKII pathway. This initiates the fetal gene program, ultimately leading to concentric hypertrophy of cardiomyocytes. Alternatively, high AC signaling could also induce hypertrophy by activation of EPAC-driven pathways (39-42). Calcium handling further deteriorates due to unfavorable cell shape and reduced cTnI phosphorylation. Slow calcium wave propagation leads to interrupted and fused calcium transients, particularly at high heart frequencies. This might lead to incomplete relaxation during diastole, a phenotype which is reminiscent of HFpEF.

5.4 Possible implications for HF treatment

Provided that these mechanisms can be translated to the patient's situation, it is conceivable that modulation of the AC pathway with small molecules could be a potential therapeutic approach for both HFrEF and HFpEF. HFrEF is already treated with β-adrenoceptor inhibitors (9). Therefore, one would suggest that AC inhibition would also be beneficial for the treatment of HFrEF. In fact, inhibition of AC5 and AC6 prevents the initiation of a fetal gene program that is characteristic of hypertrophic remodeling during HFrEF progression. Even though β-blockers are an established effective therapy for HFrEF, they have unfavourable effects in many patient populations (e.g. patients with COPD and diabetes, 131, 132). An AC inhibitor could be a good alternative for these patients. With progression of HF, β-adrenoceptors and $G\alpha_s$ proteins decouple (reviewed in (133)). An AC inhibitor could still target the AC signaling pathway even in the absence of a β-adrenoceptor. On the other hand, inhibition of AC5 and AC6 also reduced calcium transient amplitude. This negative inotropic effect could further impair contractility in HFrEF patients. However, β-blockers share this characteristic and are despite this effect clinically effective (96), making it very likely that this could apply for potential AC inhibitors as well.

A therapy with AC inhibitors could be a potential therapeutic option for patients with HFpEF. Even though HFpEF is traditionally not linked to overactivity of the sympathetic nervous system, the data from ChiPSC22 CMs suggest that inhibition of AC5 and AC6

could be a new strategy for the treatment of this disease. Genetic elimination of AC5 and AC6 rescued hiPSC CMs from concentric hypertrophy, which is key characteristic of HFpEF (129). AC5- and AC6 KO also accelerated calcium transient kinetics and prevented the fusion of calcium transients at high frequencies. Fusion of calcium transients and a slow calcium transient decay lead to incomplete relaxation of the heart muscle which is also typical for HFpEF (96, 97). As a result, inhibition of AC5 and AC6 could improve relaxation of the heart muscle and improve filling of the left ventricle in HFpEF. Interestingly, β-blockers failed to show a beneficial effect in HFpEF in clinical settings (134). One possible explanation could be that β-blockers could also inhibit the anti-apoptotic effect of the β_2-adrenoceptor. The anti-apoptotic effect of the β_2-adrenoceptor is caused by activation of $G\alpha_i$ proteins, followed by phosphatidylinositol 3-kinase and Akt activation (13). Apoptosis of cardiomyocytes is crucial in the progression of HFpEF (14). Another possible explanation is that there is no clear overactivity of the SNS in HFpEF that could be inhibited by β-blockers (15). However, this PhD thesis provided evidence that basal AC activity is already sufficient to induce a HFpEF-like phenotype in human cardiomyocytes. Reduction of basal AC activity by an AC inhibitor could be a completely new strategy for the treatment of HFpEF. Most importantly, anti-apoptotic signaling of the β_2-adrenoceptor would not be inhibited because inhibition occurs downstream of the receptor and the anti-apoptotic effect is independent of ACs. Currently, there are no successful treatment options for HFpEF. β-blockers and RAAS inhibitors failed to improve the health status of patients suffering from HFpEF (134). Thus, successful AC inhibitors will address a high unmet medical need. A pharmacological intervention of an AC inhibitor is illustrated in Figure 43B.

To sum up, pharmacological inhibition of AC5 and AC6 could be a viable strategy for the treatment or prevention of HF. The characterization of an AC5/AC6 inhibitor (BAY 1232055) in this PhD thesis supports this notion. In previous studies, BAY 1232055 did not improve cardiac performance in rodent hearts and the optimization of this compound was halted (internal communication). In addition, the AC5 inhibitor BAY 1232055 showed no selectivity over AC6 and inhibition of AC6 could be detrimental to the heart. This assumption was made based on rodent studies that showed cardioprotective effects of AC6 (see introduction). However, it is possible that BAY 1232055 improves cardiac performance in the human heart even though there is no effect in the rodent heart. At the same time, selectivity over AC6 might not be necessary as supported by the current findings.

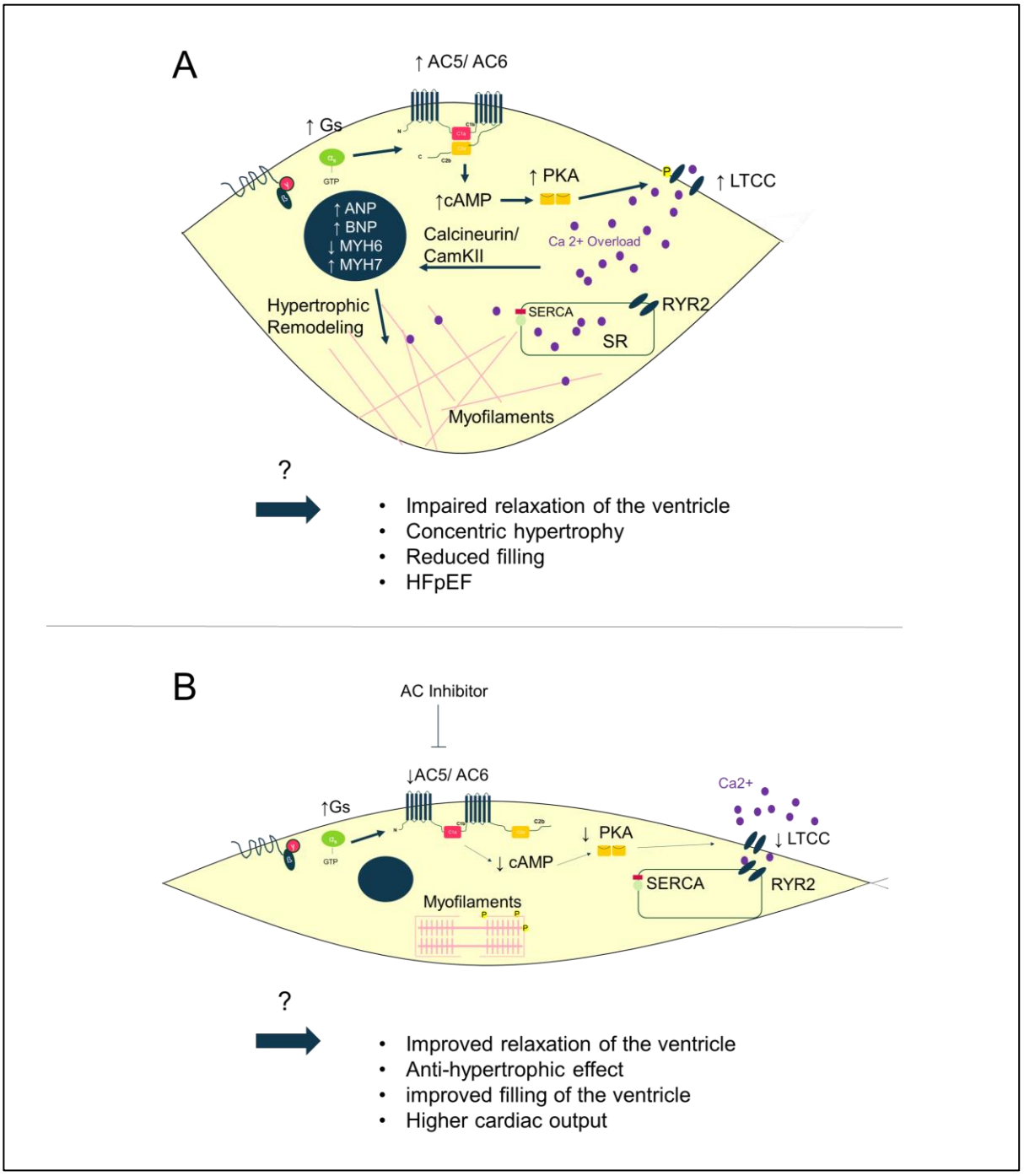

Figure 43: Proposed working model of AC5/AC6-driven HFpEF and small molecule modulation of the pathway.

A: Uncoupling of β-adrenoceptors leads to high basal $G\alpha_s$ activity that activates AC5 and AC6. High catalytic activity of AC5/AC6 leads to a strong cAMP signal that activates PKA. PKA phosphorylates L-type calcium channel (LTCC), which leads to elevated calcium levels that cannot be buffered by the SR. Excessive cardiomyocyte calcium levels activate calcineurin/CaMKII, which induce the fetal gene program. This leads to hypertrophic remodeling. Hypertrophy leads to spatial separation of RYR2 and LTCC. Together, this could have mechanical effects on the heart. B: Application of an AC inhibitor reduces AC5 and AC6 catalytic activity despite high basal $G\alpha_s$ activity. Consequently, cAMP levels and PKA activity are low. This results in a smaller influx of calcium that can be buffered by intracellular calcium stores. Under low calcium levels, there is no activity of calcineurin or CaMKII, and no activation of the fetal gene program and no hypertrophic remodeling occur. Upon AC elimination, the basal phosphorylation of cTnI is elevated by an unknown pathway. The anti-hypertrophic effect, improved calcium handling and elevated phosphorylation of cTnI could improve cardiac output.

5.5 Comparison to previous findings

The current findings are in line with results from AC5 KO mice. In this animal model, AC5 KO protects the heart from hypertrophic remodeling and a HFrEF-like phenotype after aortic banding (63). Likewise, AC5 KO protected hiPSC CMs from hypertrophic remodeling. AC5 KO mice also exhibit an increased LV +dP/dt (62). Reduced time to peak of the calcium transient in AC5 KO hiPSC CMs suggest that AC5 KO could also increase LV +dP/dt in human hearts. AC5 KO mice also exhibit a higher left ventricular pressure. Uncomplete calcium transients were observed in paced wild-type cardiomyocytes. Uncomplete calcium transients result in smaller amplitudes that could reduce left ventricular pressure in the human heart. AC5 KO prevented uncomplete calcium transients, which could increase the left ventricular pressure in the human heart. On the other hand, AC5 KO cardiomyocytes showed smaller calcium transient amplitude than wild-type cells under spontaneous beating.

What differences exist between the AC6 KO hiPSC model from this study and rodent AC6 KO models? The AC6 KO mouse generated by Tang *et al*. showed reduced LV pressure, reduced LV +dP/dt and -dP/dt under baseline conditions and stimulation with a β-adrenoceptor agonist (53). The smaller pressure of the ventricle and the lower contractility and slower relaxation might have been a result of aberrant calcium handling in these cells. Isolated cardiomyocytes from this study showed smaller SR calcium stores and slower calcium uptake in the SR. Slower calcium handling might be a result of increased PLN phosphorylation in isolated cardiomyocytes from AC6 KO mice. AC6 KO did not affect basal cAMP levels and reduced isoprenaline stimulated cAMP levels to 58% of control value.

In contrast, AC6 KO hiPSC CMs showed accelerated calcium handling in this PhD thesis. One explanation for this inconsistency could be that Tang *et al*. only investigated SR calcium handling. However, SR calcium stores do not play an important role in this hiPSC CMs. In addition, PLN is not detectable at the protein level. Thus, possible effects of AC6 KO on SR calcium handling by phosphorylation of PLN could be missed in the current work. In addition, AC6 KO accelerated whole cell calcium transients presumably by increased basal phosphorylation of cTnI, increased sarcolemmal calcium cycling and improved cell morphology. Thus, AC6 KO improves calcium cycling in a situation when SR calcium cycling is diminished. Diminished SR

calcium cycling is a hallmark of HF (93). Thus, AC6 KO could improve calcium handling in a disease state. In contrast, Tang *et al.* looked at the effects of AC6 KO in healthy cardiomyocytes only.

Later studies investigated the effect of AC6 activation in a HF-like state (135). Interestingly, AC6 activation did not alter calcium handling in this study. On the other hand, cardiac contractility and cTnI phosphorylation were increased by AC6 activation. These effects are not consistent to this PhD thesis where KO of AC6 in hiPSC CMs increased basal cTnI phosphorylation. In the end, this hiPSC model investigated the prevention of HF by AC6 KO while Lai *et al.* investigated the effect of AC6 in pre-existing HF. Thus it is possible that inhibition of AC6 activity could prevent HF, whereas once HF is already established activation of AC6 could be of therapeutic value. This hypothesis should be tested in future studies.

The inconsistent data between humans and rodents could also result from differences in physiology. For example, the mouse heart is approximately 1500-fold smaller and the heart rate is about 10-fold higher than that of the human heart (2). AC5/AC6 elimination mainly improved calcium transient kinetics. Studying calcium transient kinetics in a heart that beats 10 times faster than the human heart is unlikely to translate into the human background. Next to anatomical differences, human and rodent cardiomyocytes have many differences on the molecular level. For example, it is commonly accepted that the most important human ion channel for repolarization of the action potential, $K_v11.1$, is absent in mice. The experiments using BAY 1232055 suggest that the compound could improve relaxation of the heart via accelerated calcium transient decay. A completely different type of repolarization and relaxation in mouse hearts could conceal this effect. AC isoforms show strong paralogous conservation within a species. However, there is a lower degree of interspecies conservation of the same AC isoform (analysis via multiple sequence alignment of AC5, AC6 in human and rodent hearts, data not shown). Because of the different amino acid sequence, AC6 could have different effects in the human than in the rodent heart. This could potentially explain why cardioprotective effects of AC6 are reported in rodents while AC6 seems to be rather detrimental in this hiPSC model. This may also explain why a human phase 2 study for gene transfer of AC6 in HF patients does not proceed for years (60).

It is an open question which factor is the major determinant of the different effect of AC6 in the mouse and the human. A different physiology of the two model systems or a different sequence of human and mouse AC6? This question can be answered by overexpressing the murine AC6 sequence in hiPSC CMs and compare this effect to overexpression of the human AC6 sequence. According to the present results, overexpression of the human AC6 sequence should induce a HF-like phenotype (slow calcium kinetics, fused calcium transients, hypertrophy). If the murine AC6 sequence shows a different effect, this must be sequence-dependent because the physiology of the model is the same.

5.6 Bridging conflicting results from animal and human study

The inconsistence between rodent data and the data from this hiPSC model, if validated in future work, open also ethical questions. Is it approprite to proceed with the development of a drug in humans without showing an effect in animal models? Or is it ethically correct to withdraw the development of a drug that could possibly improve the life of patients? Until now, there is no legal basis for drug development without animal testing. The solution to this dilemma could be more advanced hiPSC-based models like engineered heart tissue (136). By arranging hiPSC CMs in a three-dimensional pattern, this model tries to mimic the physical and hemodynamic forces in the heart. It also allows direct measurement of mechanical force during contraction. Until now, the favorable effect of AC inhibition on cellular structure and calcium handling was only tested in a two-dimensional hiPSC CM format. In the next step, AC inhibition should be tested in engineered heart tissue. This would reveal if the effects really translate into better contractility and relaxation of human heart tissue. From a legal standpoint, animal testing would still be necessary before proceeding to testing in patients. However, one could directly test the compound in animal models with physiologies more similar to that of humans like pigs or monkeys. Thereby the lives of rodent animals can be spared.

In any case, optimization of BAY 1232055 is necessary. This compound shows comparable potency compared to reports of the commercially available AC inhibitors SQ22,536, NKY80 and Ara-A tested in membrane extracts from HEK 293 cells (137). However, in this PhD thesis, no inhibition of AC activity in hiPSC CMs was detectable

by SQ22,536, NKY80, or Ara-A (data not shown). This is probably because of low cell permeability of the compounds. Thus, cell permeability of BAY 1232055 seems already to be sufficient. The low potency of BAY 1232055 might rather be a common characteristic of AC inhibitors. Low potency of AC inhibitors is problematic because other ATP binding enzymes might also be targeted. Many P-site inhibitors are nucleoside-based. A possible off-target effect of nucleoside based inhibitors could be interference with DNA synthesis and purine metabolism (138) and interactions with PDEs are also conceivable. The CRISPR-mediated KO cell lines developed here could be used for optimization of BAY 1232055 and the identification of new AC inhibitors in a high-throughput screening. A requirement would be upscaling of the differentiation because here significant batch-to-batch differences were observed. The first step of the screening cascade would be identification of new hits in a primary screen of wild-type cardiomyocytes in a cAMP HTRF assay. In the second step, the hits could be validated in CRISPR-mediated KO cells. If the activity of the compound persists in these cells, it is probably a false positive hit. Comparison of IC_{50} values of wild-type, AC5- and AC6 KO CMs would also allow determination of selectivity of the compound. Selectivity should also be determined over non-cardiac ACs. Differentiation of hiPSCs into different organ types could also be used to assess possible side effects of AC5 or AC6 inhibition. Safety testing in hiPSC-derived neurons would be particularly interesting because the brain shows a particularly high expression of AC5 (GTEx portal). *De novo* gain of function mutations of AC5 were also linked to a neurological disease called familial dyskinesia with facial myokymia (139, 140). The compound BAY 1232055 as a rather hydrophobic compound would probably pass the blood-brain barrier, so side effects on neurons must be closely evaluated. The third step in the screening cascade would then be testing in engineered heart tissue. For this purpose, the already generated knockout hiPSC clones could be used as well.

6 Limitations

Some experiments were conducted with only three independent biological replicates sampled on three different days (N=3). This includes all qPCR- and cAMP assays and one Simple Western assay. The low replicate number resulted in non-parametrical testing with low statistical power. In these analyses, a *p*-value = 0.1 was considered a clear trend. Future experiments with higher sample numbers are required to verify that the effects are significant.

7 Summary and future perspectives

This work identified and established AC5 and AC6 activity as a potential new disease mechanism in HFpEF. Targeting these pathways might be a new therapeutic option for a disease with high unmet medical need. The hiPSC model uncovered AC5- and AC6 dependent effects that were not observed in animal models. Thus, the usage of hiPSC CMs could save animal lives by concentrating on the relevant species. However, further studies are necessary to validate the findings from this PhD thesis. An effect of AC5- and AC6 KO on cardiomyocyte maturity could not be completely out ruled. The development of inducible CRISPR-mediated KO cell lines and the measurement in more complex cellular assays like engineered heart tissue could help to resolve these concerns. CRISPR-mediated KO of AC5 and AC6 in hiPSC CMs accurately predicted the effect of a small molecule with AC5 and AC6 inhibitory properties. Prediction of the effects of this drug before high-throughput screening could save resources and time in the drug development process. A new screening cascade for more potent AC5/AC6 inhibitors could be set up with the AC5- and AC6 KO clones. Primary and secondary screens, safety pharmacology and 3D model would be possible thanks to the versatile differentiation possibilities of the generated KO clones. Thus, optimization of BAY 1232055 for the treatment of HFpEF could be pursued if desired.

8 References

1. Silbernagl S. Physiologie: Funktion des Lebendigen. In: Pape H-C, Kurtz A, Silbernagl S, editors. Physiologie. 8., unveränderte Auflage ed: Georg Thieme Verlag; 2018.
2. Liu J, Laksman Z, Backx PH. The electrophysiological development of cardiomyocytes. Advanced drug delivery reviews. 2016;96:253-73.
3. Klöcker N, Piper H-M. Herzerregung. In: Brandes R, Lang F, Schmidt RF, editors. Physiologie des Menschen: mit Pathophysiologie. Berlin, Heidelberg: Springer Berlin Heidelberg; 2019. p. 187-98.
4. Xie A, Zhou A, Liu H, Shi G, Liu M, Boheler KR, et al. Mitochondrial Ca^{2+} flux modulates spontaneous electrical activity in ventricular cardiomyocytes. PloS one. 2018;13(7):e0200448-e.
5. Daut J. Herzmechanik. In: Brandes R, Lang F, Schmidt RF, editors. Physiologie des Menschen: mit Pathophysiologie. Berlin, Heidelberg: Springer Berlin Heidelberg; 2019. p. 165-86.
6. Hamlin RL, del Rio C. dP/dtmax — A measure of 'baroinometry'. Journal of Pharmacological and Toxicological Methods. 2012;66(2):63-5.
7. Tanai E, Frantz S. Pathophysiology of Heart Failure. Comprehensive Physiology. 2015;6(1):187-214.
8. Ferrari R, Böhm M, Cleland JG, Paulus WJ, Pieske B, Rapezzi C, et al. Heart failure with preserved ejection fraction: uncertainties and dilemmas. European journal of heart failure. 2015;17(7):665-71.
9. Bloom MW, Greenberg B, Jaarsma T, Januzzi JL, Lam CSP, Maggioni AP, et al. Heart failure with reduced ejection fraction. Nature reviews Disease primers. 2017;3:17058.
10. Williams DM, Evans M. Are SGLT-2 Inhibitors the Future of Heart Failure Treatment? The EMPEROR-Preserved and EMPEROR-Reduced Trials. Diabetes therapy : research, treatment and education of diabetes and related disorders. 2020;11(9):1925-34.
11. Butler J, Lam CSP, Anstrom KJ, Ezekowitz J, Hernandez AF, O'Connor CM, et al. Rationale and Design of the VITALITY-HFpEF Trial. Circulation Heart failure. 2019;12(5):e005998.
12. El-Armouche A, Eschenhagen T. β-Adrenergic stimulation and myocardial function in the failing heart. Heart Failure Reviews. 2008;14(4):225.
13. Zhu WZ, Zheng M, Koch WJ, Lefkowitz RJ, Kobilka BK, Xiao RP. Dual modulation of cell survival and cell death by beta(2)-adrenergic signaling in adult mouse cardiac myocytes. Proceedings of the National Academy of Sciences of the United States of America. 2001;98(4):1607-12.
14. Simmonds SJ, Cuijpers I, Heymans S, Jones EAV. Cellular and Molecular Differences between HFpEF and HFrEF: A Step Ahead in an Improved Pathological Understanding. Cells. 2020;9(1):242.
15. Verloop WL, Beeftink MMA, Santema BT, Bots ML, Blankestijn PJ, Cramer MJ, et al. A systematic review concerning the relation between the sympathetic nervous system and heart failure with preserved left ventricular ejection fraction. PloS one. 2015;10(2):e0117332-e.
16. Tesmer JJ, Sunahara RK, Gilman AG, Sprang SR. Crystal structure of the catalytic domains of adenylyl cyclase in a complex with Gsalpha.GTPgammaS. Science (New York, NY). 1997;278(5345):1907-16.
17. Dessauer CW, Watts VJ, Ostrom RS, Conti M, Dove S, Seifert R. International Union of Basic and Clinical Pharmacology. CI. Structures and Small Molecule Modulators of Mammalian Adenylyl Cyclases. Pharmacological reviews. 2017;69(2):93-139.
18. Halls ML, Cooper DMF. Adenylyl cyclase signalling complexes - Pharmacological challenges and opportunities. Pharmacology & therapeutics. 2017;172:171-80.
19. Dessauer CW, Tesmer JJ, Sprang SR, Gilman AG. Identification of a Gialpha binding site on type V adenylyl cyclase. The Journal of biological chemistry. 1998;273(40):25831-9.
20. Wei JW, Wang MC. Muscarinic M2 receptors coupled to inhibition of adenylate cyclase in rat heart. The Chinese journal of physiology. 1990;33(4):315-27.
21. Katada T. The inhibitory G protein G(i) identified as pertussis toxin-catalyzed ADP-ribosylation. Biological & pharmaceutical bulletin. 2012;35(12):2103-11.

22. Zhu WZ, Zheng M, Koch WJ, Lefkowitz RJ, Kobilka BK, Xiao RP. Dual modulation of cell survival and cell death by beta(2)-adrenergic signaling in adult mouse cardiac myocytes. Proceedings of the National Academy of Sciences of the United States of America. 2001;98(4):1607-12.
23. Hanlon CD, Andrew DJ. Outside-in signaling – a brief review of GPCR signaling with a focus on the Drosophila GPCR family. Journal of Cell Science. 2015;128(19):3533-42.
24. Kamp TJ, Hell JW. Regulation of cardiac L-type calcium channels by protein kinase A and protein kinase C. Circulation research. 2000;87(12):1095-102.
25. Marx SO, Reiken S, Hisamatsu Y, Jayaraman T, Burkhoff D, Rosemblit N, et al. PKA phosphorylation dissociates FKBP12.6 from the calcium release channel (ryanodine receptor): defective regulation in failing hearts. Cell. 2000;101(4):365-76.
26. Kiss E, Edes I, Sato Y, Luo W, Liggett SB, Kranias EG. beta-Adrenergic regulation of cAMP and protein phosphorylation in phospholamban-knockout mouse hearts. The American journal of physiology. 1997;272(2 Pt 2):H785-90.
27. Furukawa Y, Wallick DW, Martin PJ, Levy MN. Chronotropic and dromotropic responses to stimulation of intracardiac sympathetic nerves to sinoatrial or atrioventricular nodal region in anesthetized dogs. Circulation research. 1990;66(5):1391-9.
28. Joyner RW, Kumar R, Wilders R, Jongsma HJ, Verheijck EE, Golod DA, et al. Modulating L-type calcium current affects discontinuous cardiac action potential conduction. Biophysical journal. 1996;71(1):237-45.
29. Lampe PD, Lau AF. The effects of connexin phosphorylation on gap junctional communication. The international journal of biochemistry & cell biology. 2004;36(7):1171-86.
30. Campbell AS, Johnstone SR, Baillie GS, Smith G. β-Adrenergic modulation of myocardial conduction velocity: Connexins vs. sodium current. Journal of molecular and cellular cardiology. 2014;77:147-54.
31. Simmerman HK, Jones LR. Phospholamban: protein structure, mechanism of action, and role in cardiac function. Physiological reviews. 1998;78(4):921-47.
32. Bers DM. Cardiac excitation-contraction coupling. Nature. 2002;415(6868):198-205.
33. Zhang YH, Hancox JC. Regulation of cardiac Na^{+}-Ca^{2+} exchanger activity by protein kinase phosphorylation--still a paradox? Cell Calcium. 2009;45(1):1-10.
34. Piccini I, Fehrmann E, Frank S, Muller FU, Greber B, Seebohm G. Adrenergic Stress Protection of Human iPS Cell-Derived Cardiomyocytes by Fast Kv7.1 Recycling. Frontiers in physiology. 2017;8:705.
35. Marx SO, Kurokawa J, Reiken S, Motoike H, D'Armiento J, Marks AR, et al. Requirement of a Macromolecular Signaling Complex for β Adrenergic Receptor Modulation of the KCNQ1-KCNE1 Potassium Channel. Science (New York, NY). 2002;295(5554):496-9.
36. Schinner C, Vielmuth F, Rotzer V, Hiermaier M, Radeva MY, Co TK, et al. Adrenergic Signaling Strengthens Cardiac Myocyte Cohesion. Circulation research. 2017;120(8):1305-17.
37. DiFrancesco D, Tortora P. Direct activation of cardiac pacemaker channels by intracellular cyclic AMP. Nature. 1991;351(6322):145-7.
38. Alig J, Marger L, Mesirca P, Ehmke H, Mangoni ME, Isbrandt D. Control of heart rate by cAMP sensitivity of HCN channels. Proceedings of the National Academy of Sciences of the United States of America. 2009;106(29):12189-94.
39. Cheng X, Ji Z, Tsalkova T, Mei F. Epac and PKA: a tale of two intracellular cAMP receptors. Acta biochimica et biophysica Sinica. 2008;40(7):651-62.
40. Metrich M, Lucas A, Gastineau M, Samuel JL, Heymes C, Morel E, et al. Epac mediates beta-adrenergic receptor-induced cardiomyocyte hypertrophy. Circulation research. 2008;102(8):959-65.
41. Brand T, Schindler R. New kids on the block: The Popeye domain containing (POPDC) protein family acting as a novel class of cAMP effector proteins in striated muscle. Cellular signalling. 2017;40:156-65.
42. Gingold-Belfer R, Bergman M, Alcalay Y, Schlesinger H, Aravot D, Berman M, et al. Popeye domain-containing 1 is down-regulated in failing human hearts. International journal of molecular medicine. 2011;27(1):25-31.

43. Omori K, Kotera J. Overview of PDEs and Their Regulation. Circulation research. 2007;100(3):309-27.
44. Francis SH, Turko IV, Corbin JD. Cyclic nucleotide phosphodiesterases: relating structure and function. Progress in nucleic acid research and molecular biology. 2001;65:1-52.
45. Tobise K, Ishikawa Y, Holmer SR, Im MJ, Newell JB, Yoshie H, et al. Changes in type VI adenylyl cyclase isoform expression correlate with a decreased capacity for cAMP generation in the aging ventricle. Circulation research. 1994;74(4):596-603.
46. Espinasse I, Iourgenko V, Defer N, Samson F, Hanoune J, Mercadier JJ. Type V, but not type VI, adenylyl cyclase mRNA accumulates in the rat heart during ontogenic development. Correlation with increased global adenylyl cyclase activity. Journal of molecular and cellular cardiology. 1995;27(9):1789-95.
47. Scarpace PJ, Matheny M, Tumer N. Myocardial adenylyl cyclase type V and VI mRNA: differential regulation with age. Journal of cardiovascular pharmacology. 1996;27(1):86-90.
48. Hu CL, Chandra R, Ge H, Pain J, Yan L, Babu G, et al. Adenylyl cyclase type 5 protein expression during cardiac development and stress. American journal of physiology Heart and circulatory physiology. 2009;297(5):H1776-82.
49. Tang T, Hammond HK, Firth A, Yang Y, Gao MH, Yuan JX, et al. Adenylyl cyclase 6 improves calcium uptake and left ventricular function in aged hearts. Journal of the American College of Cardiology. 2011;57(18):1846-55.
50. Timofeyev V, Myers RE, Kim HJ, Woltz RL, Sirish P, Heiserman JP, et al. Adenylyl cyclase subtype-specific compartmentalization: differential regulation of L-type Ca^{2+} current in ventricular myocytes. Circulation research. 2013;112(12):1567-76.
51. Nikolaev VO, Moshkov A, Lyon AR, Miragoli M, Novak P, Paur H, et al. Beta2-adrenergic receptor redistribution in heart failure changes cAMP compartmentation. Science (New York, NY). 2010;327(5973):1653-7.
52. Wright PT, Nikolaev VO, O'Hara T, Diakonov I, Bhargava A, Tokar S, et al. Caveolin-3 regulates compartmentation of cardiomyocyte beta2-adrenergic receptor-mediated cAMP signaling. Journal of molecular and cellular cardiology. 2014;67:38-48.
53. Tang T, Gao MH, Lai NC, Firth AL, Takahashi T, Guo T, et al. Adenylyl cyclase type 6 deletion decreases left ventricular function via impaired calcium handling. Circulation. 2008;117(1):61-9.
54. Tang T, Lai NC, Wright AT, Gao MH, Lee P, Guo T, et al. Adenylyl cyclase 6 deletion increases mortality during sustained beta-adrenergic receptor stimulation. Journal of molecular and cellular cardiology. 2013;60:60-7.
55. Gao MH, Bayat H, Roth DM, Yao Zhou J, Drumm J, Burhan J, et al. Controlled expression of cardiac-directed adenylylcyclase type VI provides increased contractile function. Cardiovascular research. 2002;56(2):197-204.
56. Lai NC, Tang T, Gao MH, Saito M, Takahashi T, Roth DM, et al. Activation of cardiac adenylyl cyclase expression increases function of the failing ischemic heart in mice. Journal of the American College of Cardiology. 2008;51(15):1490-7.
57. Gao MH, Tang T, Lai NC, Miyanohara A, Guo T, Tang R, et al. Beneficial effects of adenylyl cyclase type 6 (AC6) expression persist using a catalytically inactive AC6 mutant. Molecular pharmacology. 2011;79(3):381-8.
58. Chou JL, Huang CL, Lai HL, Hung AC, Chien CL, Kao YY, et al. Regulation of type VI adenylyl cyclase by Snapin, a SNAP25-binding protein. The Journal of biological chemistry. 2004;279(44):46271-9.
59. Chang C-P, Lee C-T, Hou W-H, Lin M-S, Lai H-L, Chien C-L, et al. Type VI adenylyl cyclase negatively regulates GluN2B-mediated LTD and spatial reversal learning. Scientific Reports. 2016;6(1):22529.
60. Hammond HK, Penny WF, Traverse JH, Henry TD, Watkins MW, Yancy CW, et al. Intracoronary Gene Transfer of Adenylyl Cyclase 6 in Patients With Heart Failure: A Randomized Clinical Trial. JAMA Cardiol. 2016;1(2):163-71.

61. Lee K-W, Hong J-H, Choi IY, Che Y, Lee J-K, Yang S-D, et al. Impaired D2 Dopamine Receptor Function in Mice Lacking Type 5 Adenylyl Cyclase. The Journal of Neuroscience. 2002;22(18):7931-40.
62. Tang T, Lai NC, Roth DM, Drumm J, Guo T, Lee KW, et al. Adenylyl cyclase type V deletion increases basal left ventricular function and reduces left ventricular contractile responsiveness to beta-adrenergic stimulation. Basic research in cardiology. 2006;101(2):117-26.
63. Okumura S, Takagi G, Kawabe J, Yang G, Lee MC, Hong C, et al. Disruption of type 5 adenylyl cyclase gene preserves cardiac function against pressure overload. Proceedings of the National Academy of Sciences of the United States of America. 2003;100(17):9986-90.
64. Yan L, Vatner DE, O'Connor JP, Ivessa A, Ge H, Chen W, et al. Type 5 adenylyl cyclase disruption increases longevity and protects against stress. Cell. 2007;130(2):247-58.
65. Zhao Z, Babu GJ, Wen H, Fefelova N, Gordan R, Sui X, et al. Overexpression of adenylyl cyclase type 5 (AC5) confers a proarrhythmic substrate to the heart. American journal of physiology Heart and circulatory physiology. 2015;308(3):H240-9.
66. Bruneau BG. Signaling and transcriptional networks in heart development and regeneration. Cold Spring Harbor perspectives in biology. 2013;5(3):a008292.
67. Abu-Issa R, Kirby ML. Heart field: from mesoderm to heart tube. Annual review of cell and developmental biology. 2007;23:45-68.
68. Arnold SJ, Robertson EJ. Making a commitment: cell lineage allocation and axis patterning in the early mouse embryo. Nature reviews Molecular cell biology. 2009;10(2):91-103.
69. Takahashi K, Yamanaka S. A decade of transcription factor-mediated reprogramming to pluripotency. Nature Reviews Molecular Cell Biology. 2016;17(3):183-93.
70. Takahashi K, Yamanaka S. Induction of Pluripotent Stem Cells from Mouse Embryonic and Adult Fibroblast Cultures by Defined Factors. Cell. 2006;126(4):663-76.
71. Takahashi K, Tanabe K, Ohnuki M, Narita M, Ichisaka T, Tomoda K, et al. Induction of Pluripotent Stem Cells from Adult Human Fibroblasts by Defined Factors. Cell. 2007;131(5):861-72.
72. Yu J, Vodyanik MA, Smuga-Otto K, Antosiewicz-Bourget J, Frane JL, Tian S, et al. Induced Pluripotent Stem Cell Lines Derived from Human Somatic Cells. Science (New York, NY). 2007;318(5858):1917-20.
73. Lickert H, Kutsch S, Kanzler B, Tamai Y, Taketo MM, Kemler R. Formation of multiple hearts in mice following deletion of beta-catenin in the embryonic endoderm. Developmental cell. 2002;3(2):171-81.
74. Ueno S, Weidinger G, Osugi T, Kohn AD, Golob JL, Pabon L, et al. Biphasic role for Wnt/β-catenin signaling in cardiac specification in zebrafish and embryonic stem cells. Proceedings of the National Academy of Sciences. 2007;104(23):9685-90.
75. Zhang M, Schulte JS, Heinick A, Piccini I, Rao J, Quaranta R, et al. Universal cardiac induction of human pluripotent stem cells in two and three-dimensional formats: implications for in vitro maturation. Stem cells (Dayton, Ohio). 2015;33(5):1456-69.
76. Musunuru K, Sheikh F, Gupta RM, Houser SR, Maher KO, Milan DJ, et al. Induced Pluripotent Stem Cells for Cardiovascular Disease Modeling and Precision Medicine: A Scientific Statement From the American Heart Association. Circulation: Genomic and Precision Medicine. 2018;11(1):e000043.
77. Colatsky T, Fermini B, Gintant G, Pierson JB, Sager P, Sekino Y, et al. The Comprehensive in Vitro Proarrhythmia Assay (CiPA) initiative — Update on progress. Journal of Pharmacological and Toxicological Methods. 2016;81:15-20.
78. Moretti A, Bellin M, Welling A, Jung CB, Lam JT, Bott-Flügel L, et al. Patient-specific induced pluripotent stem-cell models for long-QT syndrome. The New England journal of medicine. 2010;363(15):1397-409.
79. Bellin M, Casini S, Davis RP, D'Aniello C, Haas J, Ward-van Oostwaard D, et al. Isogenic human pluripotent stem cell pairs reveal the role of a KCNH2 mutation in long-QT syndrome. The EMBO journal. 2013;32(24):3161-75.
80. Fineran PC, Charpentier E. Memory of viral infections by CRISPR-Cas adaptive immune systems: acquisition of new information. Virology. 2012;434(2):202-9.

81. Horvath P, Barrangou R. CRISPR/Cas, the immune system of bacteria and archaea. Science (New York, NY). 2010;327(5962):167-70.
82. Deltcheva E, Chylinski K, Sharma CM, Gonzales K, Chao Y, Pirzada ZA, et al. CRISPR RNA maturation by trans-encoded small RNA and host factor RNase III. Nature. 2011;471(7340):602-7.
83. Jinek M, Chylinski K, Fonfara I, Hauer M, Doudna JA, Charpentier E. A programmable dual-RNA-guided DNA endonuclease in adaptive bacterial immunity. Science (New York, NY). 2012;337(6096):816-21.
84. Ran FA, Hsu PD, Wright J, Agarwala V, Scott DA, Zhang F. Genome engineering using the CRISPR-Cas9 system. Nat Protoc. 2013;8(11):2281-308.
85. Csobonyeiova M, Polak S, Danisovic L. Toxicity testing and drug screening using iPSC-derived hepatocytes, cardiomyocytes, and neural cells. Canadian journal of physiology and pharmacology. 2016;94(7):687-94.
86. Merkert S, Schubert M, Olmer R, Engels L, Radetzki S, Veltman M, et al. High-Throughput Screening for Modulators of CFTR Activity Based on Genetically Engineered Cystic Fibrosis Disease-Specific iPSCs. Stem cell reports. 2019;12(6):1389-403.
87. Doench JG, Fusi N, Sullender M, Hegde M, Vaimberg EW, Donovan KF, et al. Optimized sgRNA design to maximize activity and minimize off-target effects of CRISPR-Cas9. Nature biotechnology. 2016;34:184.
88. Dias TP, Pinto SN, Santos JI, Fernandes TG, Fernandes F, Diogo MM, et al. Biophysical study of human induced Pluripotent Stem Cell-Derived cardiomyocyte structural maturation during long-term culture. Biochemical and biophysical research communications. 2018;499(3):611-7.
89. Chanthra N, Abe T, Miyamoto M, Sekiguchi K, Kwon C, Hanazono Y, et al. A Novel Fluorescent Reporter System Identifies Laminin-511/521 as Potent Regulators of Cardiomyocyte Maturation. Scientific Reports. 2020;10(1):4249.
90. Dambrot C, Braam SR, Tertoolen LG, Birket M, Atsma DE, Mummery CL. Serum supplemented culture medium masks hypertrophic phenotypes in human pluripotent stem cell derived cardiomyocytes. Journal of cellular and molecular medicine. 2014;18(8):1509-18.
91. Gaudin C, Ishikawa Y, Wight DC, Mahdavi V, Nadal-Ginard B, Wagner TE, et al. Overexpression of Gs alpha protein in the hearts of transgenic mice. The Journal of clinical investigation. 1995;95(4):1676-83.
92. Chopra A, Tabdanov E, Patel H, Janmey PA, Kresh JY. Cardiac myocyte remodeling mediated by N-cadherin-dependent mechanosensing. American Journal of Physiology-Heart and Circulatory Physiology. 2011;300(4):H1252-H66.
93. Kho C, Lee A, Hajjar RJ. Altered sarcoplasmic reticulum calcium cycling--targets for heart failure therapy. Nat Rev Cardiol. 2012;9(12):717-33.
94. Bhupathy P, Babu GJ, Periasamy M. Sarcolipin and phospholamban as regulators of cardiac sarcoplasmic reticulum Ca^{2+} ATPase. Journal of molecular and cellular cardiology. 2007;42(5):903-11.
95. Blaustein MP, Lederer WJ. Sodium/Calcium Exchange: Its Physiological Implications. Physiological reviews. 1999;79(3):763-854.
96. Lou Q, Janardhan A, Efimov IR. Remodeling of calcium handling in human heart failure. Adv Exp Med Biol. 2012;740:1145-74.
97. Gwathmey JK, Warren SE, Briggs GM, Copelas L, Feldman MD, Phillips PJ, et al. Diastolic dysfunction in hypertrophic cardiomyopathy. Effect on active force generation during systole. The Journal of clinical investigation. 1991;87(3):1023-31.
98. Davies CH, Davia K, Bennett JG, Pepper JR, Poole-Wilson PA, Harding SE. Reduced Contraction and Altered Frequency Response of Isolated Ventricular Myocytes From Patients With Heart Failure. Circulation. 1995;92(9):2540-9.
99. Bristow MR, Ginsburg R, Umans V, Fowler M, Minobe W, Rasmussen R, et al. Beta 1- and beta 2-adrenergic-receptor subpopulations in nonfailing and failing human ventricular myocardium: coupling of both receptor subtypes to muscle contraction and selective beta 1-receptor down-regulation in heart failure. Circulation research. 1986;59(3):297-309.

100. Brodde OE, Schüler S, Kretsch R, Brinkmann M, Borst HG, Hetzer R, et al. Regional distribution of beta-adrenoceptors in the human heart: coexistence of functional beta 1- and beta 2-adrenoceptors in both atria and ventricles in severe congestive cardiomyopathy. Journal of cardiovascular pharmacology. 1986;8(6):1235-42.
101. Kao DP, Lowes BD, Gilbert EM, Minobe W, Epperson LE, Meyer LK, et al. Therapeutic Molecular Phenotype of β-Blocker–Associated Reverse-Remodeling in Nonischemic Dilated Cardiomyopathy. Circulation: Cardiovascular Genetics. 2015;8(2):270-83.
102. Man J, Barnett P, Christoffels VM. Structure and function of the Nppa-Nppb cluster locus during heart development and disease. Cellular and molecular life sciences : CMLS. 2018;75(8):1435-44.
103. Whisnant RE, Gilman AG, Dessauer CW. Interaction of the two cytosolic domains of mammalian adenylyl cyclase. Proceedings of the National Academy of Sciences of the United States of America. 1996;93(13):6621-5.
104. Suryanarayana S, Pinto C, Mou TC, Richter M, Lushington GH, Seifert R. The C1 homodimer of adenylyl cyclase binds nucleotides with high affinity but possesses exceedingly low catalytic activity. Neuroscience letters. 2009;467(1):1-5.
105. Zhang G, Liu Y, Ruoho AE, Hurley JH. Structure of the adenylyl cyclase catalytic core. Nature. 1997;386(6622):247-53.
106. Dessauer CW, Watts VJ, Ostrom RS, Conti M, Dove S, Seifert R. International Union of Basic and Clinical Pharmacology. CI. Structures and Small Molecule Modulators of Mammalian Adenylyl Cyclases. Pharmacological reviews. 2017;69(2):93-139.
107. Jeong J-Y, Yim H-S, Ryu J-Y, Lee HS, Lee J-H, Seen D-S, et al. One-Step Sequence- and Ligation-Independent Cloning as a Rapid and Versatile Cloning Method for Functional Genomics Studies. Applied and Environmental Microbiology. 2012;78(15):5440-3.
108. Popp MW, Maquat LE. Leveraging Rules of Nonsense-Mediated mRNA Decay for Genome Engineering and Personalized Medicine. Cell. 2016;165(6):1319-22.
109. Baker JG. The selectivity of beta-adrenoceptor agonists at human beta1-, beta2- and beta3-adrenoceptors. British journal of pharmacology. 2010;160(5):1048-61.
110. Baker JG. The selectivity of beta-adrenoceptor antagonists at the human beta1, beta2 and beta3 adrenoceptors. British journal of pharmacology. 2005;144(3):317-22.
111. Takimoto E, Soergel DG, Janssen PML, Stull LB, Kass DA, Murphy AM. Frequency- and Afterload-Dependent Cardiac Modulation In Vivo by Troponin I With Constitutively Active Protein Kinase A Phosphorylation Sites. Circulation research. 2004;94(4):496-504.
112. Dewenter M, von der Lieth A, Katus HA, Backs J. Calcium Signaling and Transcriptional Regulation in Cardiomyocytes. Circulation research. 2017;121(8):1000-20.
113. Kao DP, Lowes BD, Gilbert EM, Minobe W, Epperson LE, Meyer LK, et al. Therapeutic Molecular Phenotype of β-Blocker-Associated Reverse-Remodeling in Nonischemic Dilated Cardiomyopathy. Circulation Cardiovascular genetics. 2015;8(2):270-83.
114. Giacomelli E, Mummery CL, Bellin M. Human heart disease: lessons from human pluripotent stem cell-derived cardiomyocytes. Cellular and Molecular Life Sciences. 2017;74(20):3711-39.
115. Snir M, Kehat I, Gepstein A, Coleman R, Itskovitz-Eldor J, Livne E, et al. Assessment of the ultrastructural and proliferative properties of human embryonic stem cell-derived cardiomyocytes. American Journal of Physiology-Heart and Circulatory Physiology. 2003;285(6):H2355-H63.
116. Nakao K, Minobe W, Roden R, Bristow MR, Leinwand LA. Myosin heavy chain gene expression in human heart failure. The Journal of clinical investigation. 1997;100(9):2362-70.
117. Reiser PJ, Portman MA, Ning XH, Schomisch Moravec C. Human cardiac myosin heavy chain isoforms in fetal and failing adult atria and ventricles. American journal of physiology Heart and circulatory physiology. 2001;280(4):H1814-20.
118. Drawnel FM, Archer CR, Roderick HL. The role of the paracrine/autocrine mediator endothelin-1 in regulation of cardiac contractility and growth. Br J Pharmacol. 2013;168(2):296-317.
119. Iwase M, Uechi M, Vatner DE, Asai K, Shannon RP, Kudej RK, et al. Cardiomyopathy induced by cardiac Gs alpha overexpression. The American journal of physiology. 1997;272(1 Pt 2):H585-9.

120. Ojala TH, Hornberger LK. Fetal heart failure. Frontiers in bioscience (Scholar edition). 2010;2:891-906.
121. Crossman DJ, Ruygrok PN, Soeller C, Cannell MB. Changes in the organization of excitation-contraction coupling structures in failing human heart. PloS one. 2011;6(3):e17901.
122. Duan JJ, Ma JH, Zhang PH, Wang XP, Zou AR, Tu DN. Verapamil blocks HERG channel by the helix residue Y652 and F656 in the S6 transmembrane domain. Acta pharmacologica Sinica. 2007;28(7):959-67.
123. Fritz AL, Adil MM, Mao SR, Schaffer DV. cAMP and EPAC Signaling Functionally Replace OCT4 During Induced Pluripotent Stem Cell Reprogramming. Molecular therapy : the journal of the American Society of Gene Therapy. 2015;23(5):952-63.
124. Ramirez-Correa GA, Cortassa S, Stanley B, Gao WD, Murphy AM. Calcium sensitivity, force frequency relationship and cardiac troponin I: critical role of PKA and PKC phosphorylation sites. Journal of molecular and cellular cardiology. 2010;48(5):943-53.
125. Wu H, Lee J, Vincent LG, Wang Q, Gu M, Lan F, et al. Epigenetic Regulation of Phosphodiesterases 2A and 3A Underlies Compromised beta-Adrenergic Signaling in an iPSC Model of Dilated Cardiomyopathy. Cell stem cell. 2015;17(1):89-100.
126. Satoh H, Delbridge LM, Blatter LA, Bers DM. Surface:volume relationship in cardiac myocytes studied with confocal microscopy and membrane capacitance measurements: species-dependence and developmental effects. Biophysical journal. 1996;70(3):1494-504.
127. Matsumoto G, Tasaki I. A study of conduction velocity in nonmyelinated nerve fibers. Biophysical journal. 1977;20(1):1-13.
128. Tong J, Qi Y, Wang X, Yu L, Su C, Xie W, et al. Cell micropatterning reveals the modulatory effect of cell shape on proliferation through intracellular calcium transients. Biochimica et Biophysica Acta (BBA) - Molecular Cell Research. 2017;1864(12):2389-401.
129. Heerebeek Lv, Borbély A, Niessen HWM, Bronzwaer JGF, Velden Jvd, Stienen GJM, et al. Myocardial Structure and Function Differ in Systolic and Diastolic Heart Failure. Circulation. 2006;113(16):1966-73.
130. Aksel T, Choe Yu E, Sutton S, Ruppel KM, Spudich JA. Ensemble force changes that result from human cardiac myosin mutations and a small-molecule effector. Cell reports. 2015;11(6):910-20.
131. Lipworth B, Wedzicha J, Devereux G, Vestbo J, Dransfield MT. Beta-blockers in COPD: time for reappraisal. The European respiratory journal. 2016;48(3):880-8.
132. Tsujimoto T, Kajio H, Shapiro MF, Sugiyama T. Risk of All-Cause Mortality in Diabetic Patients Taking β-Blockers. Mayo Clinic proceedings. 2018;93(4):409-18.
133. Lucia Cd, Eguchi A, Koch WJ. New Insights in Cardiac β-Adrenergic Signaling During Heart Failure and Aging. Frontiers in Pharmacology. 2018;9(904).
134. Yoon S, Eom GH. Heart failure with preserved ejection fraction: present status and future directions. Exp Mol Med. 2019;51(12):1-9.
135. Lai NC, Tang T, Gao MH, Saito M, Takahashi T, Roth DM, et al. Activation of cardiac adenylyl cyclase expression increases function of the failing ischemic heart in mice. Journal of the American College of Cardiology. 2008;51(15):1490-7.
136. Mannhardt I, Breckwoldt K, Letuffe-Brenière D, Schaaf S, Schulz H, Neuber C, et al. Human Engineered Heart Tissue: Analysis of Contractile Force. Stem cell reports. 2016;7(1):29-42.
137. Brand CS, Hocker HJ, Gorfe AA, Cavasotto CN, Dessauer CW. Isoform selectivity of adenylyl cyclase inhibitors: characterization of known and novel compounds. The Journal of pharmacology and experimental therapeutics. 2013;347(2):265-75.
138. Seifert R, Lushington GH, Mou TC, Gille A, Sprang SR. Inhibitors of membranous adenylyl cyclases. Trends in pharmacological sciences. 2012;33(2):64-78.
139. Chen YZ, Friedman JR, Chen DH, Chan GC, Bloss CS, Hisama FM, et al. Gain-of-function ADCY5 mutations in familial dyskinesia with facial myokymia. Annals of neurology. 2014;75(4):542-9.
140. Chen YZ, Matsushita MM, Robertson P, Rieder M, Girirajan S, Antonacci F, et al. Autosomal dominant familial dyskinesia and facial myokymia: single exome sequencing identifies a mutation in adenylyl cyclase 5. Archives of neurology. 2012;69(5):630-5.

VI Danksagung

Ich danke Dr. Kirsten Leineweber, Dr. Stefan Frank und Dr. Eva Hippe für die Chance, diese Arbeit bei der Bayer AG schreiben zu können. Danke für Eure kontinuierliche Unterstützung und dass ihr mich auf diesem Weg begleitet habt.

Ich danke ebenso Prof. Dr. med. Dobromir Dobrev für die fachliche Betreuung. Ihre stets hilfreichen Impulse trugen maßgeblich zum Erfolg dieser Arbeit bei. Darüber hinaus danke ich Prof. Dr. rer. nat Gero Hilken ebenfalls für die Betreuung dieser Arbeit.

Vielen Dank an Dr. Monique Wölfer und Maximilian Koch für eure Unterstützung im Laboralltag. Ebenso danke ich Stefan Neumann, Dr. Greta Ziemann und Dr. Mark Meininghaus für die großartige Zusammenarbeit bei der Entwicklung der KinEva Software.

VII Lebenslauf

Der Lebenslauf ist in der Online-Version aus Gründen des Datenschutzes nicht enthalten.

VIII Eidesstattliche Erklärung

Erklärung:

Hiermit erkläre ich, gem. § 7 Abs. (2) d) + f) der Promotionsordnung der Fakultät für Biologie zur Erlangung des Dr. rer. nat., dass ich die vorliegende Dissertation selbständig verfasst und mich keiner anderen als der angegebenen Hilfsmittel bedient, bei der Abfassung der Dissertation nur die angegeben Hilfsmittel benutzt und alle wörtlich oder inhaltlich übernommenen Stellen als solche gekennzeichnet habe.

Essen, den _____ _____

Unterschrift des Doktoranden

Erklärung:

Hiermit erkläre ich, gem. § 7 Abs. (2) e) + g) der Promotionsordnung der Fakultät für Biologie zur Erlangung des Dr. rer. nat., dass ich keine anderen Promotionen bzw. Promotionsversuche in der Vergangenheit durchgeführt habe und dass diese Arbeit von keiner anderen Fakultät/Fachbereich abgelehnt worden ist.

Essen, den _____ _____

Unterschrift des Doktoranden

Erklärung:

Hiermit erkläre ich, gem. § 6 Abs. (2) g) der Promotionsordnung der Fakultät für Biologie zur Erlangung der Dr. rer. nat., dass ich das Arbeitsgebiet, dem das Thema „Target validation of adenylyl cyclase 5 and adenylyl cyclase 6 in human induced pluripotent stem cell-derived cardiomyocytes“ zuzuordnen ist, in Forschung und Lehre vertrete und den Antrag von Pascal Lambertz befürworte und die Betreuung auch im Falle eines Weggangs, wenn nicht wichtige Gründe dem entgegenstehen, weiterführen werde.

Prof. Dr. med. Dobromir Dobrev

Name des Mitglieds der Universität Duisburg-Essen in Druckbuchstaben

Essen, den _____ _____

Unterschrift des Mitglieds der Universität Duisburg-Essen